

Some pages of this thesis may have been removed for copyright restrictions.

If you have discovered material in AURA which is unlawful e.g. breaches copyright, (either yours or that of a third party) or any other law, including but not limited to those relating to patent, trademark, confidentiality, data protection, obscenity, defamation, libel, then please read our [Takedown Policy](#) and [contact the service](#) immediately

VIBRATIONAL METHODS APPLIED TO
NDT TESTING AND FLUID DENSITY MEASUREMENT

JAMAL A. MUADDI

... of ...
... which ...
... industrial ...
...
...

Submitted to
The University of Aston in Birmingham
for the degree of
Doctor of Philosophy

January 1982

VIBRATIONAL METHODS APPLIED TO
NDT TESTING AND FLUID DENSITY MEASUREMENT

Jamal A. Muaddi

A thesis submitted to
The University of Aston in Birmingham
for the degree of
Doctor of Philosophy 1982

Summary

A system for the NDT testing of the integrity of composite materials and of adhesive bonds has been developed to meet industrial requirements. The vibration techniques used were found to be applicable to the development of fluid measuring transducers.

The vibrational spectra of thin rectangular bars were used for the NDT work. A machined cut in a bar had a significant effect on the spectrum but a genuine crack gave an unambiguous response at high amplitudes. This was the generation of fretting crack noise at frequencies far above that of the drive.

A specially designed vibrational decrement meter which, in effect, measures mechanical energy loss enabled a numerical classification of material adhesion to be obtained. This was used to study bars which had been flame or plasma sprayed with a variety of materials. It has become a useful tool in optimising coating methods. A direct industrial application was to classify piston rings of high performance I.C. engines. Each consists of a cast iron ring with a channel into which molybdenum, a good bearing surface, is sprayed. The NDT classification agreed quite well with the destructive test normally used.

The techniques and equipment used for the NDT work were applied to the development of the tuning fork transducers investigated by Hassan into commercial density and viscosity devices. Using narrowly spaced, large area tines a thin lamina of fluid is trapped between them. It stores a large fraction of the vibrational energy which, acting as an inertia load reduces the frequency. Magnetostrictive and piezoelectric effects together or in combination enable the fork to be operated through a flange. This allows it to be used in pipeline or 'dipstick' applications.

Using a different tine geometry the viscosity loading can be predominant. This as well as the signal decrement of the density transducer makes a practical viscometer.

Key Words

NDT, BONDING, FLUIDS, DENSITY, VISCOSITY.

ACKNOWLEDGEMENTS

Page

I wish to express my sincere thanks to Dr. J. F. W. Bell for his guidance and encouragement throughout the progress of this project.

I would also like to thank Professor E. J. Davies, Head of the Electrical and Electronic Engineering Department, for the provision of laboratory facilities.

The workshop staff and departmental technicians provided invaluable help and assistance, particularly Mr. F. Hunt, Mr. B. Hale, Mr. W. Harper and Mr. B. Cox (Metallurgy Department) for plating the transducers.

The Associated Engineering Company suggested the industrial application of the Q-meter and provided the piston rings and a range of specially coated samples.

Finally, it is a pleasure to thank Helen Turner for typing the thesis.

CONTENTS

Clamped Bar

26

	<u>Page</u>
Summary	ii
Acknowledgements	iii
Contents	iv
List of Figures	viii
List of Tables	xii

CHAPTER 1

REVIEW OF THE USE OF VIBRATIONS FOR NDT AND THE MEASUREMENT OF FLUID PROPERTIES	1
1.1 Introduction	1
1.2 Vibrational Techniques for Evaluating Materials	4
1.3 Electromechanical Resonator as Measuring Transducers.	8
1.4 Review of some Measuring Transducers based on Mechanical Resonators using the Frequency Domain Technique.	10
1.4.1 Fluid Density Transducers	10
1.4.2 Viscosity Transducers	14

CHAPTER 2

THE PHENOMENON OF RESONANCE AS APPLIED TO SOLIDS OF SIMPLE GEOMETRY	17
2.1 Introduction	17
2.2 Phenomenological Approach to Q and Loss Factors	18
2.3 Rectangular Bar Resonator	24
2.3.1 Clamped-Free Bar	26

	<u>Page</u>
2.3.2 Free-Free and Clamped-Clamped Bar	26
2.4 Tuning Fork Resonator	28
2.4.1 Introduction	28
2.4.2 Some Applications of the Tuning Fork	32
2.5 Split Ring Resonator	33
 <u>CHAPTER 3</u>	
THE TESTING AND EVALUATING OF COMPONENTS AND MATERIALS BY MECHANICAL RESONANCE	37
3.1 Introduction	37
3.2 Vibration of Simple Bars Containing Defects	38
3.3 Decrement Q-Meter	53
3.3.1 Introduction	53
3.3.2 Electronic Design	54
3.3.2.a Zero Crossing Comparator	57
3.3.2.b Decrement Comparator	57
3.3.2.c The Switching Bistable	58
3.4 Evaluating the Design	58
3.5 Experimental Results	62
3.5.1 Testing Adhesive Bonds	62
3.5.2 Influence of Coating Thickness	65
3.5.3 Temperature Effect on Q	65
 <u>CHAPTER 4</u>	
INDUSTRIAL APPLICATION	71
4.1 Introduction	71
4.2 Electronic Design	73
4.2.1 Introduction	73

	<u>Page</u>
4.2.2 Transmitter and Control System	75
4.2.3 Receiver and Phase Adjustment	81
4.2.4 Q-Meter	81
4.3 Testing Procedure	83
4.3.1 Introduction	83
4.3.2 Experimental Results	87
<u>CHAPTER 5</u>	
THE DESIGN OF TUNING FORK TRANSDUCER FOR MEASURING FLUID DENSITY AND VISCOSITY	95
5.1 Introduction	95
5.2 Driver	100
5.2.1 Introduction	100
5.2.2 Drive Channel	100
5.3 Receiver and Decrement Signal Processing	105
5.3.1 Introduction	105
5.3.2 Input Voltage Follower	107
5.3.3 Zero Crossing Comparator	107
5.4 Error Measurement	108
5.4.1 Signal Channel	108
5.4.2 Decrement Channel	108
5.5 The Control System	110
5.5.1 Introduction	110
5.6 Transducer Evaluation	119

	<u>Page</u>
<u>CHAPTER 6</u>	
DENSITY AND VISCOSITY MEASUREMENT	133
6.1 Introduction	133
6.2 Vibrating Body-Fluid Interaction	136
6.3 Driving Techniques	139
6.4 Theoretical Consideration	144
6.4.1. Introduction	144
6.4.2 Centre Clamped Circular Plate	145
6.4.3 The Fluid Loading effects in Practical Designs	149
6.4.3.a Fluid Loading effects on the Narrow Tuning Fork	149
6.4.3.b Fluid Loading effects on the Wide Tuning Fork	152
6.4.4 The Dynamic Mass of the Resonator	154
6.5 Experiments and Calibration	156
6.6 Development of the Transducer	161
6.7 Recommendation of the Transducer	167
6.7.1 Introduction	167
6.7.2 Viscosity Measurement	169
6.8 Magnetostrictive Material	171
6.9 Conclusions	175
List of Symbols	177
Appendix 1	179
References	182

LIST OF FIGURES

<u>Figure</u>		<u>Page</u>
1.1	An idealised mechanical system with mass, spring and damping.	2
1.2	Solartron liquid density transducer.	10
1.3	Solartron gas density transducer.	12
1.4	Agar vibrating spool density transducer.	13
1.5	Viscometer for biological fluids.	15
2.1	An idealised mechanical system with mass, spring and damping.	20
2.2	Damped oscillatory motion.	21
2.3	R.L.C. electric circuit resonator	23
2.4	Shapes of the first three characteristic functions for a clamped free bar.	27
2.5	Shapes of the first three characteristic functions for a free-free bar.	29
2.6	A general view of the transducer.	30
2.7	A double resonator used for ultrasonic thermometry.	33
2.8	A piston ring clamped firmly at the centre.	35
2.9	The first three modes as classified experimentally for a free split ring.	35
3.1	The experimental arrangement for observing the resonant frequency response.	39
3.2	Experimental and theoretical values of (f_n/f_1) versus n .	42
3.3	Steel bars showing the position of the cuts.	44
3.4	f_n/B_n^2 against cut depth.	45
3.5	f_n/B_n^2 against cut depth.	46
3.6	Photographs showing the crack noise component in the pick-up signal of a glass bar containing crack.	49

<u>Figure</u>		<u>Page</u>
3.7	Photograph showing the crack noise in the pick-up signal of a glass bar containing a crack.	51
3.8	Photographs showing the crack noise in the pick-up signal of a glass bar containing crack.	52
3.9	Signal schematic diagram to give account of Q.	56
3.10	The experimental set-up for measuring the decay rate of oscillations.	60
3.11	The variation of Q^{-1} with coating weight.	66
3.12	The variation of Q^{-1} with coating thickness.	66
3.13	The variation of Q^{-1} with temperature.	69
4.1	Photographs showing the experimental arrangement for testing piston rings.	72
4.2	Block diagram of the electronic system to drive, receive and measure the decay rate of oscillations for piston rings.	74
4.3	Block diagram of phase locked loop.	76
4.4	Circuit detail of the driver and the receiver of the automatic Q-meter.	78
4.5	Waveforms of the driver system giving an interlaced signal.	79
4.6	Drive power amplifier and gating circuit to obtain the required signal.	80
4.7	Circuit detail of the Q-meter.	82
4.8	Waveforms at different points in the Q-meter.	84
4.9	Modes of vibration of the piston ring when it is clamped firmly at the centre.	86
5.1	A typical transducer used for measuring liquid density.	97
5.2	The functional block diagram of the electronic system of the transducer.	99
5.3	The drive channel and the receive channel of the transducer.	102

<u>Figure</u>		<u>Page</u>
5.4	Photographs showing the drive and decrement modes.	103
5.5	The required waveform for gating bursts of oscillations from the VCO.	104
5.6	The required waveforms to drive the transducer.	106
5.7	The circuit diagram for error measurement.	109
5.8	Drive and decrement signal samples.	111
5.9	Photographs showing the drive, decrement and the output of the two integrators.	113
5.10	Drive and decrement samples and the output of the two integrators.	114
5.11	Functional block diagram of the control system.	115
5.12	The circuit detail of the error measurement.	117
5.13	The read-out frequency of the three conditions of controller.	118
5.14	The decrement wave form and the error signal for aluminium transducer.	120
5.15	Frequency fluctuation of the aluminium transducer vibrating in air, oil and water.	122
5.16	Frequency fluctuation of the nickel silver transducer vibrating in air, oil and water.	123
5.17	Frequency fluctuation of the nickel silver transducer vibrating in air, oil and water.	125
5.18	The variation of the frequency of the aluminium transducer vibrating in water as the density changes.	126
5.19	The variation of the frequency of the nickel silver transducer vibrating in water when a sugar solution was added to the water.	127
5.20	Frequency fluctuation of the nickel silver transducer vibrating in oil.	129
5.21	The variation of the frequency of the aluminium transducer with temperature vibrating in air.	130

<u>Figure</u>		<u>Page</u>
5.22	The variation of the frequency of the aluminium transducer with temperature vibrating in oil.	131
6.1	A general view of the liquid density transducer.	134
6.2	Photograph of the viscosity transducer design.	135
6.3	Circular tuning fork.	146
6.4	Narrow tuning fork.	151
6.5	Wide tuning fork.	153
6.6	Mechanical vibrator system with mass M , spring and an added mass Δm .	156
6.7	The calibration curves for four transducers using a range of liquids.	163
6.8	The final electronic circuit design for the transducer.	165
6.9	A final density transducer design.	166
6.10	Frequency fluctuations of transducers vibrating in oil.	168
6.11	Magnetostrictive drive force for a sinusoidally alternating magnetisation in the case of non-biased excitation.	174
6.12	Magnetostrictive driving force for a sinusoidally alternating magnetisation in the case of a biased excitation.	174

LIST OF TABLES

<u>Table</u>		<u>Page</u>
2.1	A number of typical systems for steady-state vibrations.	19
2.2	Results of the large curved tuning fork.	36
2.3	Results of the small curved tuning fork.	36
3.1	Comparison of experimental and theoretical results of steel bar free at both ends.	41
3.2	The experimental results of measuring the resonant frequency for two steel bars containing cuts and vibrating at different modes.	47
3.3	Experimental results of measuring the Q for different resonators.	61
3.4	Comparison of (Q_D) and (Q_B) for aluminium rectangular bars of different thickness.	63
3.5	Experimental results of testing the adhesive bond of steel bars.	64
3.6	Experimental results of measuring Q of steel bars coated with chrome and alumina.	67
3.7	Experimental results of measuring Q of aluminium bars coated with chrome and alumina.	68
3.8	Experimental results of measuring Q and frequency of a hot steel bar cooling down.	70
4.1	Experimental results of measuring the Q of badly bonded rings.	88
4.2	Experimental results of measuring the Q of well-bonded rings.	89
4.3	Experimental results of measuring the Q of unknown rings.	91
6.1	The characteristic of the transducers used for liquid density measurements.	158
6.2	Experimental results of measuring frequencies for various transducers using a range of liquids.	162

<u>Table</u>		<u>Page</u>
6.3	Experimental results of measuring Q-factor of various transducers using a range of liquids.	170
6.4	Experimental results of measuring frequencies for viscosity transducers using a range of liquids.	170
6.5	The characteristic of the transducer used for viscosity measurements.	172

CHAPTER 1

REVIEW OF THE USE OF VIBRATIONS FOR NDT AND THE MEASUREMENT OF FLUID PROPERTIES

1.1 INTRODUCTION

The usefulness of using vibration as an NDT to study the defect structure of solids, strength of adhesive bond and measuring physical quantities has created an interest in industry. Therefore the development of instrumentation applications lying in this field has great possibilities.

In this work the technique adopted is to measure the energy dissipated in a vibrating system as a result of the internal elastic dissipation of the material or a defect in any coating is based on measuring the decay rate of oscillations. This gives the quality factor "Q" of each particular resonance when a body or structure is set in motion and the excitation source is removed. This can be understood by considering a simple lumped electrical resonator (RLC circuit) or an idealised mechanical vibrator with a single degree of freedom as shown in Fig. 1.1. In the absence of the driving force the vibration of the system will decay exponentially as will be discussed in the next chapter as in equation (1.1).

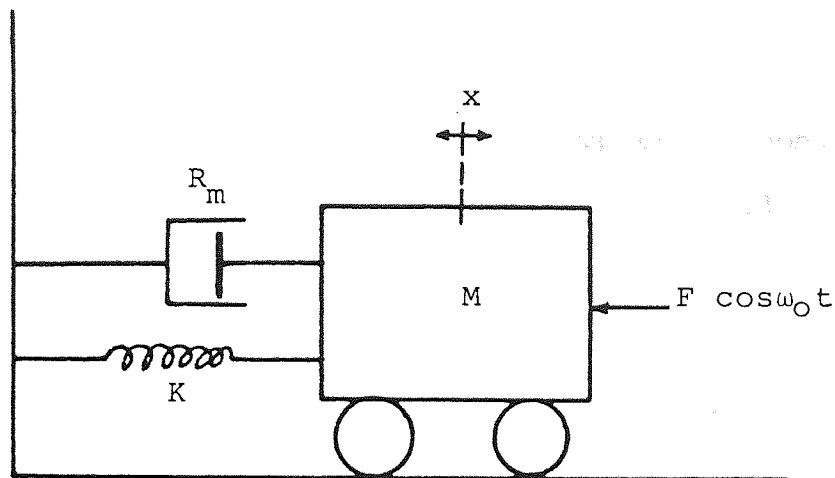


Fig. 1.1 An idealised mechanical system with mass, spring and damping.

$$A_n = A_0 \exp\left(-\frac{\pi n}{Q}\right) \quad (1.1)$$

where

- A_0 the initial amplitude
- A_n the amplitude after number of oscillations
- n the number of oscillations
- Q the 'Q' factor.

The model of the mechanical vibrator consists of a mass M , spring of stiffness K and velocity dependent viscous damping $R_m \dot{x}$. Resonance of the structure can also be the fundamental principle of measuring physical quantities such as density, viscosity and temperature.

The equation of motion of the system after disturbance is given by:

$$M\ddot{X} + R_m\dot{X} + KX = 0 \quad (1.2)$$

This is a well known damped simple harmonic motion equation where the system returns to rest under the influence of the mechanical dissipation. However, the oscillations may be maintained at the natural frequency of resonance $\omega_0 = \sqrt{\frac{K}{M}}$ by supplying a driving force to the system. Equation (1.3) now describes the motion

$$M\ddot{X} + R_m\dot{X} + KX = F\cos\omega_0 t \quad (1.3)$$

where $F\cos\omega_0 t$ is the driving force of the system.

Thus any factor contributing to a variation in K or M will result in a change in the frequency of the maintained oscillator and this frequency may be employed as a measure of such factors. For fluid movement Hassan (1980) has shown that by changing the geometrical design either the K factor or the M factor can be predominant. There is also an associated change in R_m which, because of its relationship to Q, can set a limit to the effectiveness of the vibrations of the transducer. Changes in stiffness of the system may be arranged to arise from a direct effect of changes in compressive or tensile stress on such a physical element as a vibrating wire or prismatic beams. This may be used to design load cells and pressure transducers. The dependence of resonant frequency on temperature may be utilised to design a thermometer.

1.2 VIBRATIONAL TECHNIQUES FOR EVALUATING MATERIALS

There are two widely used techniques for measuring the quality factor or the internal friction (Q^{-1}). These are the bandwidth and the decay methods. They were originated by Förster (1937).

For the samples exhibiting large internal friction, the bandwidth technique is most effective because the large bandwidth Δf may be measured more accurately. This is shown in equation (1.4).

$$Q = \frac{f_r}{\Delta f} \quad (1.4)$$

where

f_r is the resonant frequency

$\Delta f = f_2 - f_1$, where f_2 and f_1 are the frequencies at half power points.

The second method is more effective with specimens having low loss, where the time for the decay of oscillations is large. In this method Q^{-1} may be

determined by stopping the drive and counting the number of oscillations for the amplitude to fall to a precalculated fraction of its initial value.

A variety of instruments for measuring Q^{-1} using the decay technique has been described in literature. In the devices described by Fusfeld (1950) and Pattison (1954) , the decaying signal was rectified and smoothed. The resulting envelope was used to trigger further circuitry, producing time markers for pre-selected amplitudes of oscillation. Measuring the resonant frequency of the sample and the time interval between these markers by means of a counter allows Q to be calculated. At low frequencies the technique of rectification loses precision because of the difficulty in smoothing the rectified signal. Moreover the filter components should ideally be changed for each value of decrement and frequency. The frequency range of these devices is approximately 50 Hz - 10 KHz. A rate of about 20 readings per minute with two operators can be taken from the Fusfeld instrument.

Swartz (1964) circumvented these limitations by eliminating the rectification procedure and using the decaying oscillation directly to trigger the threshold level devices. Q is measured by counting the number of oscillations between two preset amplitudes of frequency below 80 Hz for Q values below 100.

The devices of Mason (1969) and Eder (1973) work in a similar way by counting the decrement oscillations. The frequency range for the Mason device is 5 Hz to 25 KHz for Q values between 6 and 200; while for the second device is 10 Hz to 40 KHz for values of Q between some tens and some millions. This device is designed for piezoelectric crystals only. For measuring other resonators, a power amplifier with a special drive and detector units must be provided.

Recently, Klimasara (1976) and Simpson (1977) described an electronic system which utilised a phase locked loop for the automatic measurement of the internal friction by means of a frequency modulation technique. The second device is limited to a Q factor below 10^3 .

An electronic instrument based on the decrement technique was specially designed by the author to give a numerical method of evaluating the integrity of solids, the testing adhesive bonds and similar components assemblies. Recent improvements in I.C. electronic comparators have been a major factor in achieving an instrument of high accuracy.

The principle of the instrument is the exponential equation of damped amplitude (equation (1.1)). It counts the number of oscillations of the freely decaying vibration between two defined levels of amplitude. Noting

that A_o/A_n has been chosen to be 23.14 and that $\ln 23.14$ is equal to π then equation (1.1) establishes that n is equal to Q . That is to say that the number of pulses counted equals to Q value of the test sample. An electro-magnetic transducer and a miniature microphone was used to drive the samples and pick-up the vibration as will be discussed in detail in Chapter 3.

Using the same method of measuring Q , the instrument was further developed for a particular industrial application requirement. The application area was the testing the quality of piston rings of high performance internal combustion engines where the bearing surface is molybdenum, flame sprayed onto a cast iron ring. The required inspection rate was 100 rings per hour. The design now operates automatically as will be described in Chapter 4. It uses a drive and pick-up control loop to find the resonance of each ring, even when there is a considerable frequency variation between the rings. The instrument can also be applied to other areas where self-excited vibration is needed. Both instruments operate within the audible frequency range for values of Q between some tens and some thousands. The accuracy of the instrument is better than 1% for this wide range of Q .

1.3 ELECTROMECHANICAL RESONATORS AS MEASURING TRANSDUCERS

The techniques and equipment used for the above work are applicable to the development of vibrating transducers for measuring physical quantities such as fluid density and viscosity. A commercial device to use in oil pipe lines and 'dip-stick' samplers was attempted.

The tuning fork transducer investigated by Hassan (1980) was considered to have the best development potential. A tuning fork is a dynamically clamped system and because of the high 'Q' it has a very good frequency stability.

The principle of the design of this resonator sensor for liquid density measurement lies in the thin layer of fluid trapped between the vibrating tines. It becomes part of the transducer, contributing an inertia load which lowers the resonant frequency. This design can in principle be used for viscosity measurement by calibrating the Q-factor of the resonator as a function of liquid viscosity. The viscosity can also be measured using a different tine geometry where the width of the tines is very small compared to the thickness. The large area exerts a shearing effect on the liquid. Unlike the vibrating plate transducer the immersion depth is not critical.

The problem of making the transducer operate through

a flange in an oil pipe line or pressure vessel wall was overcome. Two techniques were used to operate the transducer. Both use a magnetostrictive drive and in one the detector is also magnetostrictive but in the other it was piezoelectric. The latter appears to be the most satisfactory as it gives the higher frequency stability (10 ppm) and better signals in high viscosity liquids.

The energy is led through the flange as magnetic flux and converted to vibration energy by magnetostrictive nickel. The general vibration of the unit gives an adequate detector signal.

Devices for density and viscosity applications were produced. In the former a typical design gave a change in frequency which was as much as 25% when the probe was immersed in water. The density and viscosity transducers will be discussed in Chapters 5 and 6.

A brief discussion of operating principles and main features of some of the commercial transducers based on mechanical resonators is given in the following section.

1.4 A REVIEW OF SOME MEASURING TRANSDUCERS BASED ON MECHANICAL RESONATORS, USING THE FREQUENCY DOMAIN TECHNIQUE

1.4.1 Fluid Density Transducer

(a) Solartron Density Transducers. (Potter (1969))

The transducer as shown in Fig. 1.2 consists of a pair of nickel-iron alloy tubes welded parallel to each other. Two electromagnetic drive and pick-up coils are used to drive the tubes which are dynamically balanced in the fundamental flexural mode. The tubes and coils are held to the transducer case with anti-vibration mounts and the liquid, whose density is to be measured, flows equally through both tubes.

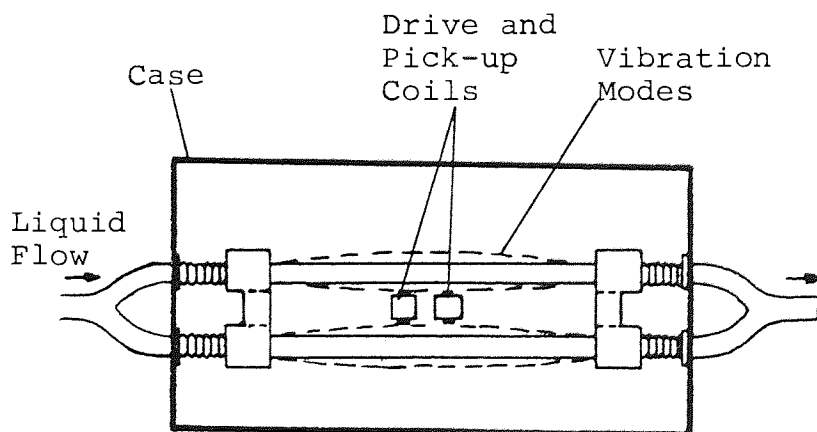


Fig. 1.2 Solartron liquid density transducer.

Since the natural frequency of oscillation of the tubes is a function of their mass, it is also a function of the density of the liquid contained in the tubes. By measuring this frequency, it is therefore possible to compute the liquid density. There is a 20% reduction in frequency when the tubes are filled with water. The use of a nickel alloy with a combination of cold working and heat treatment gives a very low temperature coefficient of less than 20 ppm/dec °C to the instrument. The density/frequency relationship is given by:

$$\rho_{\ell} = \frac{1}{K_0} \left| \left(\frac{f_0}{f_{\ell}} \right)^2 - 1 \right| \quad (1.5)$$

where

ρ_{ℓ} = liquid density

f_{ℓ} = frequency at density being measured

f_0 = frequency at zero density

K_0 = sensitivity constant.

New liquid density transducers have been developed by Solartron. In these instruments the sensing element is a straight smooth bore tube vibrated at one of its natural frequencies. The liquid whose density is to be measured flows through the tube.

Two identical transducers are available, the vibrating tube in one is manufactured from "Nispan C" material providing a very good stability and low temperature coefficient. In the other transducer the vibrating tube

is manufactured from stainless steel 316 which has better corrosion resistance but a higher temperature coefficient. The transducer occupied an area about 100 cm × 20 cm.

(b) Solartron Gas Density Transducer. (Potter (1969))

The sensing element of this transducer as shown in Fig. 1.3 is a thin walled cylinder (nickel-iron alloy) resonated in "hoop" (distortion) mode. The maximum vibrating amplitude occurs at the middle of the cylinder length with nodes at the ends. The cylinder is therefore clamped at one end with a heavy node-forming ring at the other end. The gas, whose density is to be measured, is passed over the inside and outside of the sensing element cylinder eliminating any stress effects due to the pressure of the gas. Gas is thus brought into oscillation by the vibrating walls and contributes to the mass of the walls by an amount which depends on the density of the gas. An increase in density will increase the

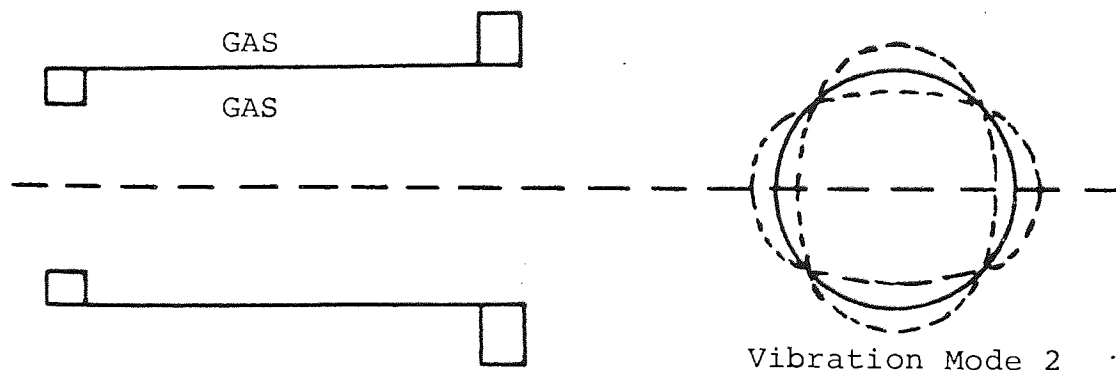


Fig. 1.3 Solartron Gas Density Transducer

effective mass of the vibrating system and thus lower the natural resonant frequency. The cylinder wall thickness varies between 50 and 150 micron depending on the density range to be measured. The thin wall is essential to achieve an acceptable sensitivity.

(c) Agar Vibrating Spool Density Meter. (Agar (1969))

The principle of operation is shown in Fig. 1.4. The sensing element is a tube thickened at the two ends (a spool), which also vibrates in a distortion mode of oscillation. The spool is maintained in oscillation by a feedback amplifier. The fluid to be measured is allowed to surround the spool and thus is set in oscillation as well. The model is essentially that of the mass spring system of Fig. 1.1. An increase in the density of the liquid lowers the frequency of oscillation. A 10% reduction in frequency is equivalent

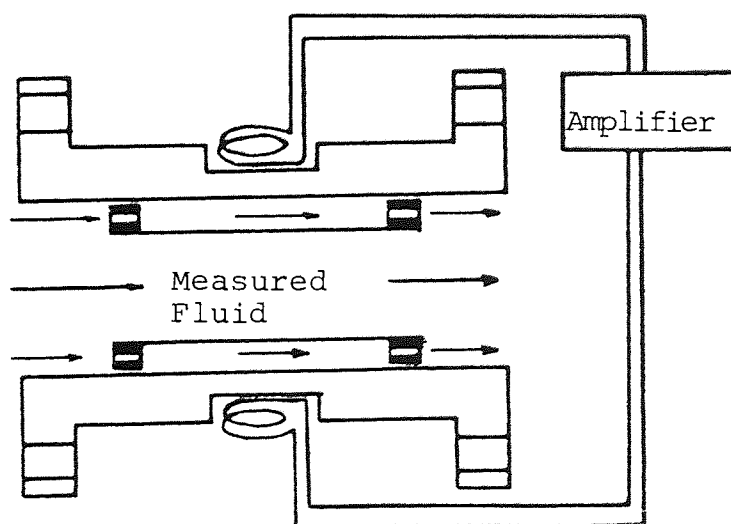


Fig. 1.4 Principle of Operation of Liquid Density Meter.

to a 100 Kg m^{-3} change in density. (Berger (1978))

Unlike the tuning fork design used in this work there is no fluid velocity magnification and sensitivity is only achieved by a major sacrifice of resonator robustness.

1.4.2 Viscosity Transducer

Liquid viscosity can be measured by two frequency domain methods. One is based on the resonant system, where the transducer is part of a self-oscillating circuit, Haynes (1973) and Miyake (1977). The second method is based on measuring the amplitude decrement of a driven resonator, Taraba (1967), White (1968), Chung (1973) and Berger (1978).

The most common viscometer operating on the first method is a torsionally vibrating crystal. The piezoelectric crystal generates shear (viscous) stresses in the medium to be measured. Both a reactance and a resistance loading occurs in the crystal which lowers its frequency and raises the measured resistance loss. The viscosity may then be determined by measuring the change in the impedance of the crystal. A brief discussion of a transducer operating on the amplitude decrement is given below.

(a) Viscometer Designed for Biological Fluids. (Berger (1978))

The basic principle of design involves the measurement of the decay constant of a tuning fork which is damped by the fluid immersion of one of the needle-like tines projecting as shown in Fig. 1.5.

The electromagnetic driver and receiver is connected as part of an amplifier and phase locked loop circuit.

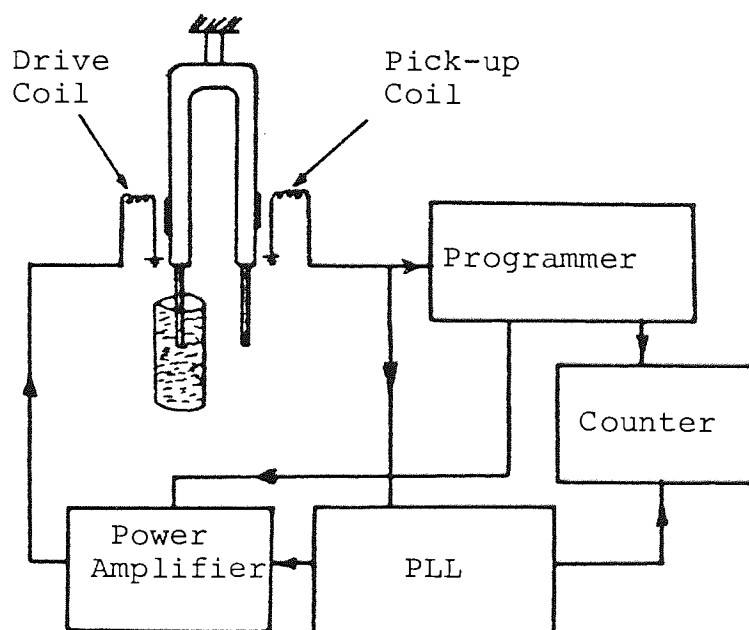


Fig. 1.5 Schematic diagram of tuning fork viscometer and associated electronics.

In operation, the tuning fork is part of an oscillatory system and quickly builds up to a pre-established maximum amplitude. The driver amplitude is then shut off by a programmer system and the amplitude of the oscillations

decay exponentially. An electronic counter counts the number of oscillations, until the amplitude of oscillation decays to $1/e$ of the initial maximum amplitude. The electronic programmer then turns on the drive, and the fork is driven to the maximum amplitude to start the cycle over again.

The digital read out of the counter is a function of the viscosity of the fluid and the length of the immersed part of the needle.

CHAPTER 2

THE PHENOMENON OF RESONANCE AS APPLIED TO SOLIDS OF SIMPLE GEOMETRY

2.1 INTRODUCTION

With the increasing mechanisation and specialisation of industrial society, the nondestructive testing of engineering components such as the determination of the material integrity, the strength of an adhesive bond and the measurement of the physical properties of fluids has become economically important. The work described in this thesis has resulted in the use of vibration generation and measurement to carry out these tasks. Specifically the nondestructive testing by vibration of piston rings appeared to be possible. These consist of a channelled ring (of cast iron) into which molybdenum, which constitutes the contact surface with the piston cylinder, is sprayed. Initial tests were carried out on simple rectangular steel bars with various coatings. Having established that the quality of the adhesive could be measured, the work proceeded to the realisation of a practical high testing rate technique of ring quality control.

In parallel with this, the development of a vibrating

transducer for measuring fluid density and viscosity using an electromechanical resonator was undertaken. Simplicity, robustness and reliability relative to existing transducers were achieved.

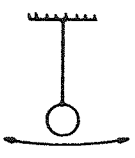
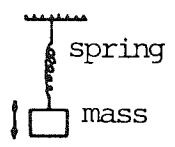
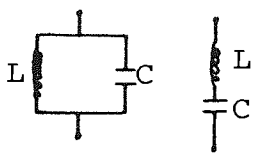
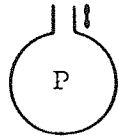

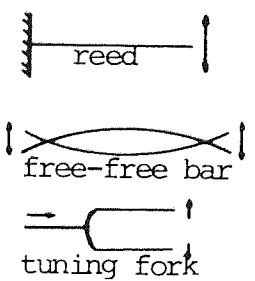

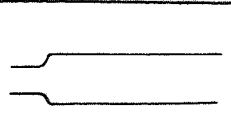
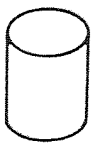
An electronic instrument to measure the decay rate of vibrations was developed and used to measure the mechanical losses of resonators such as the rectangular bar, piston rings and tuning forks. The principle of the instrument is to observe the exponential decay of the vibration when the driving force is removed (see Chapter 3). The basic operating technique adopted for the transducer is thus that of the frequency domain, as described in Chapter 1. Table 2.1 shows a number of typical systems for steady-state vibration and gives some idea of the universality of the phenomenon.

2.2 PHENOMENOLOGICAL APPROACH TO Q AND LOSS FACTORS

If a solid specimen is made to vibrate and the excitation source removed, the vibrations then present are termed 'free vibrations' since they are present without the continuing external stimulus and occur at the natural frequency of the specimen. In any real solid these free vibrations die away with time because of the presence of various mechanisms of energy dissipation e.g. presence of a crack, an elasticity or dislocation movements in the micro-crystals of the material and acoustic

TABLE 2.1

A Number of Typical Systems for Steady State Vibration

Resonator	Energy Types	Schematic Diagram	Remarks
Simple Pendulum	Kinetic Gravity Potential		In clocks accurate time-keeping depends on the feature of resonance that the period is independent of amplitude.
Mass on Spring	Kinetic Mechanical Stress		A circular form is the balance wheel movement of a watch.
Electrical Inductance and Capacitance	Magnetic and Electrical Fields		Selective tuned circuit used in radio reception.
Helmholtz Bottle	Gas Kinetic Compression		Beer bottle type musical instrument.
Diatomic Molecule	Atomic Kinetic Bond Strain		One of the infinity of molecular resonances. Can be analysed by mechanical or quantum methods.
Flexure of Beams and Bars	Kinetic Strain		Usually classified according to boundary conditions, free, clamped or simply supported.
Electrical Transmission Line	Electromagnetic Field		Analysed in terms of two waves travelling in opposite directions.
Acoustic Transmission Line	Kinetic Pressure		The upper represents two parallel wires, the lower an organ pipe.
Cylindrical Resonator	Electromagnetic Mechanical Kinetic-pressure or Stress		As a cavity electro-magnetic and acoustic properties are completely analysible. In the case of a solid only partial solutions have been obtained.

radiation, Norwick (1953), Bickford (1973), Zener (1943) and Lazon (1964). Considering the solid body to be isolated so that dissipation due to support conditions, radiation of sound into the surrounding medium can be neglected, the dissipation mechanisms inherent to the solid material collectively produce what is referred to as internal friction (which is the inverse of the quality factor Q). The instrument developed measures internal friction, the greater the decrement, the higher the internal friction, some of which is associated with the parameter being tested. The Q may be understood by considering an electrical resonator (RLC circuit) or an idealised mechanical vibrator with a single degree of freedom. Such a system, as shown in Fig. 2.1 consists of a spring of stiffness K , viscous damping $R_m \dot{x}$ and a mass, M , represents the material. In the case of a bar or a piston ring the components are distributed but can nevertheless be represented by this lumped component model.

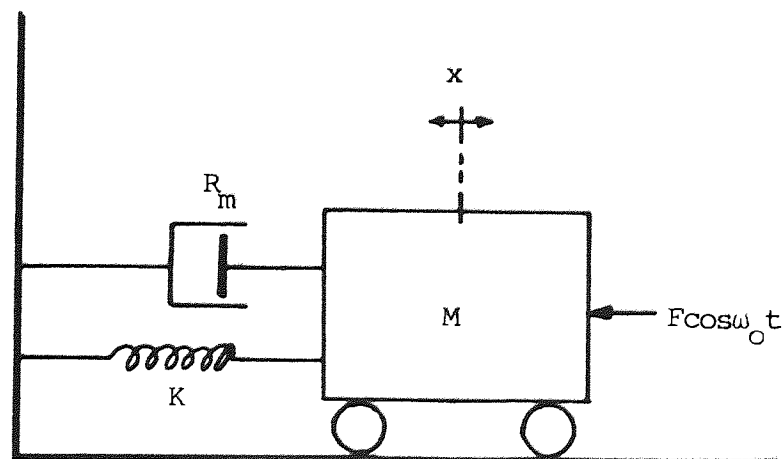


Fig. 2.1 An idealised mechanical system with mass, spring and damping.

The equation of motion for the system is given by

$$M\ddot{X} + R_m\dot{X} + KX = F \cos\omega_0 t \quad (2.1)$$

In the absence of the driving force $F\cos\omega t$ the motion is governed by equation (2.2)

$$M\ddot{X} + R_m\dot{X} + KX = 0 \quad (2.2)$$

when the decrement is low, the condition applicable throughout this work, the system vibrates at its natural frequency $\omega_0 = (K/M)^{\frac{1}{2}}$ and the general solution is given by equation (2.3)

$$X = A_0 \exp\left(-\frac{R_m t}{2M}\right) \sin(\omega_0 t + \phi) \quad (2.3)$$

A is the amplitude of vibration (A_0 at time $t = 0$) and it will decay exponentially with time by a term $\exp\left(-\frac{R_m t}{2M}\right)$ as shown in Fig. 2.2.

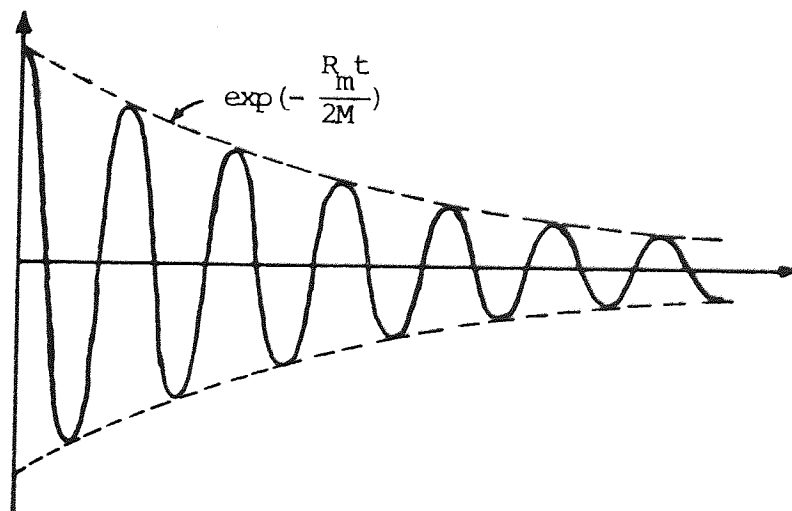


Fig. 2.2 Damped oscillatory motion. The amplitude decays with $\exp\left(-\frac{R_m t}{2M}\right)$.

After n vibrations the amplitude at time $t=t_n$ is given by

$$A_n = A_0 \exp\left(-\frac{R_m t_n}{2M}\right) \quad (2.4)$$

and the decay of energy is given by

$$E_n = E_0 \exp\left(-\frac{R_m t_n}{M}\right) \quad (2.5)$$

The Q factor which can be defined in both mechanical and electrical terms as

$$Q = 2\pi \frac{\text{energy stored}}{\text{energy lost per cycle}}$$

$$Q = 2\pi \frac{E_n}{-dE_n} = \frac{2\pi E_n}{R_m E_n T/M} = \frac{\omega M}{R_m} \quad (2.6)$$

where $-dE_n = R_m E_n T/M$ is the energy lost per cycle of period T .

Equation (2.6) relates R_m of equation (2.2) to Q .

It follows that

$$E_n = E_0 \exp\left(-\frac{\omega t_n}{Q}\right) = E_0 \exp\left(-\frac{2\pi n}{Q}\right) \quad (2.7)$$

where n is the number of oscillations.

In equation (2.7) the time and frequency terms have been eliminated, and Q is expressed in terms of amplitude and the number of oscillations as

$$A_n = A_0 \exp\left(-\frac{\pi n}{Q}\right) \quad (2.8)$$

This equation is the basis of the instrument developed.

The Q-factor can also be measured by bandwidth (Δf) which is the frequency difference between the half power points, but this method is inaccurate for the low decrement, sharply tuned resonators of this work.

It is worthwhile evaluating the bandwidth in terms of Q by considering an electrical resonator as shown in Fig. 2.3 in the series and parallel model forms. It can be readily shown that the Q-factor is given by $(\frac{\omega l}{r})$ and $(R/\omega l)$ for the series and parallel models respectively.

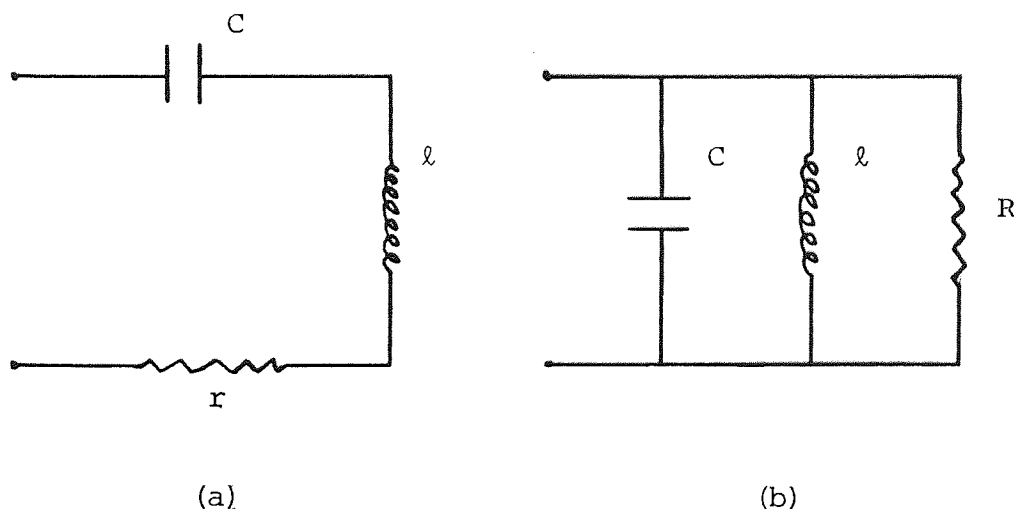


Fig. 2.3 R.L.C. Electric circuit capable of damped simple harmonic vibrations.
(a) in series, (b) in parallel.

Equation (2.9) gives the bandwidth

$$\Delta f = \frac{f_0}{Q} \tag{2.9}$$

Three particular resonators which have been widely used in this work are described below.

2.3 RECTANGULAR BAR RESONATOR

The flexural vibration of the bar is the most important kind of vibration for this work. To analyse the flexural vibration of the bar it is normally assumed that the vibrating bar is straight of uniform cross-section and density and symmetrical about a central plane. It is also assumed that the geometry is such (thickness \ll length) that rotational effects are negligible. With these initial conditions the equation of motion is given by Morse (1948)

$$\frac{\partial^4 y}{\partial x^4} = - \frac{\rho}{EK^2} \cdot \frac{\partial^2 y}{\partial t^2} \quad (2.10)$$

where

E is Young's modulus

ρ is the density of the bar

K is the radius of gyration for a bar of rectangular

cross-section. This is $\frac{b}{\sqrt{12}}$, where b is its thickness.

For a circular rod of radius a, $K = \frac{a}{2}$.

The solution for the equation of motion depends on the pair of boundary conditions at the ends of the bar. The particular forms of these conditions depend on the nature of the support and include:

(a) Clamped End

If the end of the bar is rigidly clamped both the displacement and the slope must be zero at the end at all times. The boundary conditions are therefore

$$y = 0 \quad \text{and} \quad \frac{\partial y}{\partial x} = 0$$

(b) Free End

At a free end there can be neither an externally applied torque nor a shearing force, and hence the bending moment and the shear force are zero in a plane located at an infinitesimal distance from the end. This means that the displacement and the slope must have finite values. The boundary conditions are

$$y \neq 0, \quad \frac{\partial y}{\partial x} \neq 0$$

$$\frac{\partial^2 y}{\partial x^2} = 0 \quad \text{and} \quad \frac{\partial^3 y}{\partial x^3} = 0$$

(c) Simply Supported

A rigid knife-edge support of the bar, prevents displacement, but the slope may have any small value. The curvature is equal to zero. Therefore the boundary conditions are:

$$y = 0, \quad \frac{\partial y}{\partial x} \neq 0 \quad \text{and} \quad \frac{\partial^2 y}{\partial x^2} = 0.$$

2.3.1 Clamped-Free Bar

The allowed frequencies for a bar of length L are given by Morse

$$f_n = \frac{\pi}{2} \cdot \frac{K}{L^2} C_o B_n^2 \quad (2.11)$$

where

C_o is the velocity of waves in the bar (rod velocity) and it is equal to $\sqrt{\frac{E}{\rho}}$

B_n is a factor determining the overtones, the values are given as $B_1 = 0.597$, $B_2 = 1.494$, $B_3 = 2.500$.

n is the mode order.

Shapes of the first three characteristic functions for a vibrating bar clamped at one end are shown in Fig. 2.4. This mode is of particular significance to the work undertaken.

2.3.2 Free-Free and Clamped-Clamped Bar

The frequencies are the same in both cases and are given by Equation (2.11). The symbols have the same meaning as before except B_n takes the values $B_1 = 1.506$, $B_2 = 2.499$.

It is apparent that B_n is practically equal to $(n+\frac{1}{2})$, where n is the mode order. Forms of characteristic functions for a vibrating bar free at both ends are shown

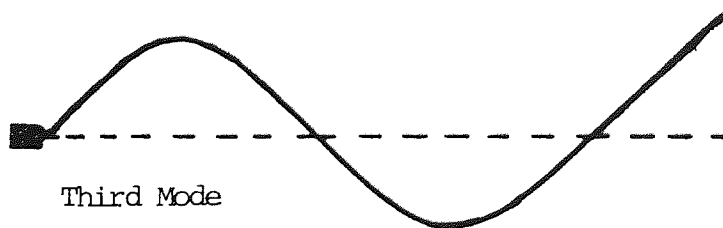
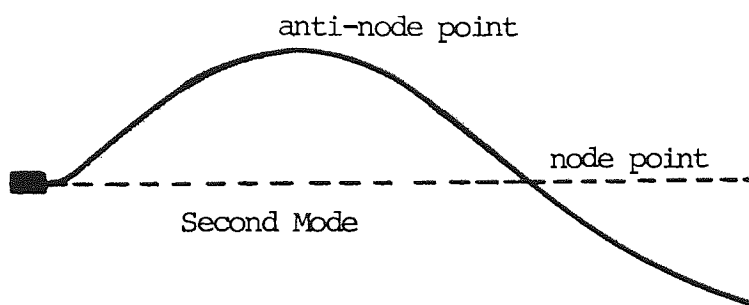
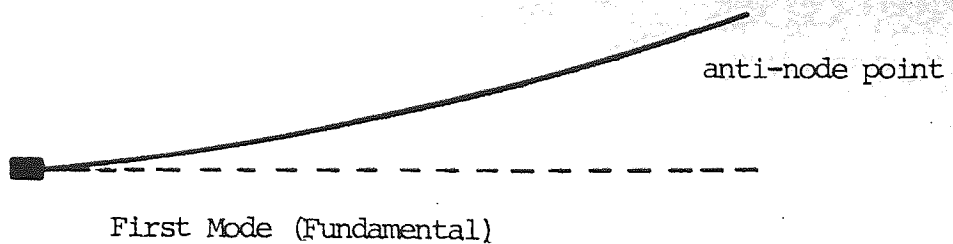


Fig. 2.4 Shapes of the first three characteristic functions for a clamped-free bar. It will be noted that the nodes are points of inflexion and that the curvature at the free end is zero. The free end is stress free and the clamp a region of maximum curvature and hence maximum stress.

in Fig. 2.5.

It was found that these formulae gave quite good agreement with the experiments but lacked complete precision because rotation is not quite insignificant.

2.4 TUNING FORK RESONATOR

2.4.1 Introduction

Resonators of this kind are used as measuring transducers where the parameters are fluid pressure, density, temperature and viscosity. Fig. 2.6 shows various designs of transducers; Fig. 2.6(a) is a liquid density transducer and 2.6(b) a liquid viscosity transducer. Each design consists of a pair of two rectangular bars clamped together at one end. Considering this structure and the flexural mode of vibration they can be regarded as double clamped-free resonators.

In the literature the most familiar double resonator is the tuning fork. The fork was invented by Shore and used by K \ddot{o} nig to establish the relationship of frequency to pitch. Chladni regarded the tuning fork as evolving from a free-free bar by bending it in the form of an elongated U. The effect of bending the bar is to cause the two nodes of the fundamental mode of vibration to move towards one another and lower the frequency of vibration. The amplitude of vibration at the antinodal mid-point of

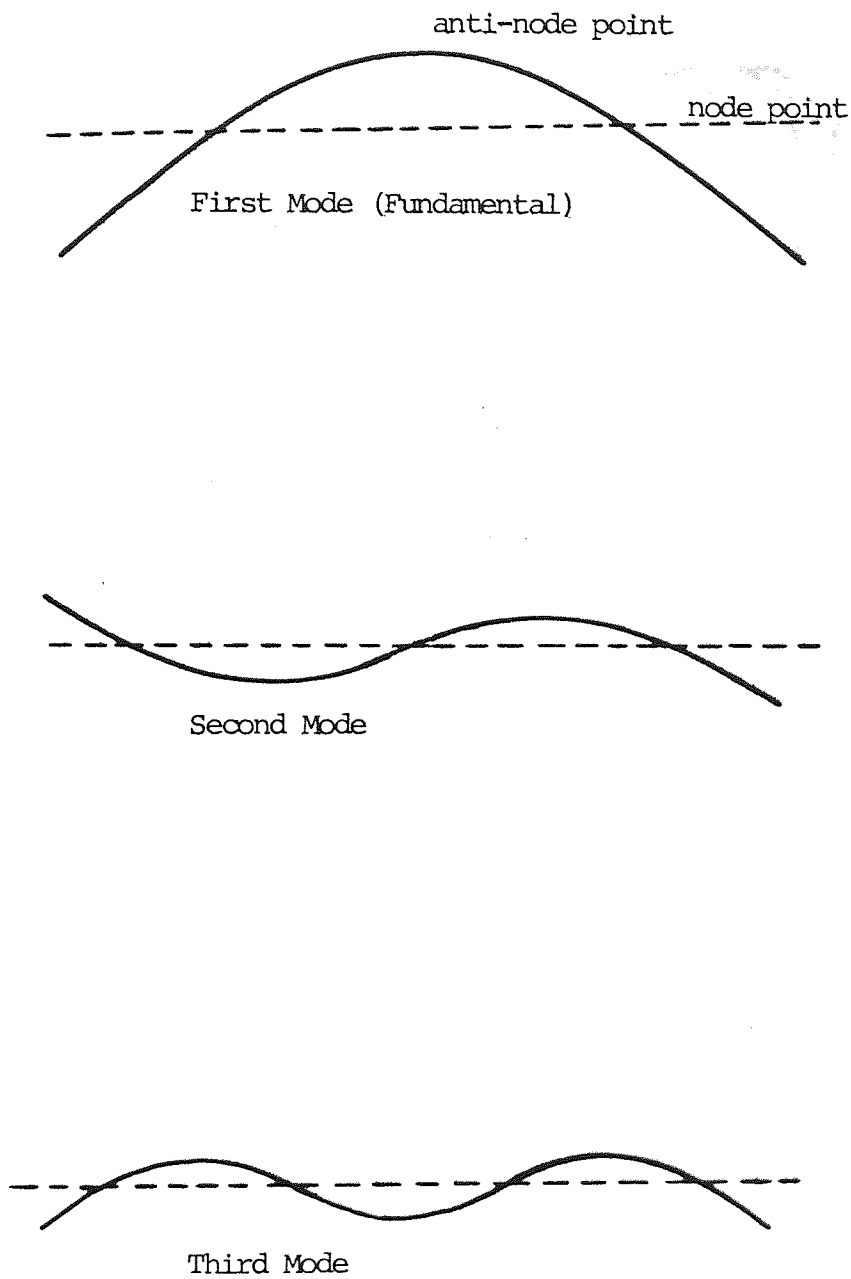
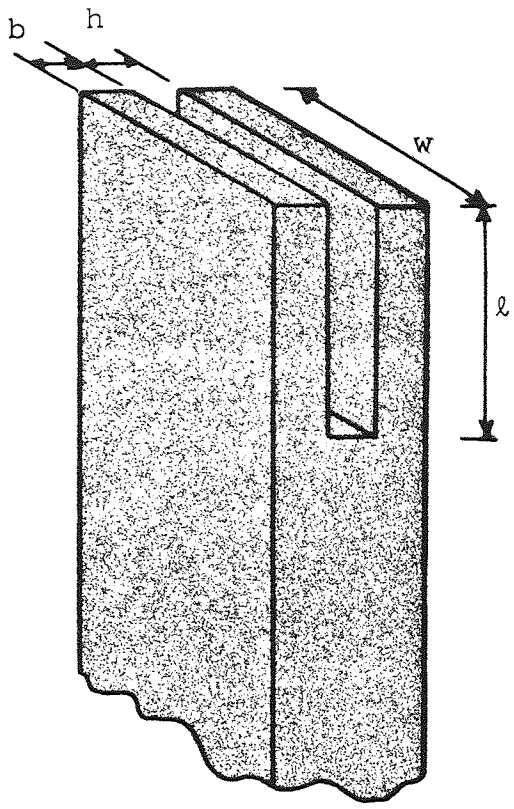
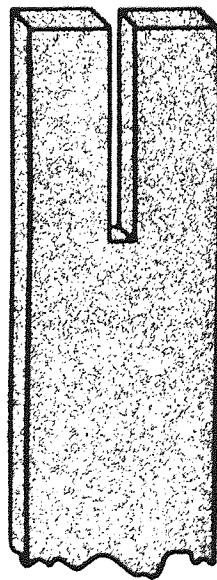
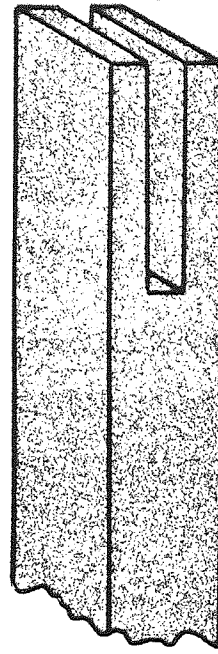


Fig. 2.5 Shapes of the first three characteristic functions for a Free-Free bar. It is of interest that compared with longitudinal resonances each mode has an extra node.



(a)



(b)

l = length of the tines

w = width of the tines

b = thickness of the tines

h = gap between the tines

Fig. 2.6 A general view of the transducer.

(a) a liquid density transducer

(b) a liquid viscosity transducer

the bend will be small but significant compared with that of the ends of the bar. Lord Rayleigh (1894) who was primarily concerned with frequency and described the tuning fork as an instrument indispensable to the acoustic investigator, favoured the clamped-free bar model.

Stephens and Bate (1966) described the tuning fork as "it is preferable to regard each tine as being equivalent to a straight bar fixed at the stem end but free at the other end". While Morse (1948) considered a tuning fork to be two vibrating bars both clamped at their lower ends.

Whatever the model considered, both bars are coupled together and vibrate in antiphase providing a mutual support. This fulfils the condition that the momentum must be conserved. In a single clamped-free bar the forces at the clamp meet this requirement.

Therefore, by considering the tuning fork as two bars clamped at one end and free at the other end, the allowed frequency is given by equation (2.11) as

$$f_n = \frac{\pi}{2} \frac{K}{\ell} C_0 B_n^2$$

where ℓ is the length of the tine

K is the radius of gyration which is equal to $b/\sqrt{12}$

b the thickness of the tine

B_n is the factor determining the overtones and it takes the values $B_1=0.597$, $B_2=1.494$, and $B_3 = 2.500$.

The first overtone of the fork is higher than the fundamental by a ratio of $(\frac{B_2}{B_1})^2$, approximately 6.3. This feature gives a valuable isolation of the fundamental which is not common to other resonators. Kalmarczie (1976) showed that in practice the value of l should be increased by about $b/2$.

2.4.2 Some Applications of the Tuning Fork

Besides the long musical history of the tuning fork, it has a variety of other applications. Lord Rayleigh used an electrically maintained one to measure temperature. They were widely used as frequency standards (James, (1961)). Other typical applications are in time and frequency measuring devices, Max (1963) and Reefman (1964) and fixed frequency filters, Wulfsberg (1950) and Holt (1960). Recently tuning forks have been used to measure the viscosity of the biological fluids, Berger (1978), and the density and pressure of liquids and gasses, Hassan (1980). A special design of the double resonator shown in Fig. 2.7, which may be taken as a type of tuning fork used successfully to develop ultrasonic thermometers, Bell (1971), Seth (1974) and Fathimani (1976).

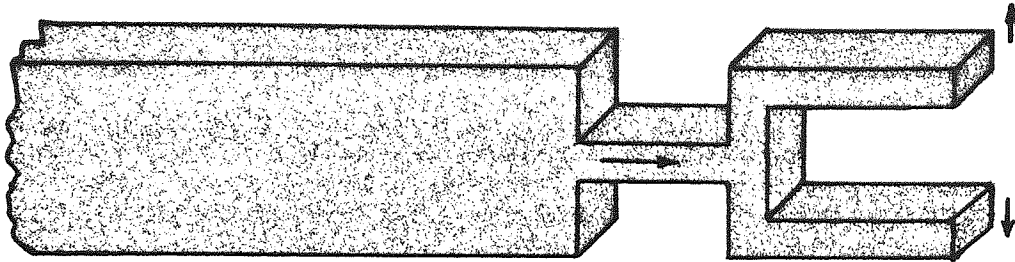


Fig. 2.7 A double resonator used for ultrasonic thermometry.

2.5 SPLIT RING RESONATOR

The vibrations of a split ring can be classified in a similar way to those of the complete ring. They are of three kinds, extensional, flexural out of plane and flexural in plane. In the case of extensional vibrations, the ring remains in its own plane being alternately stretched and contracted, while in the case of out of plane the vibrations perpendicular to the plane of the ring. The inplane vibration is the most important for this work where the split ring clamped firmly at the centre as shown in Fig. 2.8. The resonator will behave as two vibrating curved bars both clamped at one end,

because of the heavy solid clamp at the centre of the split ring. Therefore, it is possible to regard a solidly clamped split ring at the centre as a tuning fork. The centre clamp will, of course, inhibit certain modes, such as centre one in Fig. 2.9.

Some measurements of the low order free tuning fork modes were carried out on large (3" diameter) low frequency forks and small ($\frac{3}{8}$ " diameter) high frequency forks. The modes were classified (shown in Fig. 2.9) as f_0 the 'fundamental' mode with two nodes, f_1 with three nodes and f_2 with four nodes. The results are shown in Tables 2.2 and 2.3.

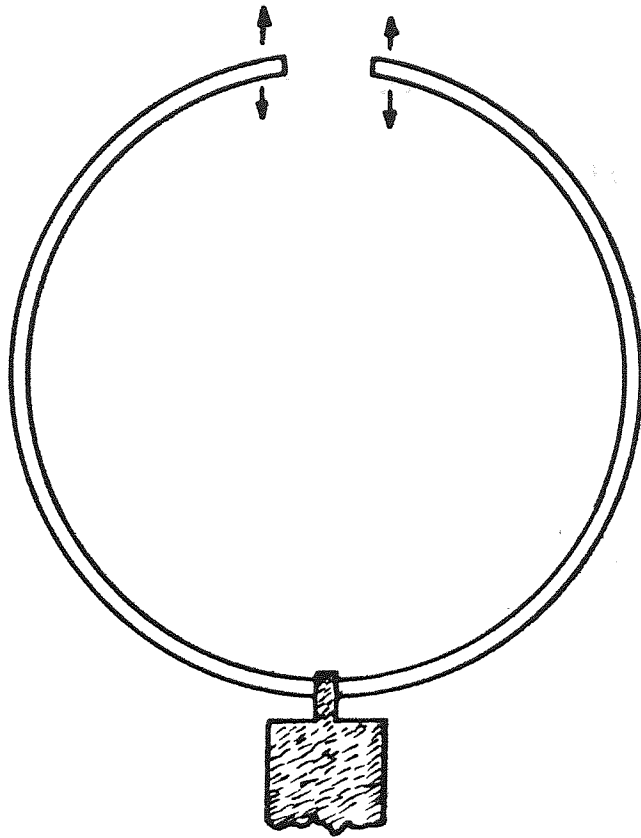


Fig. 2.8 A piston ring clamped solidly at the centre.

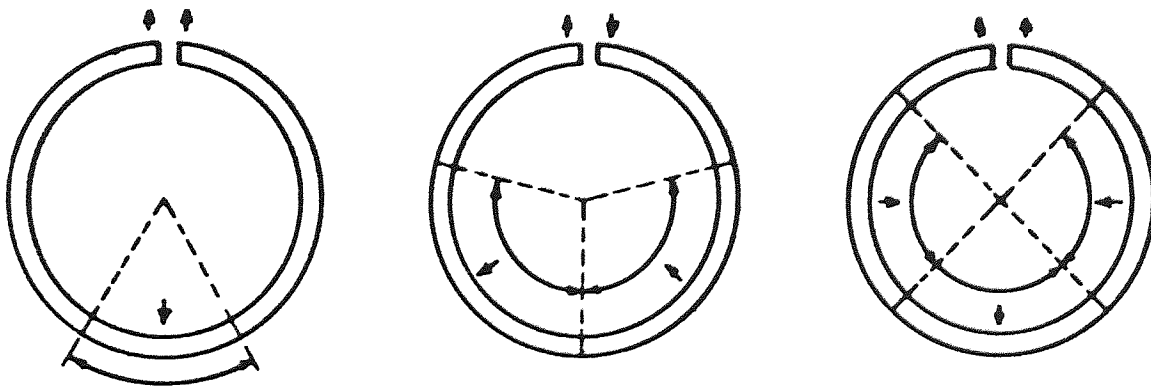


Fig. 2.9 The first three modes as classified experimentally for a free split ring. It will be noted that in the second mode, the centre has the properties of a simple support rather than a clamp.

TABLE 2.2

The Results of the Large Tuning Fork (KHz)

OD	ID	THICKNESS	f_o	f_1	f_2
3	5/4	1/4	2.994	-	2.15
3	3/2	1/4	2.370	-	2.14
3	7/4	1/4	1.783	8.313	2.18

TABLE 2.3

The Results of the Small Tuning Fork (KHz)
(frequency must be greater than 30 KHz)

OD	ID	THICKNESS	f_2
3/4	5/16	1/8	53.9
5/8	1/4	1/8	67.4
1/2	3/16	3/32	86.1

OD - outer diameter (inch)

ID - internal diameter (inch)

CHAPTER 3

THE TESTING AND EVALUATING OF COMPONENTS AND MATERIALS BY MECHANICAL RESONANCE

3.1 INTRODUCTION

In this chapter the main experimental results of developing a nondestructive technique for crack detection in metals and testing adhesive bonds will be presented.

These are concerned with the frequency characteristics of samples of various geometry such as rectangular plates containing artificial defects. The study of coating on bars involved measuring the decrement of oscillations giving the quality factor of each particular resonance. Inferior or defective coatings are expected to have a high decrement. In both cases the flexural mode was used.

It was found that there was an additional external damping arising from constraints placed on the specimen by the support system and also by the measuring devices. To obtain meaningful values for the internal damping of a material, the supports must be located as near as possible to the nodes. Expanded polystyrene, because of its lightness, was very suitable especially when cut to a wedge form.

The nodes in these flexural vibrations are points of inflection and hence the supports must occupy as small an area as possible. The supports used gave comparable performance to that of Mason (1970) and Wachtman (1958) who used fine threads. (Fig. 3.1).

3.2 VIBRATION OF SIMPLE BARS CONTAINING DEFECTS

Following the experiments of Lloyd (1976) a series of mild steel rectangular bars ($4 \times 5/4 \times 1/8$ ") were used. A standard electromagnetic transducer was effective in exciting magnetic material by direct magnetic attraction and non-magnetic conducting material by the eddy current effect. The unit is equally efficient when used in the reciprocal manner to observe vibrations. The bars were free at both ends and supported as described above by small wedges of expanded polystyrene at two convenient nodes, usually those nearer to the free ends of the bar. This produces a close approximation to a free-free condition comparable in effectiveness to the Mason arrangement.

The vibrations were picked-up by an $1/8$ " diameter miniature microphone positioned as close as possible to the vibrating surface. Moving the microphone over the surface enabled the nodes to be identified. The signal is maximum at the anti-node and reaches a null at the node. By comparing the signal phase with that of the drive

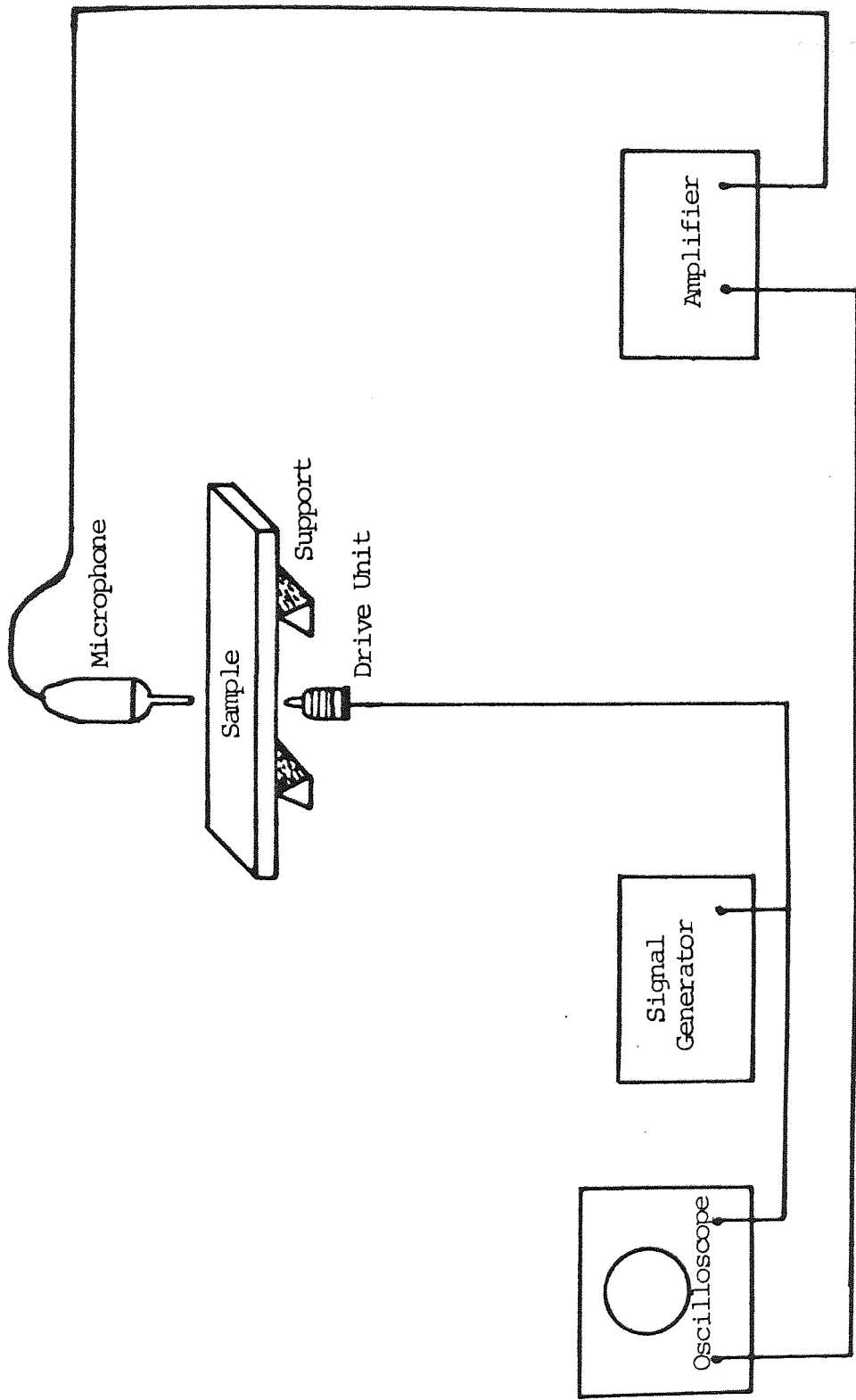


Fig. 3.1 Diagram showing the experimental set-up to observe the resonant frequency response. The drive and microphone positions are at the centre, an anti-node for odd order modes. They could not detect the even modes.

the nodal positions were obtained with high precision as, on crossing a nodal line the signal phase reverses. The anti-nodes are, of course, the best location for the drive and pick-up units. Fig. 3.1 shows a block diagram of the experimental arrangement to drive a sample into different modes and to observe the resonant frequency response of samples containing artificial defects.

Initial experiments were carried out on steel bars free at both ends and excited by electromagnetic transducers into different modes. The results are in surprisingly good agreement with the theoretical calculated values obtained using equation (2.11) are shown in Table 3.1 and Fig. 3.2. Large departures from the simple theory might be expected as the width to wavelength ratio is large, especially for the high order modes. Such departures are well known in the longitudinal vibrations of rods (Bancroft Correction) and bars (Rayleigh/Lamb Correction). In flexural vibrations the frequencies are low and lateral effects have sufficient time to be fully established, unlike the other two cases. This does not appear to have been reported previously. Some workers Leissa (1973) have used finite element technique to evaluate the phenomenon expected.

The experiment to observe the resonant frequency response of bars containing defects was performed using two identical steel specimens which were made in the

TABLE 3.1

Mode Order (n)	(f _n) Hz	f _n /f ₁ Theoretical	f _n /f ₁ Experimental	f _n /B _n ² Experimental
1	420	1	1	0.187
2	1157	2.778	2.752	0.187
3	2266	5.451	5.390	0.185
4	3741	9.002	8.900	0.185
5	5578	13.448	13.268	0.184

Comparison of experimental and theoretical results of (4" x 5/4" x 1/8") steel bar free at both ends. C₀ = 5457 metre per second. It is of interest that unlike longitudinal and torsional vibration in bars the number of nodes is not equal to the mode order but exceeds it by one.

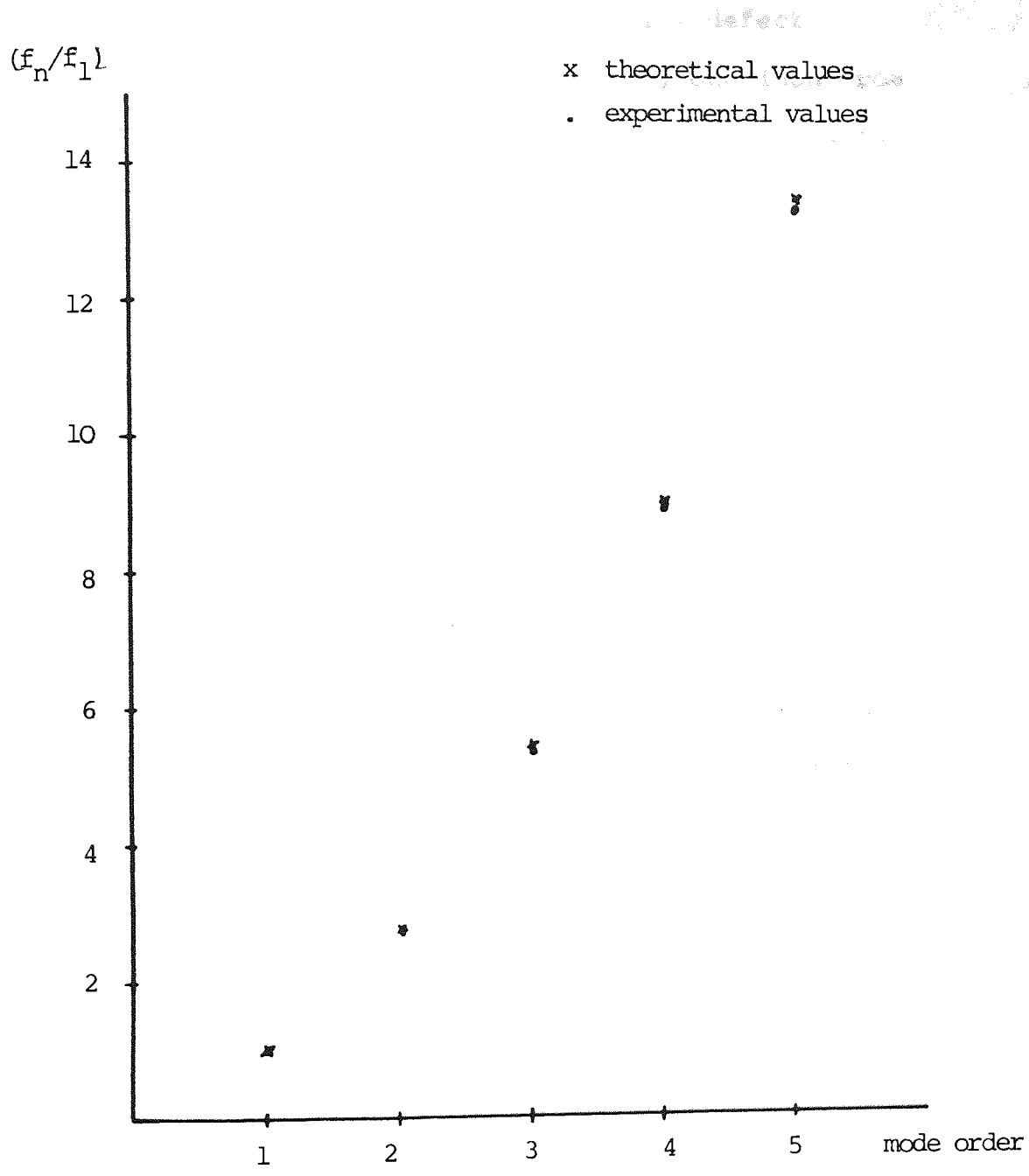


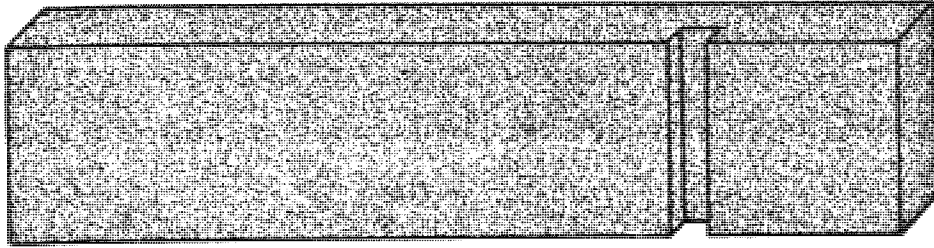
Fig. 3.2 Experimental and theoretical values of (f_n/f_1) versus n . It will be noted from Table 3.1 and the graph that the theoretical values are larger than the experimental. The reason being that, in solving the equation of motion of a bar vibrating in flexural, the rotary and lateral inertia were ignored.

standard (4"x1"x1/8") size. An artificial defect was machined in a section across the bar, one inch from the end in one case and at the middle in the second as shown in Fig. 3.3. The depth of the cut was varied in order to examine the effect upon the different modes of resonance frequency.

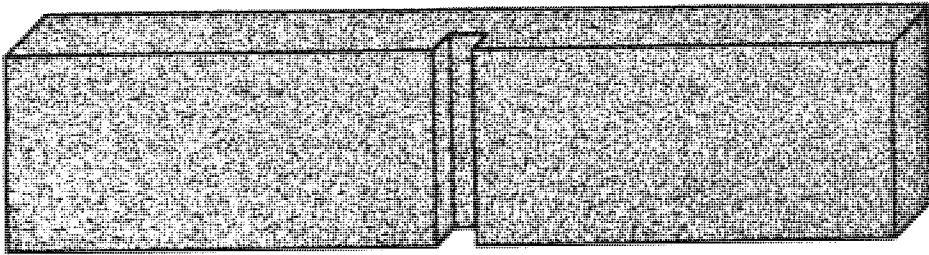
The result of the experiments show that the resonant frequency is quite sensitive to depth, and is strongly affected by the position of the cut. The decrease in resonant frequency increases rapidly with the depth of defect as shown in Figs. 3.4 and 3.5.

For the first bar, where the artificial defect was machined one inch from the end, the second mode of the resonance vibration showed the larger difference. The next most affected mode was the third and then the fundamental modes. The least affected mode was the fourth, the reason being that the cut is closest to the anti-nodal point for the second mode, while it is the least close for the fourth mode (where it is the closest to the nodal line). The closer the cut is to the anti-node (maximum stress) the more the frequency is affected.

Further experiments were carried out using the second bar, where the cut was arranged to coincide with nodal or anti-nodal lines, and the results are shown in Table 3.2. In these experiments the odd modes shows the larger effect while even modes are hardly effected by



(a)



(b)

Fig. 3.3 Steel bars of dimensions ($4" \times 1" \times 1/8"$).

(a) with cut $1/16"$ width at one inch from the end - a low stress point for the first mode.

(b) with cut $1/16"$ width at the middle of the bar where the stress is high for all odd modes and zero for even ones.

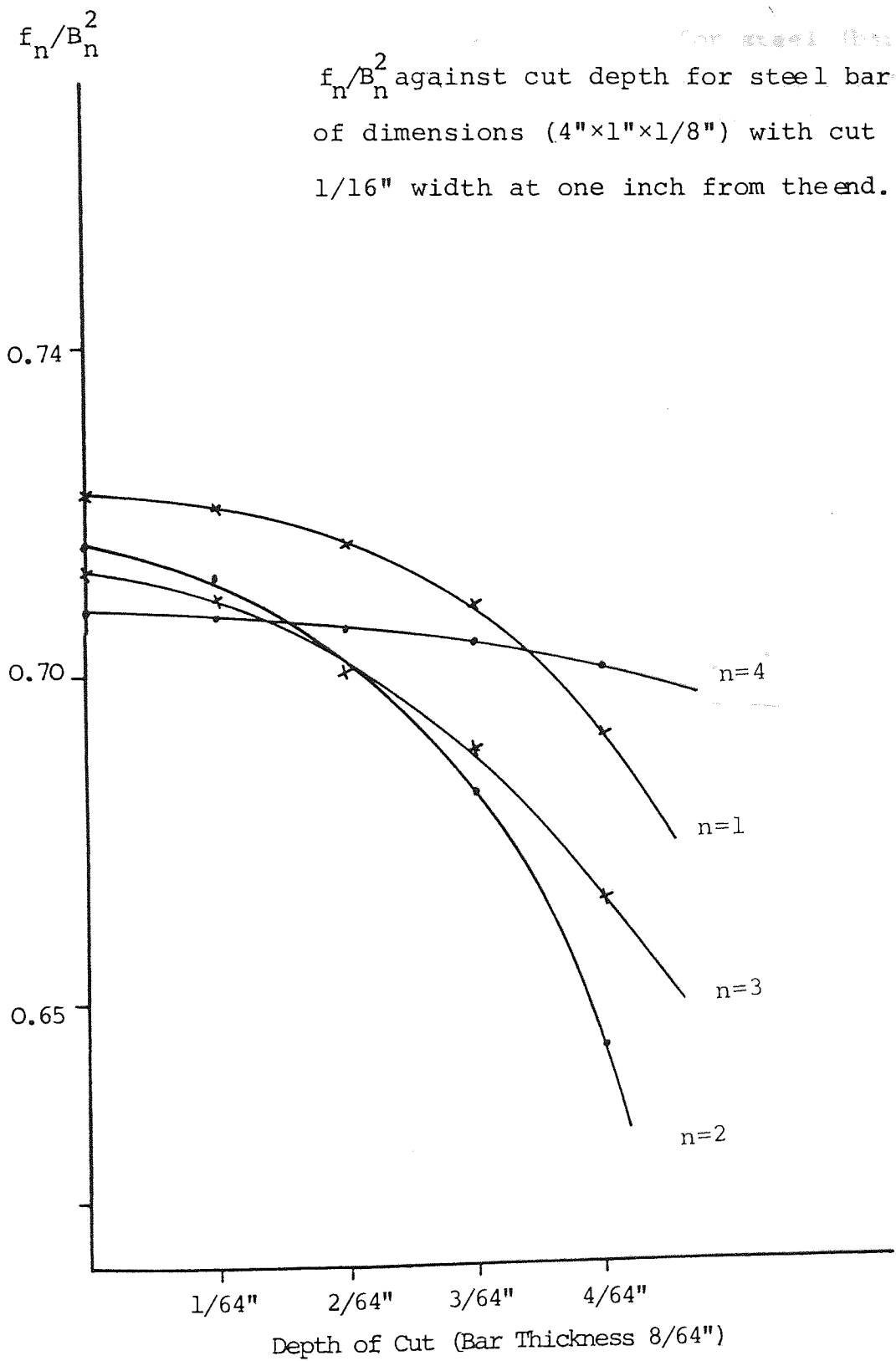


Fig. 3.4

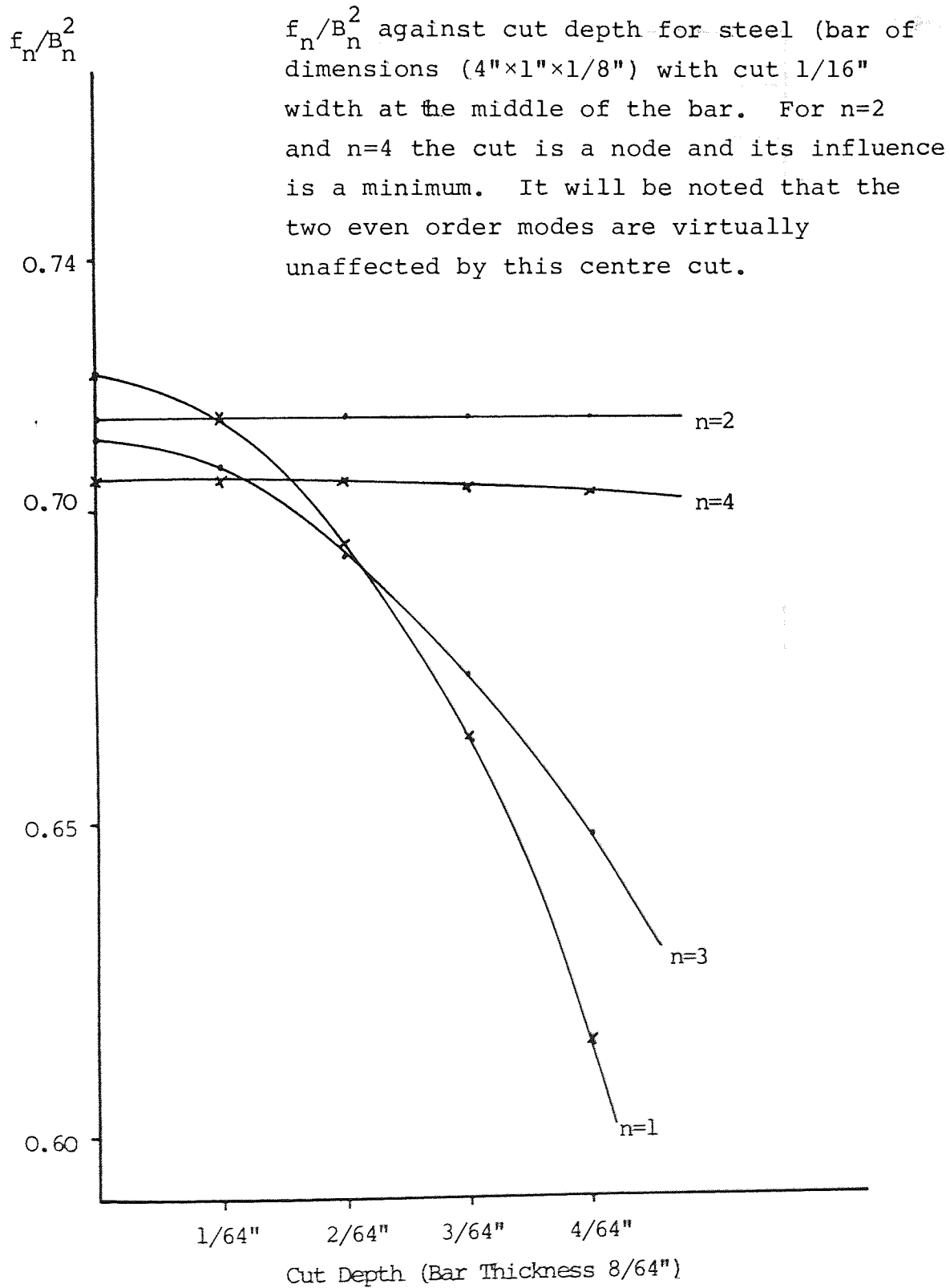


Fig. 3.5

TABLE 3.2

Cut Depth %	Drop of f_n/B_n^2 %			
	n=1	n=2	n=3	n=4
12.50	0.244	0.733	0.616	0.132
25.00	1.100	2.578	2.086	0.397
35.50	2.260	5.222	3.830	0.675
50.00	5.070	10.733	6.965	1.197

Steel bar of dimensions (4"x1"x1/8") with cut 1/16" width at one inch from the end.

Cut Depth %	Drop of f_n/B_n^2 %			
	n=1	n=2	n=3	n=4
12.50	1.046	0.022	0.620	0.021
25.00	3.815	0.045	2.558	0.098
35.50	8.123	0.090	5.243	0.154
50.00	14.892	0.157	8.960	0.343

Steel bar of dimensions (4"x1"x1/8") with cut 1/16" width at the middle of the bar.

the defect, as shown in Fig. 3.5. The reason being that the cut was at the anti-node position for the odd modes, while it was at the node position for the even modes.

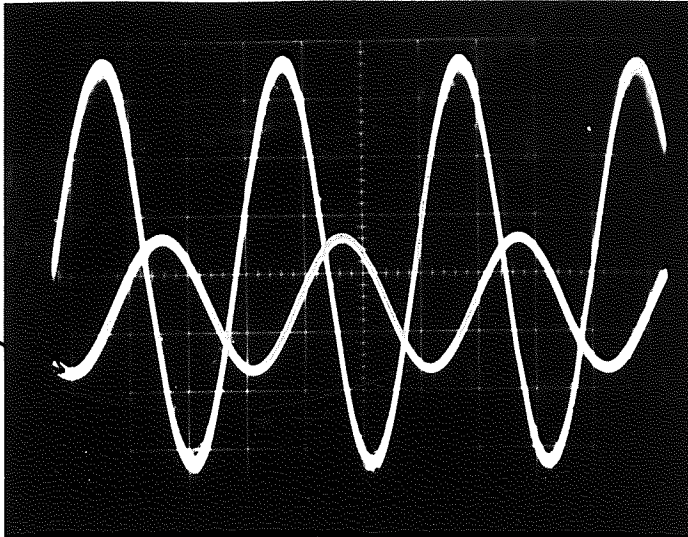
This technique was further applied to observe the spectrum response of samples containing small cracks. This is a better representation of a real situations where a local shear force can cause fretting between crack surfaces and thus generating crack noise.

The first experiment used a glass bar of dimensions (5"×1"×1/10") where a small crack had been induced at the middle. The bar was excited by the electromagnetic transducers, using as coupling a piece of shim steel (1 cm²) cemented at the middle.

The drive voltage was varied to observe the pick-up signal as a function of amplitude. When a small drive voltage was applied to excite the bar at its first mode there was a clear audible sinusoidal signal. It was detected by using 1/8" diameter microphone, as shown in Fig. 3.6(a). Rubbing between crack surfaces occurs above a critical drive voltage and crack noise was very apparent. The signal produced as shown in Fig. 3.6(b). The high harmonic component is the source of this noise.

Again the second mode was hardly affected by the crack even when a very large amplitude was applied, as shown in Fig. 3.6(c).

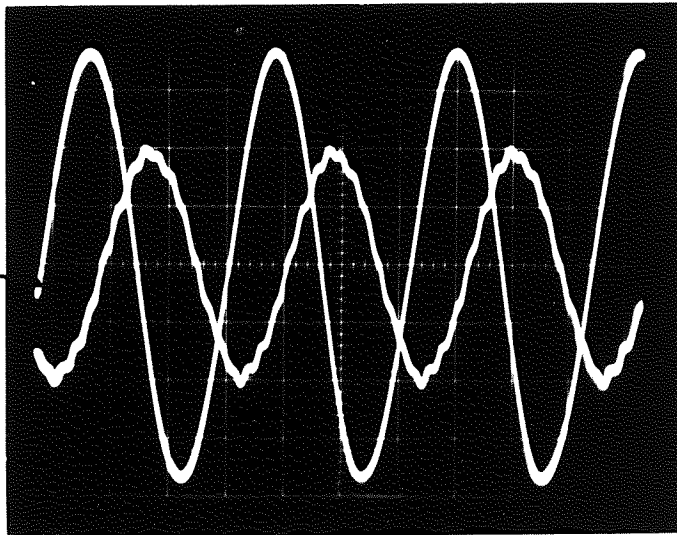
Drive
Signal



(a)

The bar vibrating at the fundamental, with a small drive signal. No crack noise is present in the pick-up signal.

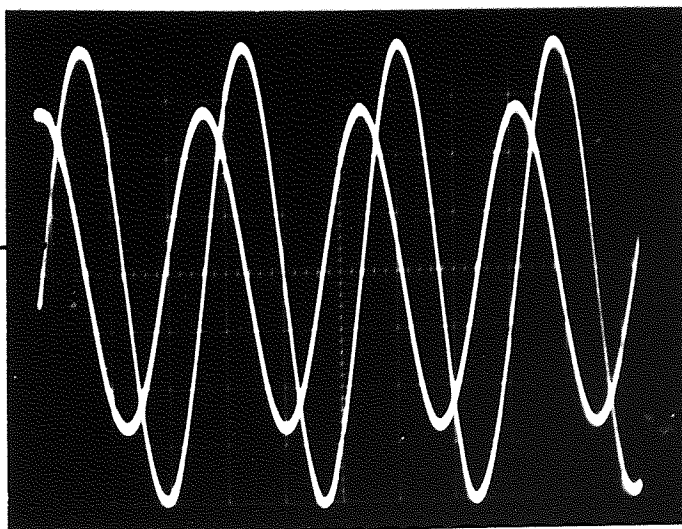
Drive
Signal



(b)

The bar vibrating at the fundamental, with a large drive signal. The crack noise component was evident in the pick-up signal.

Drive
Signal



(c)

The bar vibrating at the second mode, with a large drive signal. There is no crack noise component in the pick-up signal.

Fig. 3.6 A glass bar of dimensions (5"×1"×1/10").

The crack has been induced at the middle of the bar.

Further experiments were carried out on two more glass bars. The crack in the first bar almost coincided with a node (a zero stress region). No anomaly was observed when the bar was excited at the fundamental mode even with a large drive as shown in Fig. 3.7.

In the second bar the crack was located near the anti-node. The high frequency crack noise component was evident in the waveform when the bar was excited at the fundamental mode as shown in Fig. 3.8(a).

The bar was then excited in its second mode to the level where the crack noise developed as shown in Fig. 3.8(b). The noise was predominantly at the second harmonic of the drive frequency as this coincided with the third overtone of the bar. If it is assumed that the crack noise covers a wide spectrum, the bar will act as a selective filter and give an enhanced signal where a drive harmonic coincides with a bar resonance.

These results indicated that the modal frequency and the spectrum can be used as a nondestructive testing technique for surface opening cracks when the specimen is excited into different flexural modes.

In industrial applications where the specimen is not of simple geometry as a rectangular bar, it may be difficult to excite the specimen into different modes to improve the crack detection and to identify its position.

Drive
Signal

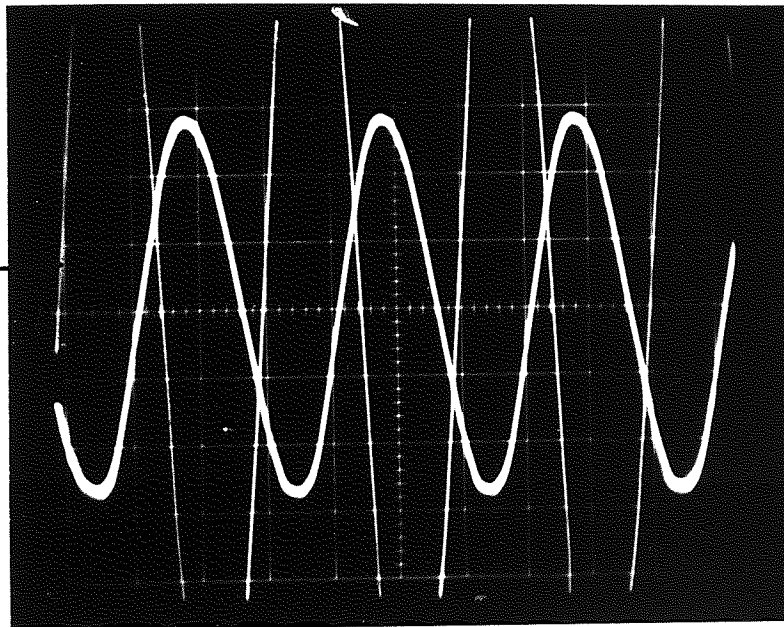
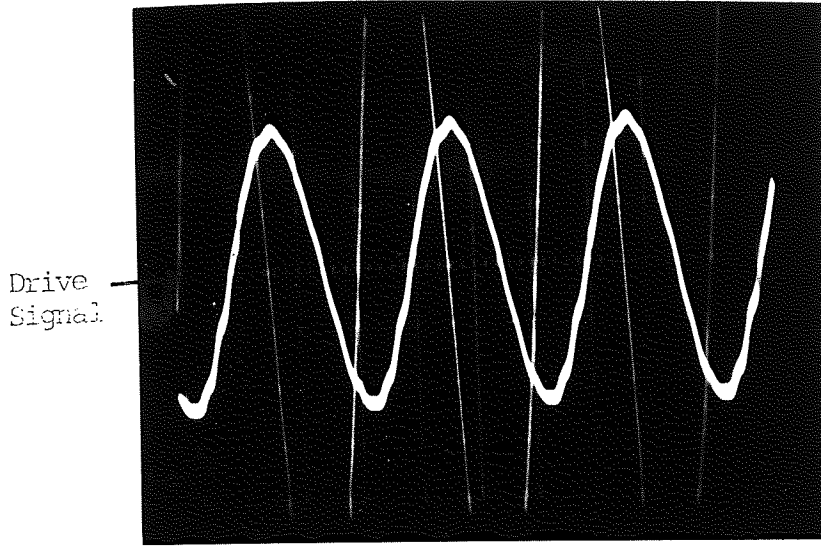
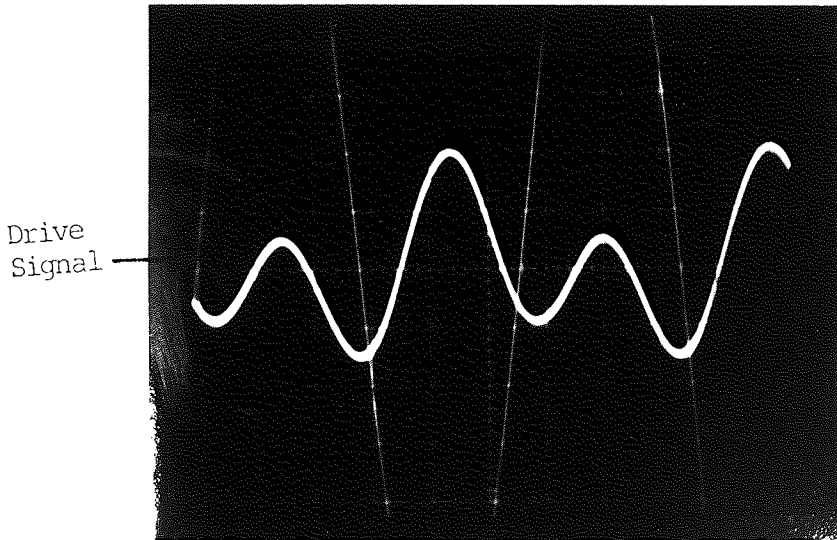


Fig. 3.7 The glass bar of dimension (5"×1"×1/10") vibrating at the fundamental mode. The crack was located at the node (zero stress). There is no crack noise in the pick-up signal even with very high amplitude drive.



(a)
The crack noise component was evident in the pick-up when the bar was excited at the fundamental mode.



(b)
The bar excited at the second mode. The crack noise that has been developed was predominantly at the second harmonic of the drive frequency.

Fig. 3.8 The glass bar of dimensions (5"×1"× $\frac{1}{8}$ " crack was located near the antinode.

A second vibrational technique, the measurement of the decay of oscillation (damping) gives an alternative technique to determine the integrity of the material. It offers an attractive numerical method of testing the strength of an adhesive bond. The development of the decrement meter used for this work is described in the next section.

3.3 DECREMENT Q-METER

3.3.1 Introduction

The measurement of the decay of oscillations or the internal friction (Q^{-1}) has been widely used in the study of the mechanical properties of materials. It is essentially a measure of energy dissipated internally within a vibrating specimen when mechanical energy is applied externally. The various methods that may be employed in the measurement of internal friction in solids are shown below:

- (a) Semi-static determination of the hysteresis loop in the stress curve during forced vibration. This method is suitable for evaluating the damping effects due to plastic deformations in the material.
- (b) Measurement of the energy input required to maintain a specimen in vibration of constant amplitude.

(c) Determination of the resonance curve during forced vibration (Bandwidth technique). In this technique the two frequencies are found at two half power points. The lower the internal friction of the specimen the sharper the resonance peak. The accuracy of this method falls off as the Q increase. As shown in

Chapter 2,

$$Q = \frac{f_r}{f_2 - f_1}$$

where

f_r is the resonant frequency

f_2 is the frequency higher than resonant frequency which has amplitude 0.707 that of resonant frequency (Half power points).

f_1 is the corresponding frequency on the other side.

(d) Measurement of the decay rate of vibration. In this technique the number of oscillations has been counted by an electronic instrument when the excitation source is removed and the vibrations are decaying freely at the natural frequency of the specimen. The accuracy of this method improves with increase in Q, while the bandwidth method is accurate for low Q.

3.3.2 Electronic Design

This section describes the electronic design developed for the measurement of the mechanical loss of resonator. The function of the electronic system is to count the number of oscillations of decaying amplitude which will be equal to the Q-factor of the material. The principle of the instrument is contained in Equation (2.8)

$$A_n = A_o \exp\left(-\frac{\pi}{Q} n\right)$$

where

A_o the initial amplitude

A_n the amplitude after a number of oscillations

n the number of oscillations

Q the Q-factor

It will be noted that both Q and Q^{-1} are dimensionless.

Numerically if A_o/A_n is equal to 23.14 then the Q-factor will be equal to the number of oscillations between these two levels of amplitude. The design is based on the measurement of this parameter.

The block diagram is shown in Fig. 3.9 and the circuit diagram and the waveforms at different points are given in Appendix A.

An essential component used in the design is the integrated circuit comparator. It has two inputs, the

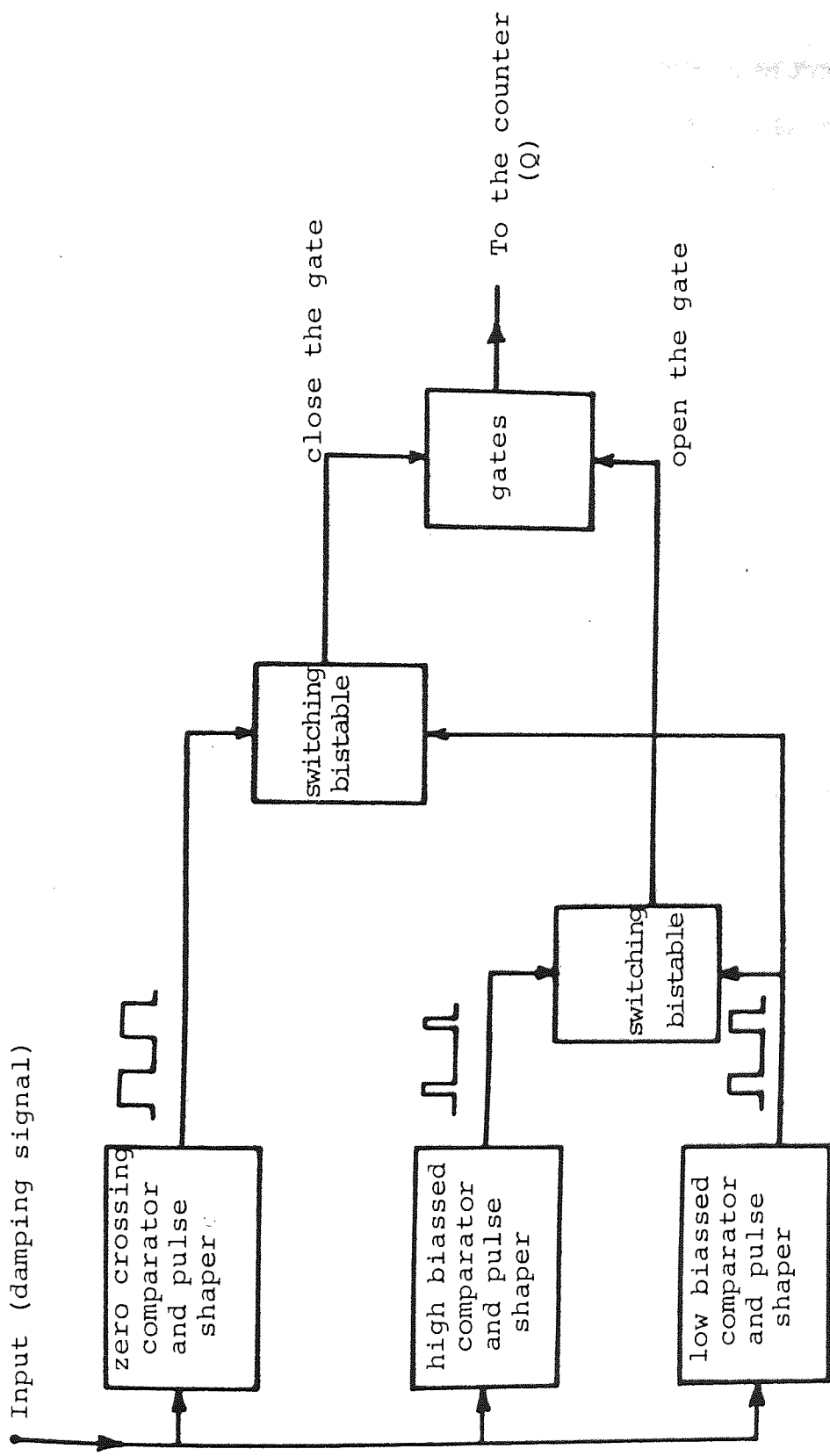


Fig. 3.9 Signal schematic diagram to give account of Q. The action of bistable (1) opens the gates, allowing the count to start and bistable (2) closes them, stopping the count.

analogue signal being applied to one and a reference voltage to the other. The output is (TTL) digital logic 1 or 0 depending on which input is the greater. The resolution is about 1 mV thus if the reference voltage is zero, a sinusoidal signal is converted to an equal mark space ratio TTL square wave. With a reference bias there is only an output when the signal exceeds the bias.

In this design the decrement signal drives three comparators. The first comparator acting as a zero crossing detector, while the second and the third comparators have high and low bias voltage respectively. These two comparators produce an output only when the amplitude of the input voltage exceeds predetermined reference levels.

3.3.2.(a) Zero Crossing Comparator

An integrated circuit voltage comparator type LM 306 giving a TTL compatible pulse output, is used to detect the zero crossing of the (analogue) decrement very accurately. The decrement signal drives the comparator which is unbiased and therefore is acting as a zero crossing detector which produces square waves.

3.3.2.(b) Decrement Comparator

This is also an integrated circuit voltage comparator type LM 306. The decrement signal drives the comparator

and the bias voltage was adjusted to identify the level of amplitude where the comparator was ceased working. Two comparators were used in the design. The first one has a high bias voltage, while the second has a low bias voltage. The ratio of the two bias voltages were adjusted to have a value 23.14.

The output of these comparators interface to TTL digital devices. The three comparator outputs were applied to three separate monostables type 74123 to produce a well defined short duration trigger pulse starting at a positive going edge.

3.3.2.(c) The Switching Bistable

Two JK flip flops with preset and clear facilities (type 7476) were used. The output of the first Flip Flop opened the gate. Since this output is going to a high logic level when the high comparator stops working the second Flip Flop closed the gate with a low logic level when the low amplitude comparator stops working.

3.4 EVALUATING THE DESIGN

In order to examine the design many experiments were performed using a range of resonator types with a wide range of Q-factor. The quality of these resonators which have been measured by the Q-meter compared with that

measured by a bandwidth technique.

An electromagnetic transducer was used to excite tuning forks and rectangular bars at the fundamental mode. The vibrations were picked up by an $\frac{1}{8}$ " diameter microphone positioned very close to the vibrating surface.

The resonance was found by displaying the drive and pick up signals on the two beams of an oscilloscope. As before the nodes were identified by comparing the signal phase with the drive when the microphone was moving over the vibrating surface.

The rectangular bar was supported at two convenient nodes by small wedges of expanded polystyrene, while the tuning fork was solidly clamped at the stem. Fig. 3.10 illustrates the system.

The pick-up signal is fed to the Q-meter and the Q measured by counting the number of pulses between the defined amplitude levels.

To examine the spread associated with the design and which is primarily associated with the uncertainty of the Trigger levels in the comparators experiments were carried out on different resonators. The results are shown in Table 3.3. Further experiments were carried out on aluminium rectangular bars of dimensions ($4" \times 1" \times \frac{1}{8}"$) free at both ends with different thicknesses and of a variety

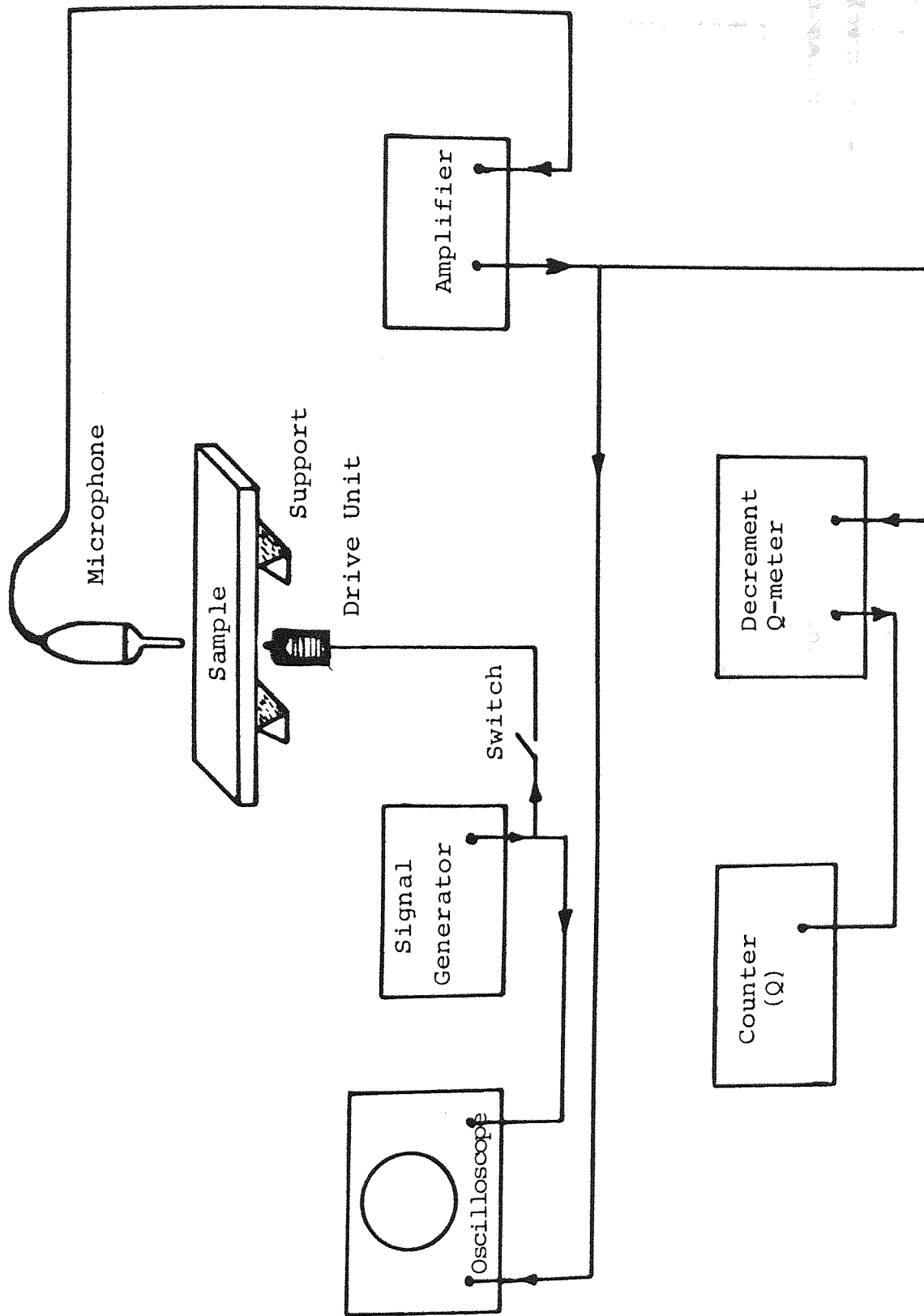


Fig. 3.10 Diagram showing the experimental set up to measure the decay rate of oscillation.

TABLE 3.3

Type of Resonator	Frequency Hz	Q	Number of Reading	Average Q	Standard Error
Steel Bar	774.7	3800, 3798, 3802, 3772, 3772, 3788, 3808, 3788, 3778, 3776, 3796	12	3790	0.34%
Steel Bar	4112.7	3088, 3098, 3068, 3076, 3054, 3092, 3066, 3046, 3034, 3058, 3058, 3038	12	3065	0.67%
Steel Bar	761.5	4558, 4558, 4556, 4556, 4562, 4566, 4584, 4558, 4560, 4558,	10	4561	0.19%
Tuning Fork	2784.1	730, 736, 738, 732, 728, 732, 730, 734, 730, 724, 736, 738	12	732	0.58%
Tuning Fork	2159.98	5326, 5318, 5316, 5336, 5332, 5338, 5346, 5344, 5330, 5330, 5330, 5318, 5320	12	5329	0.19%
Tuning Fork	5609.6	3120, 3124, 3082, 3098, 3088, 3106, 3094, 3100, 3082, 3094, 3084, 3090	12	3096	0.45%

Experimental results of measuring the Q by counting the number of oscillations between two levels of amplitudes for different resonators. It will be noted that the accuracy of the instrument is better than 1% for a wide range of Q.

of coatings. The Q was measured by the Q factor and a bandwidth technique.. The results in Table 3.4 show a good agreement between the two methods. The accuracy of the instrument is better than 1% for a wide range of Q.

3.5 EXPERIMENTAL RESULTS

Having established the basic effectiveness of the design, it was decided to examine its capability to test adhesive bonds, the influence of coating thickness and the effects of temperature on the quality factor of the resonator. These topics are of current local interest.

3.5.1 Testing Adhesive Bonds

The work described here again used the standard rectangular steel bars of dimensions (4"x1"x $\frac{1}{8}$ ") sprayed with nickel. Two sets of bars were sprayed, one set was considered to have a good adhesive bond, while the other was classified as bad.

The bars were excited at the fundamental mode as in previous experiments. The Q of each bar was measured and the results showed that it was possible to identify a good and a bad adhesive bond by the difference.- A good bar having a high Q and an inferior one a low Q. The results are shown in Table 3.5.

TABLE 3.4

Number	Frequency	$Q_D \times 10^3$	$Q_B \times 10^3$
1	1665.4	1.7	1.7
2	1666.1	1.99	1.9
3	1666.8	1.9	1.85
4	1689.3	1.24	1.21
5	1690.9	2.1	1.9
6	1718.5	1.03	1.01
7	1757.2	1.82	1.80
8	1778.2	1.80	1.80
9	1820.2	0.79	0.79
10	1891.5	0.69	0.69

Comparison of (Q_D) measured by the decrement Q-meter and (Q_B) measured by a bandwidth technique for Aluminium rectangular bars of different thickness.

TABLE 3.5

Good Sprayed Bar	Frequency (f_r) Hz	$Q \times 10^3$
Reference	1636	6.09
1	1664	4.10
2	1662	3.38
3	1663	3.58
4	1664	3.43
5	1663	3.57
Bad Sprayed Bar	Frequency (f_r) Hz	$Q \times 10^3$
6	1682	2.9
7	1692	2.69
8	1690	2.68
9	1690	2.68
10	1690	2.67

Experimental results of testing the adhesive bond of steel bars of dimension (4"×1"× $\frac{1}{8}$ ") which have been sprayed with nickel. The first group (1-5) was well bonded, while the second group (6-10) was intentionally badly bonded.

3.5.2 Influence of Coating Thickness

Experiments carried out on steel and aluminium rectangular bars of dimensions ($4 \times 1 \times \frac{1}{8}$ ") coated to different thicknesses with alumina and chrome. The results showed a dependence on the coating thickness. The Q decreased with increasing thickness (weight) of coating as shown in Fig. 3.11 and Fig. 3.12. The results are shown in Table 3.6 and Table 3.7.

It will be seen that the change is approximately linear. The value extrapolated to zero thickness coincides with the normal value of (Q^{-1}) for the plate, indicating that there is no significant loss mechanism associated with the surface layer.

3.5.3 Temperature Effects on Q

To examine the effect of the temperature on " Q ", a hot rectangular steel bar was excited at the fundamental mode. The resonant frequency (which is linear with the temperature) and the quality factor of the bar have been observed when it was cooling down. The results in Fig. 3.13 and Table 3.8 show how strongly the damping of the vibrations depend on the temperature. Work of this kind is widely carried out in the study of lattice structure and defects.

Fig. 3.11 Variation of (Q^{-1}) with coating weight of steel bars of dimension $(4" \times 1" \times \frac{1}{8}")$ coated with chrome.

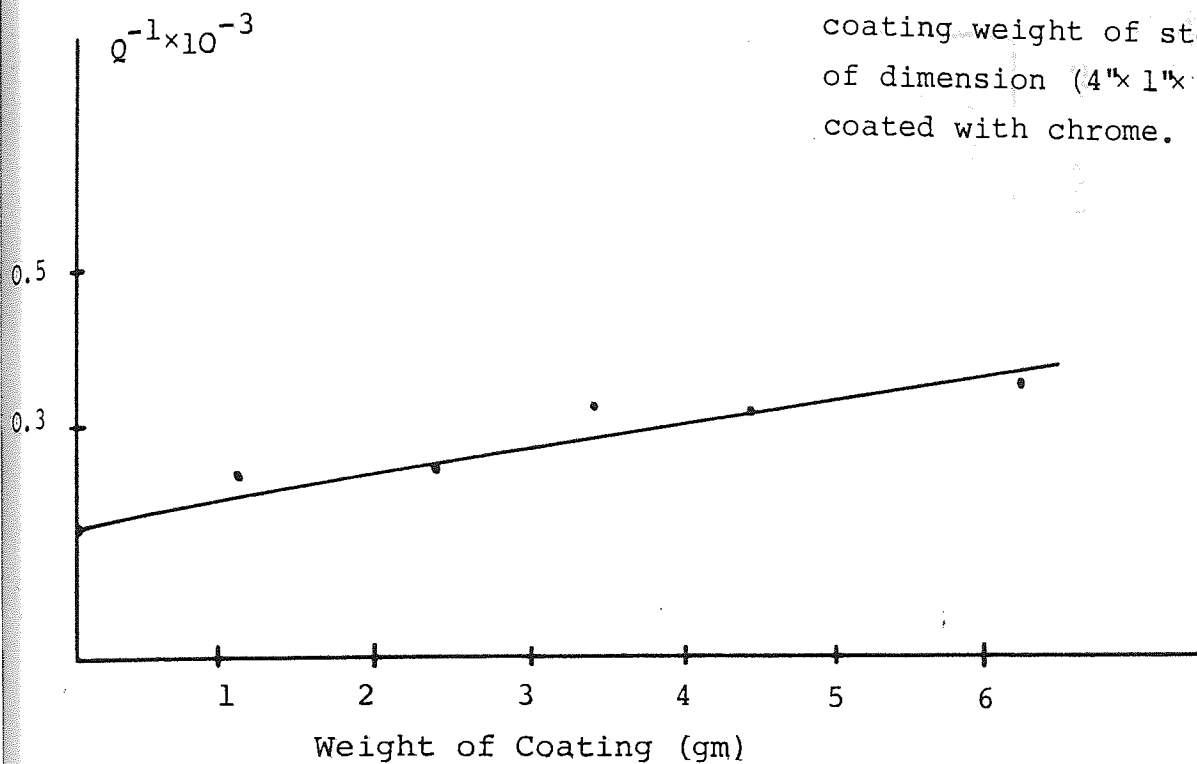


Fig. 3.12 Variation of (Q^{-1}) with coating thickness of steel bars of dimension $(4" \times 1" \times \frac{1}{8}")$ coated with alumina.

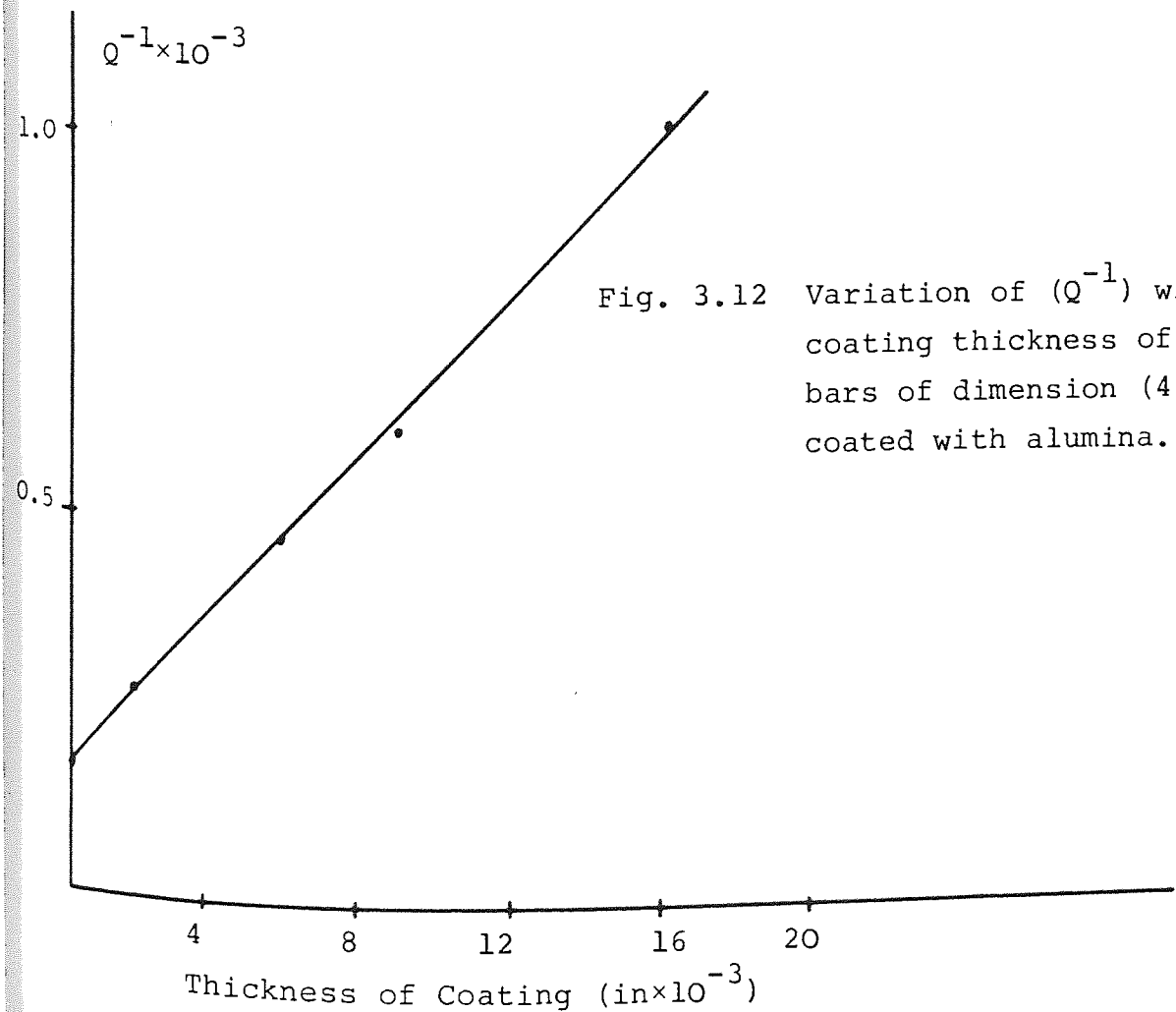




TABLE 3.6

Bar	CHROME SPRAYED COATINGS				ALUMINA SPRAYED COATINGS			
	Coating Thickness (inches)	Weight (gm)	Frequency (f_r) Hz	$Q \times 10^3$	Coating Thickness (inches)	Weight (gm)	Frequency (f_r) Hz	$Q \times 10^3$
1	0	0	1616	5.8	0	0	1621	6.1
2	0.0025	1.14	1604	4.35	0.002	0.26	1613	3.64
3	0.0045	2.40	1624	4.25	0.004	0.38	1627	3.0
4	0.006	3.40	1640	3.14	0.006	0.62	1617	2.10
5	0.009	4.52	1651	3.18	0.009	1.58	1676	1.63
6	0.015	6.25	1645	2.88	0.016	2.73	1673	0.92

Experimental results of measuring Q of steel bars coated with different thicknesses of chrome and alumina.

TABLE 3.7

CHROME SPRAYED COATINGS				ALUMINA SPRAYED COATINGS			
Bar	Coating Thickness (inches)	Weight (gm)	Frequency (f_r) Hz	Coating Thickness (inches)	Weight (gm)	Frequency (f_r) Hz	$Q \times 10^3$
1	0	0	1666	0	0	1666	1.65
2	0.002	0.85	1679	0.002	0.21	1664	1.64
3	0.0045	2.17	1691	0.004	0.78	1686	1.08
4	0.006	2.25	1717	0.006	1.19	1713	0.83
5	0.009	3.79	1757	0.009	1.90	1812	0.65
6	0.015	6.51	1778	0.015	2.87	1879	0.68

Experimental results of measuring Q of aluminium bars coated with different thicknesses of chrome and alumina.

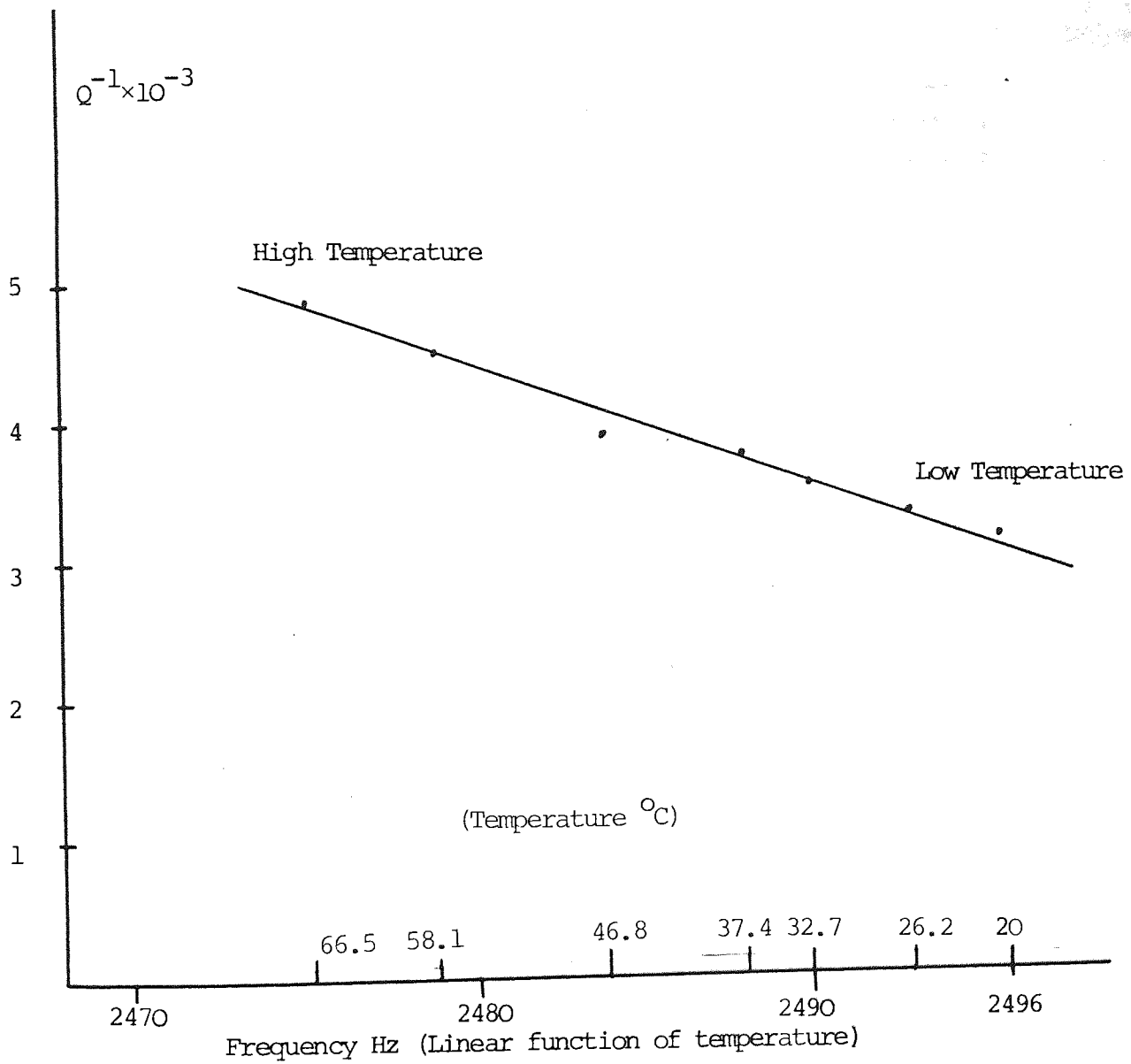


Fig. 3.13 Correlation of (Q^{-1}) with temperature of steel bar vibrating at the fundamental mode.

TABLE 3.8

Frequency (Hz)	Q	$Q^{-1} \times 10^{-3}$	Temperature °C
2475.2	206.6	4.84	66.5
2478.9	221.4	4.52	58.1
2483.9	255.4	3.92	46.8
2488.1	265	3.77	37.4
2490.2	279	3.58	32.7
2493.1	297.8	3.36	26.2
2495.9	315	3.18	20.0

Experimental results of measuring Q and frequency of a hot steel bar cooling down.

CHAPTER 4

INDUSTRIAL APPLICATION

4.1 INTRODUCTION

The main results of frequency response of steel bars containing a defect and the testing of adhesive bonds by measuring the decay rate of vibrations was presented in the previous chapter. These form a basis for assessing the capability of the decay rate technique.

While the work was in progress initial examinations of the application of the decay rate technique to an industrial problem was performed. The application area was testing piston rings for high performance internal combustion engines where the bearing surface is flame sprayed molybdenum.

The required inspection rate is 100 rings per hour. The decrement Q-meter described in Chapter 3 was further developed to operate automatically. The new design uses a drive and pick-up control loop to find the resonance of each ring even if there is a considerable frequency variation between rings. The design uses a voltage controlled oscillator and amplifier for the drive unit, an amplifier for the pick-up unit and the Q-meter. The experimental set up is shown in Fig. 4.1.

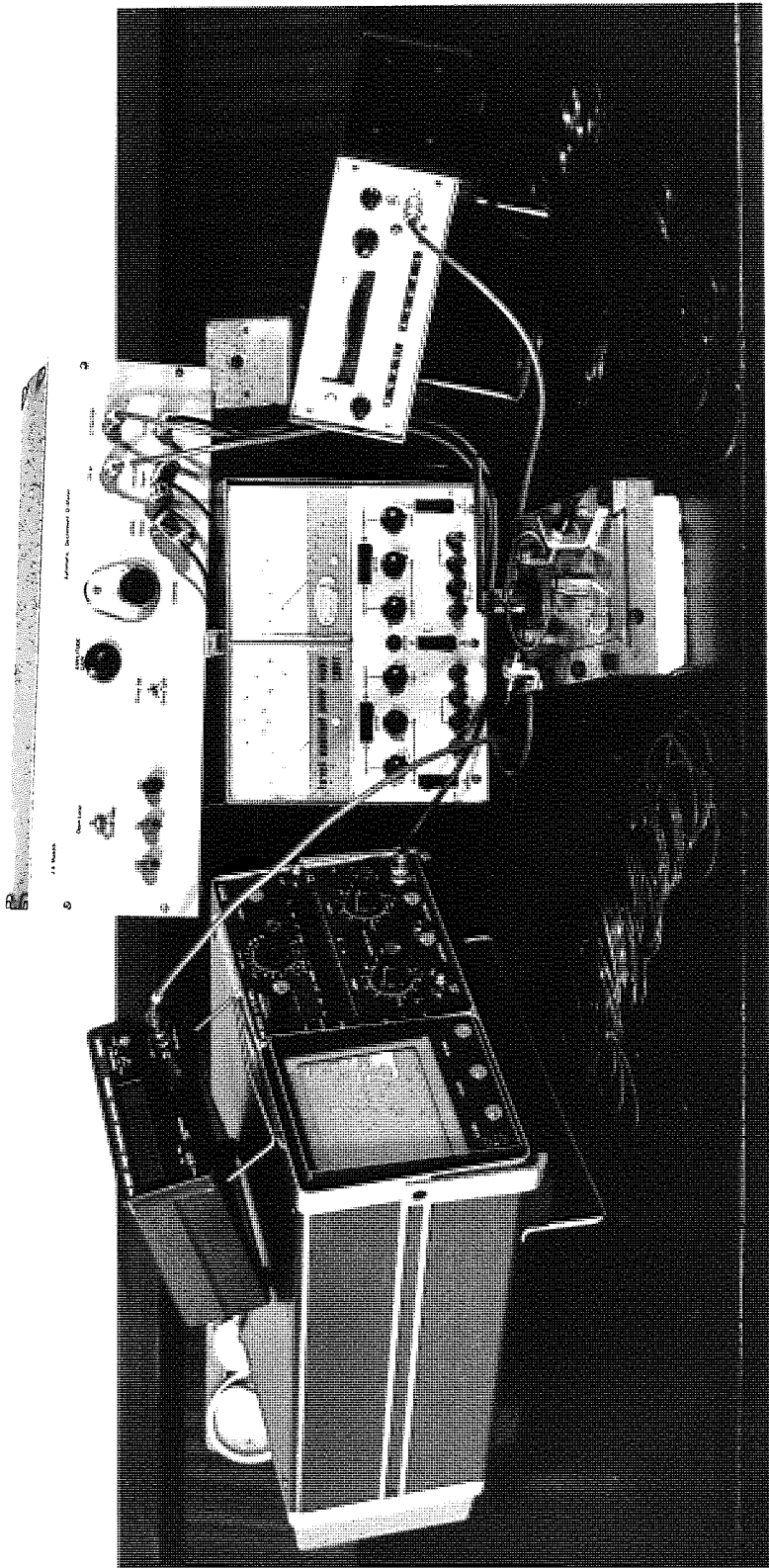


Fig. 4.1 The experimental arrangement for testing piston rings.

4.2 ELECTRONIC DESIGN

4.2.1 Introduction

To achieve the required inspection rate of 100 rings per hour it was decided to use a control loop to make the ring vibrate automatically at its natural frequency. A considerable scatter in frequencies is to be expected mainly due to variation in the amount of molybdenum sprayed on the rings. On switching off the drive the decrement of the ring is to be measured.

The control system makes use of a phase locked loop (PLL) integrated circuit. A drive amplifier is necessary to achieve sufficient amplitude to operate the Q-meter used for decrement measurement. The separate unit picks up the feedback signal and this is conveniently available for the Q-meter input.

The Q-meter in this system consists of two biased comparators (the previous design used three). The first being biased to a high voltage while the second is low. The bias ratio is 4.81. A switching bistable is used to open and close the gates. The functional block diagram of the electronic system is shown in Fig. 4.2. The electronic system that is required to perform these functions can be divided into the following subsystems.

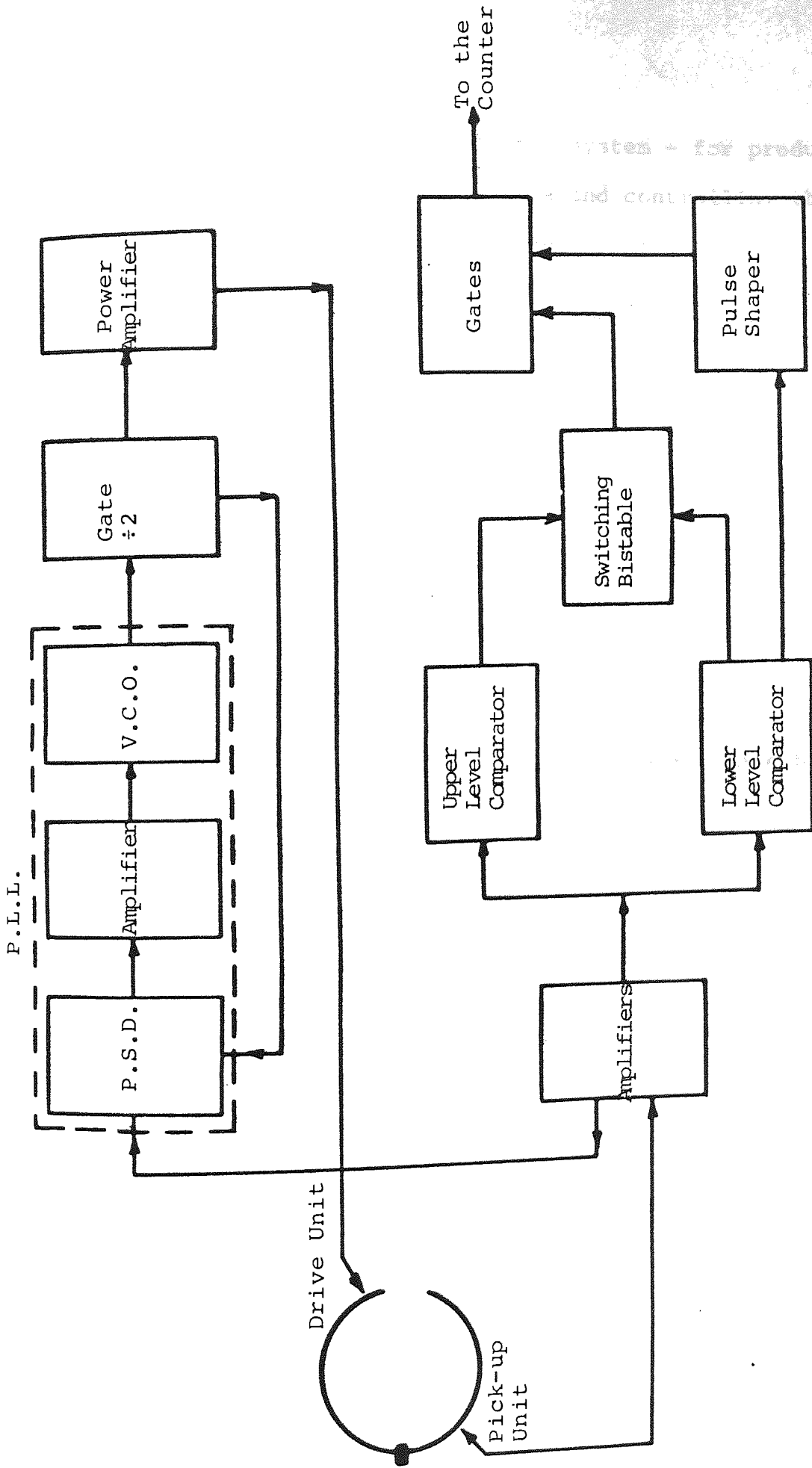


Fig. 4.2 Block diagram of the electronic system to drive, receive and measure the decay rate of oscillations.

- (1) Transmitter and control system - for producing electrical oscillations and controlling the output of the signal generator.
- (2) Receiver and phase adjustment - to amplify and shift the phase (as necessary) of the pick-up signal.
- (3) Q-meter - to measure the decay rate of oscillation for a piston ring when the drive force is removed.

4.2.2 Transmitter and Control System

The functions of this system are to generate high power electrical pulses to drive the rings, and to set a signal generator to the natural frequency of the measured ring. A 565 phase locked loop integrated circuit has the characteristics to do this.

The PLL is a feedback system comprising of a phase comparator, a low pass filter, an error amplifier in the forward signal path and a voltage controlled oscillator (VCO) in the feedback path as shown in Fig. 4.3. The basic principle of PLL operation can be briefly explained as follows:

With no signal input applied to the system the error voltage is equal to zero. The VCO operates at a set

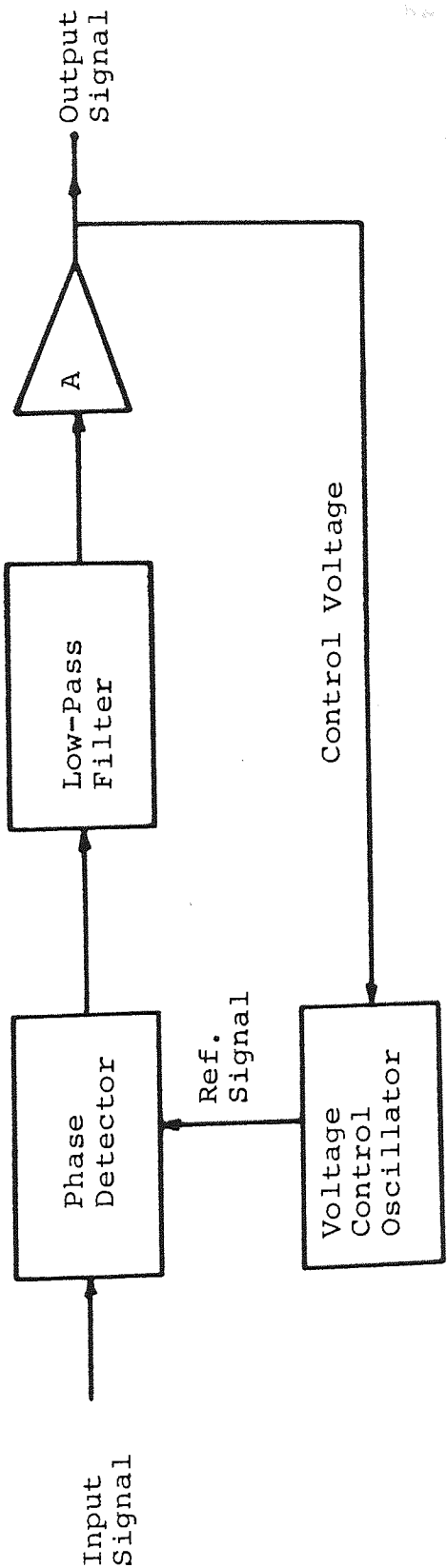


Fig. 4.3 Block diagram of phase locked loop (PLL)

frequency ω_0 which is known as the free-running frequency. If an input signal (in this design the pick-up signal) is applied to the system; the phase comparator compares the phase and the frequency of the input with the VCO frequency and generates an error voltage which is related to the phase and the frequency difference between the two signals. This error voltage is then filtered, amplified and applied to the control terminal of the VCO. In this manner, the control voltage forces the VCO frequency to vary in a direction that reduces the frequency difference between f_0 and the pick-up signal. In practice the control is in the centre of its range (ω_0) when the VCO and signal have a 90° phase difference. A signal conditioning network can achieve this, so long as the pick-up frequency is within 20% of the VCO frequency. The feedback nature of the PLL causes the VCO to synchronise with the pick-up signal. The circuit diagram of the transmitter is shown in Fig. 4.4. and the required waveform to drive the ring in Fig. 4.5.

The transmitter also contains a power amplifier shown in Fig. 4.6(a) consisting of two VMOS transistors type BD 512 (p-channel) and BD 522 (n-channel). The amplifier produces high voltage pulses of amplitude, -24 volts to +24 volts. The gating circuit of Fig. 4.6(b) produces the required signals to drive the amplifier.

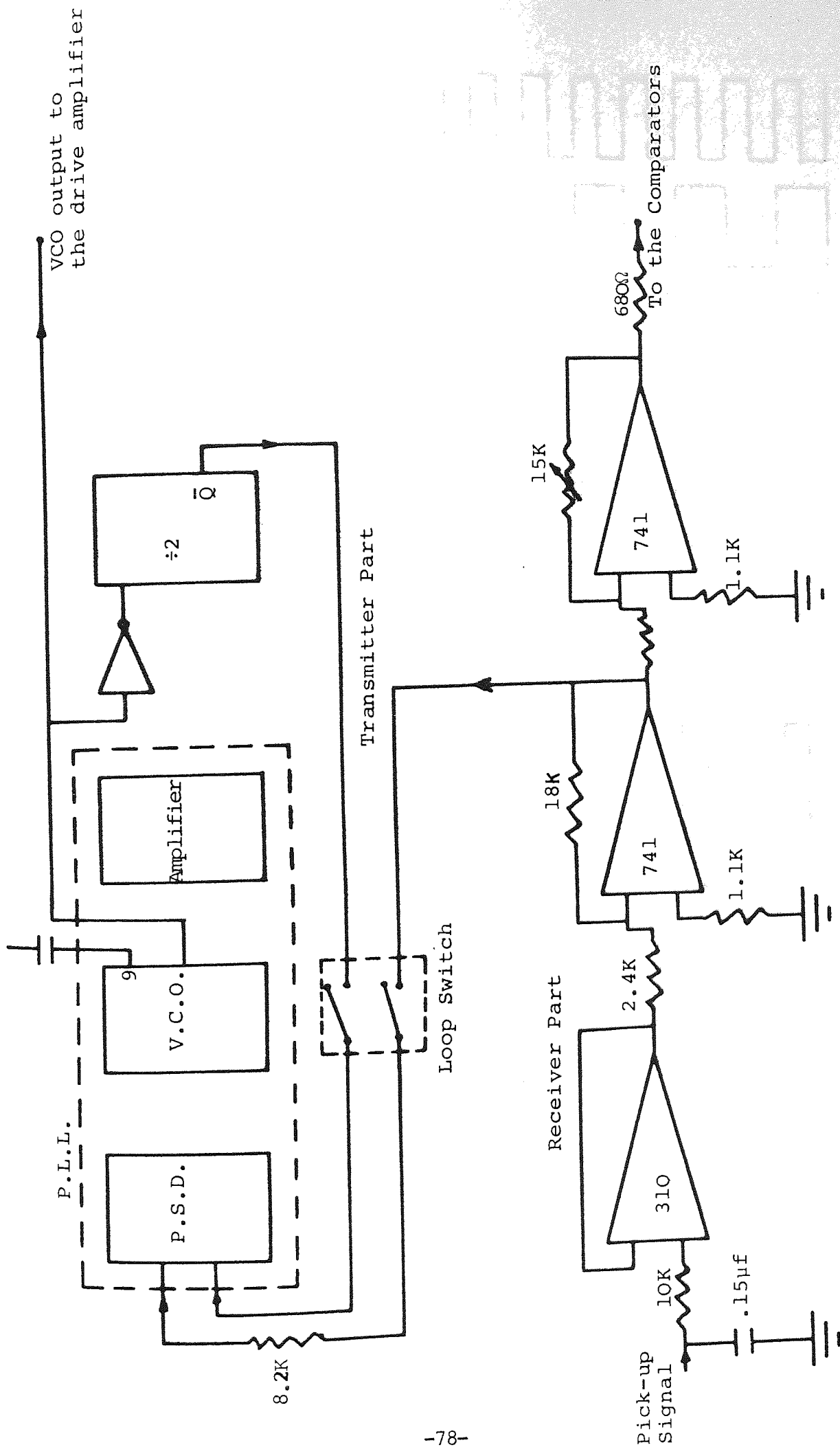


Fig. 4.4 Circuit detail of the transmitter and the receiver.

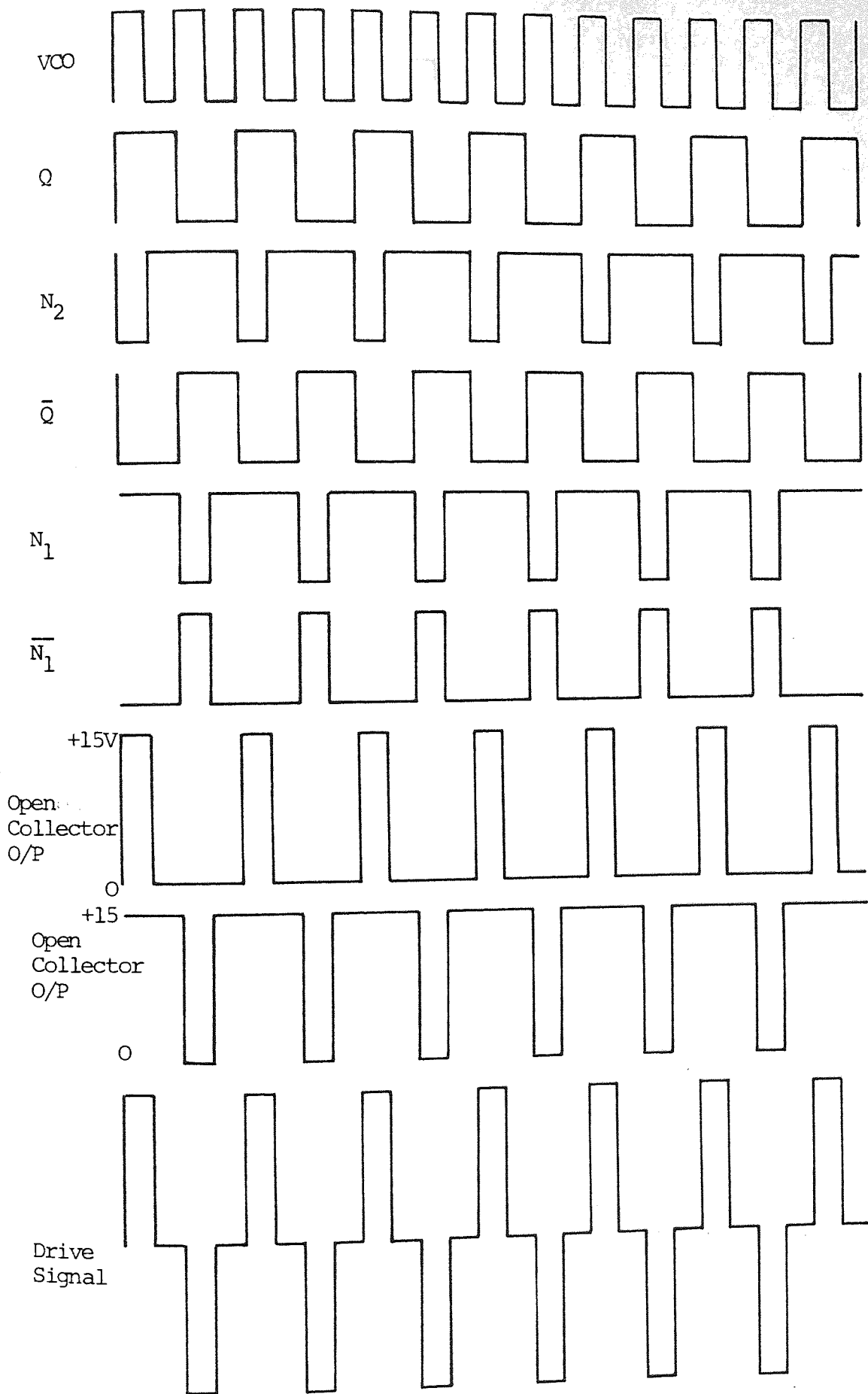
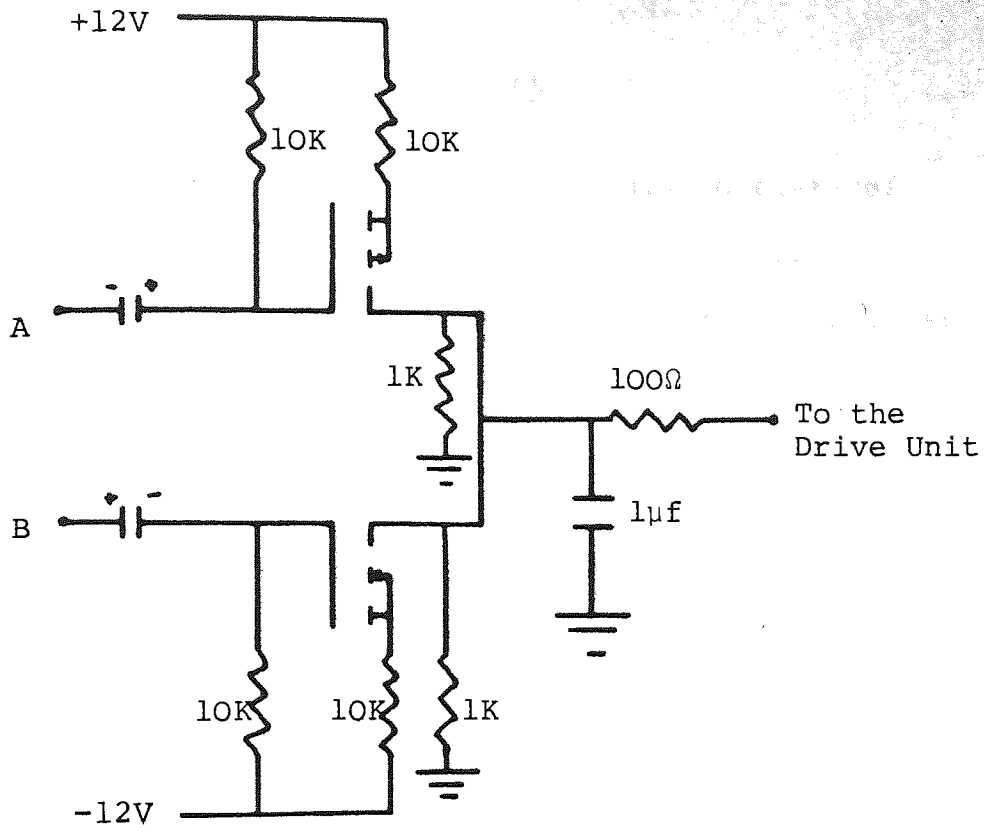
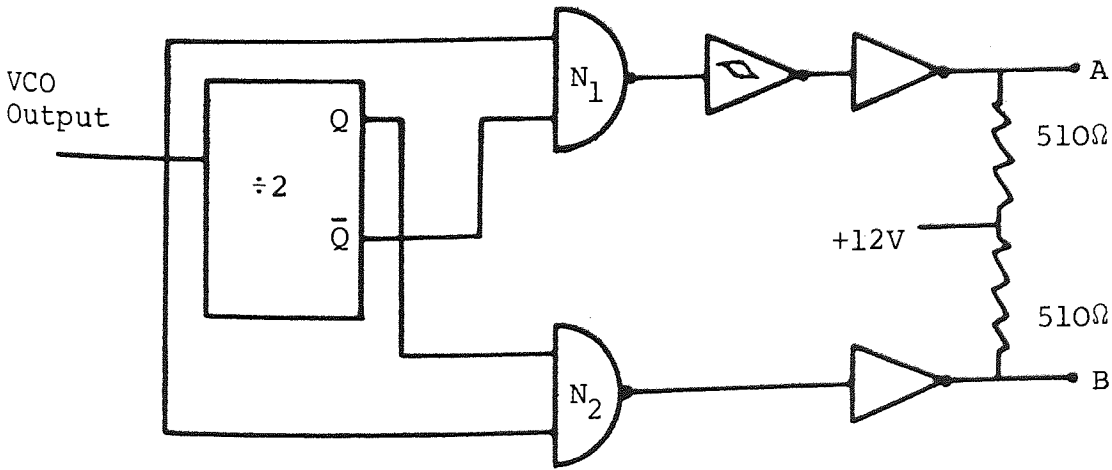


Fig. 4.5 Waveforms for the transmitter system giving an interlaced signal.



(a) Drive Power Amplifier



(b) Gating Circuit to obtain the required Signals for the Drive Amplifier

Fig. 4.6

4.2.3 Receiver and Phase Adjustment

The receiver section shown in Fig. 4.4 consists of a voltage follower which is a unity gain amplifier integrated circuit, type LM 310 and two separate amplifiers.

The input capacitor and resistor of the voltage follower were used to set the pick-up signal to the correct phase for the signal of central frequency selected.

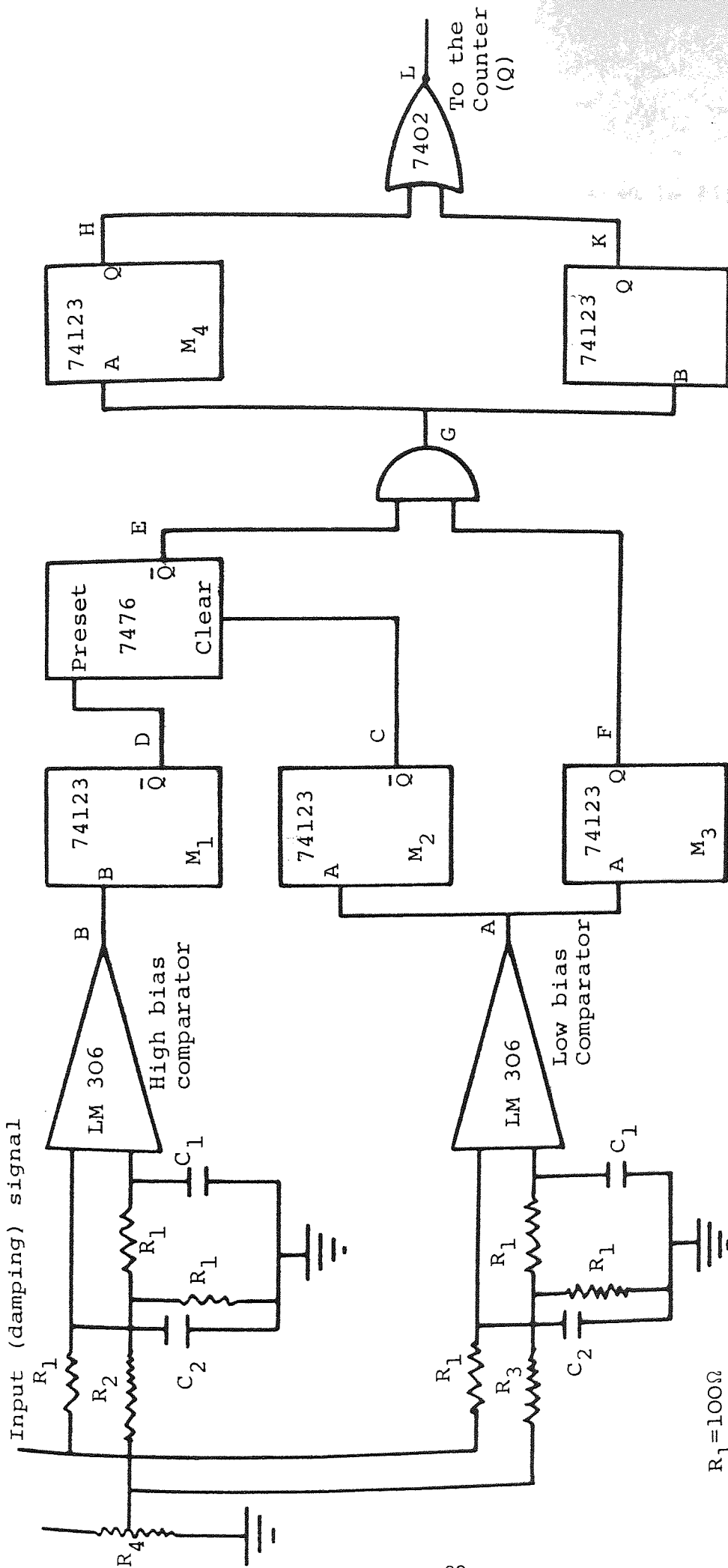
Standard IC operational amplifiers were used. The output of the first having a gain of 7.5 was fed to the PLL. The second had a variable gain, its output was fed to the two comparators of the Q-meter.

4.2.4 Q-Meter

The function and the operation of the Q-meter is the same as that discussed in Chapter 3.


The Q-meter in this system which uses two comparators, was developed to avoid spurious noise in the pick-up signal at low level amplitudes by making the ratio of the two bias voltages 4.81 rather than 23.14 as in Chapter 3. In this case the counter will read $Q/2$.

Three separate monostables were used to give a count of Q rather than $Q/2$. The monostable produces a short duration trigger pulses starting at opposite polarity edges. The full circuit diagram is shown in Fig. 4.7 and



- $R_1=100\Omega$
- $R_2=1K\Omega$
- $R_3=4.3K\Omega$
- $R_4=5K\Omega$
- $C_1=120\text{ pf}$
- $C_2=1000\text{ pf}$

Fig. 4.7 Circuit detail of the Q-Meter.



the waveform at different points is shown in Fig. 4.8.

4.3 TESTING PROCEDURE

4.3.1 Introduction

The feasibility of measuring the decay rate of oscillation to evaluate the adhesive bonds was investigated using samples of simple geometry such as the rectangular bars used in the previous experiments. The results showed that Q measurement gives a promising technique.

This section describes testing the bond integrity of the piston rings by measuring the damping. The rings are of cast iron with a channel round the outer surface. This is filled with Molybdenum by flame spraying to give the hard wearing contact with the cylinder.

Two standard electromagnetic transducers were used, one to drive the ring in the flexural in-plane mode and the other to pick-up the vibrations. These two transducers must be located at suitable points to minimise the strong direct magnetic cross-talk which can mask the signal. Since the anti-nodes are the best locations for both drive and pick-up units, the drive unit was located very close to one free end, while the pick-up unit was located very close to the vibrating surface at the anti-node in the other side of the clamp. This gave a good separation and

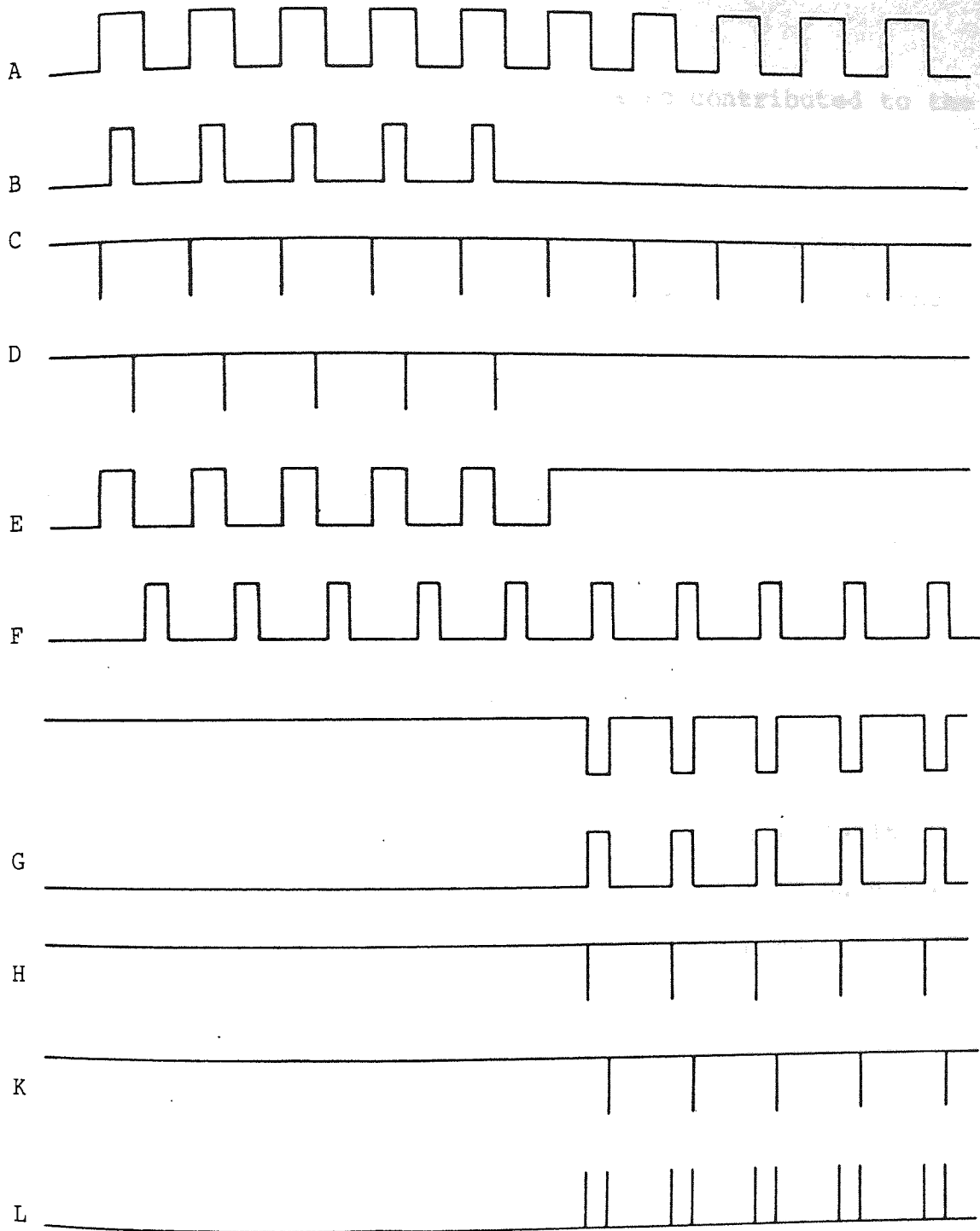


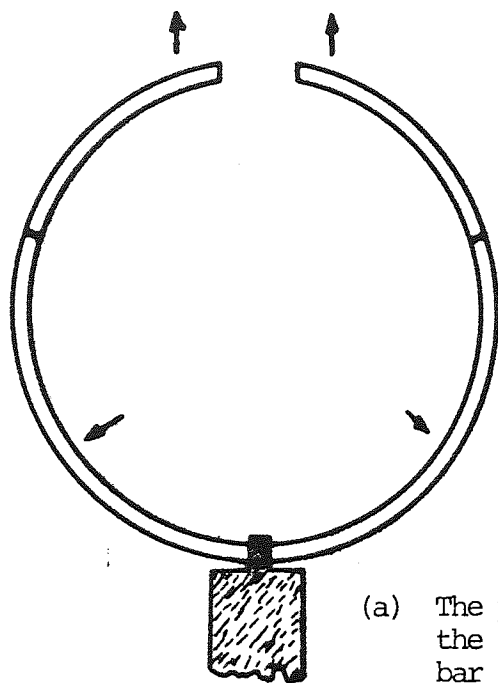
Fig. 4.8 Waveforms at different points in the Q-Meter

the angle between the two units also contributed to the reduction of the direct signal.

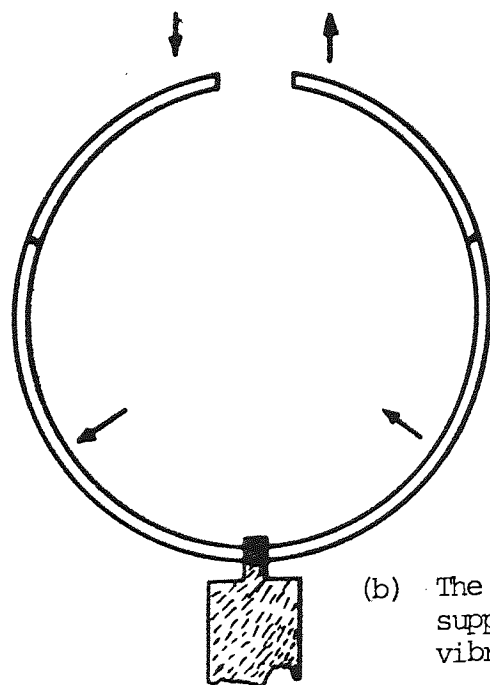
Two adjacent modes were observed during the experiments, where the ring was clamped firmly at the centre by a specially constructed jig. The strong mode was at a frequency close to the second resonance of a clamped-free bar. Near the clamp the amplitude was virtually zero and had the features of clamped support. The vibrations of this section as shown in Fig. 4.9(a) were perfectly symmetrical about the axis, the phase of the vibrations being the same on either side of the clamp.

The second mode was much weaker, and while it occurred at a lower frequency it appeared to have the same nodal pattern. Detailed examination showed that the difference appears in the phases. The vibrations are no longer mirror images and the phase across the clamp is reversed. The clamp is now behaving as a simple support. The pattern is shown in Fig. 4.9(b).

A careful study of a conventional tuning fork gave the mode shown in Fig. 4.9(a), but there was no evidence of the second mode. The strong mode was used throughout the investigation.



(a) The piston ring is vibrating in the second mode of clamped-free bar (second mode of the tuning fork)



(b) The clamp is behaving as a simple support and the piston ring vibrates as F-S-F bar.

Fig. 4.9. Piston ring clamped firmly at the centre.

4.3.2 EXPERIMENTAL RESULTS

To assess the capability of the design for the quality control of the rings, a series of experiments were carried out. Two batches of rings were available. One made as a well bonded group, while the other was intentionally badly bonded. Defective platings are expected to have high decrements, while the standard ring (not plated) has quite a low decrement. The decrement of a good plated ring will have a value somewhat lower than the standard one.

It will be noticed from the results presented in Tables 4.1 and 4.2 that the Q-meter gives a wide difference in quality factor between bad and good rings, where the best ring in the first group has a value of Q less than the worst in the second group. It is also less than Q/2 of the standard ring.

It was observed that as well as a scatter in the Q there was frequency scatter for the two groups. This was considered to be due to the known variation in the amount of molybdenum sprayed on the rings. The point was confirmed experimentally as described in Chapter 3 using rectangular bars.

The clamping point in common with the support points discussed in Chapter 3, has a major effect on the Q. Consequently, the rings must be clamped carefully at the centre.

TABLE 4.1

Ring	f_r	Q	No. of Reading	\bar{Q}	Standard Error
1	676	405,397,391,397,391,391	6	395	1.41%
3	673	423,421,427,421,429	5	424	0.86%
4	670.3	475,471,473,479,473,477	6	474	0.62%
6	668	361,375,361,363,355,361	6	362	1.83%
7	676	473,465,469,465,467	5	467	0.72%
8	669	443,465,459,441,447,457,453	7	442	2.00%
9	677	471,457,453,437,449	5	453	2.73%
10	672	457,467,459,461,449	5	458	1.4%
11	680	377,379,367,375,383	5	376	1.58%
12	680	1040,1060,1040,1050,1050,1040	6	1047	0.78%

The experimental results of measuring the Q of badly bonded rings. The standard ring (number 12) has a value of 1047

TABLE 4.2

Ring No.	f_r	Q	No. of Reading	\bar{Q}	Standard Error
3	690	719,695,689,711,699,719	6	705	1.8%
4	689	847,867,845,851,843,853	6	851	1.02%
5	688.2	699,701,687,717,703,703,705	7	712	1.24%
6	687	625,625,621,631,625,627,625	7	625	0.53%
7	687.6	631,627,623,621,617,613,619	7	612	0.99%
8	683.7	809,821,817,839,817,817,807	7	818	1.28%
9	687.2	923,939,921,939,927,921,921	7	927	0.89%
12	680	1070,1060,1060,1050,1020	5	1052	1.83%

The experimental results of measuring the Q of well-bonded rings. Ring number (12) is the standard one which has a Q value of 1052.

As far as the electronic design is concerned the standard error has been found for a wide range of readings to be about 2%. The spread associated with the design arose from the uncertainty trigger levels in the comparators.

Finally, experiments were performed on 200 unknown rings to obtain data of the quality of the plating and the inspection rate of the system. The inspection rate was near the target of 100 rings per hour, and the results are shown in Table 4.3.

Having discussed the capability of the design and the experimental results, it can be concluded that measuring the decay rate of oscillations is a quick and reliable method to identify a well plated ring from a bad one.

It is also possible to study the influence of the coating thickness (weight) and the effects of temperature on the quality factor of other resonators of simple geometry such as rectangular bars.

TABLE 4.3

The experimental results of measuring the Q of unknown rings.

The standard ring has a Q value of 1214.

Ring No.	f_r	Q
Reference	625	1214
1	648	838
2	657	777
3		
4		
5	649	546
6	651	864
7	656	744
8	661	832
9	651	940
10	655	994
11	644	612
12	647	410
13	651	754
14	646	522
15		
16	650	842
17	652	790
18		
19	654	982
(12)	647	404
22	661	702
23	662	766
24	661	636
25	658	836
26	657	812
27	648	878
28	645	724
29	663	804
30	658	668

Ring No.	f_r	Q
31	658	790
32	662	622
33	646	674
34	648	870
35	657	998
36		
37	643	858
38	657	772
39	653	540
40	652	434
(12)	647	400
41	647	714
42	648	730
43		
44		
45	660	898
46	651	868
47	663	1094
48	658	1108
49	651	612
50	654	668
51	661	684
52	646	529
53		
54	651	766
55	660	870
56	659	1020
57	651	946
58	656	780
59	653	944

TABLE 4.3 continued

Ring No.	f_r	Q
60	655	910
(12)	646	428
61	647	570
62	658	836
63	650	558
64	657	1058
65	659	1160
66	656	954
67	656	522
68	661	912
69	653	592
70	646	824
71	645	790
72	651	808
73	637	624
74	650	792
75	659	812
76	654	988
77	652	822
78	652	622
79	651	762
80	652	1000
(12)	647	411
81	653	1052
82	652	580
83	658	886
84	655	854
85	659	742
86	660	1026
87	653	980
88	651	590
89	655	780
90	652	922

Ring No.	f_r	Q
91	656	966
92	645	522
93	662	892
94		
95	663	906
96	646	962
97	647	582
98	647	640
99	658	766
100	648	664
(12)	645	396
101	637	952
102		
103	652	980
104	647	776
105	638	810
106	652	886
107		
108	654	866
109	655	572
110	656	808
111	658	562
112	633	602
113	655	736
114		
115	655	936
116	656	1016
117	639	910
118	657	966
119	652	928
120	660	958
(12)	647	407
121	655	964

TABLE 4.3 continued

Ring No.	f_r	Q
122	653	872
123		
124	646	669
125	651	606
126	657	738
127	655	600
128	648	690
129	657	508
130	644	526
131	655	604
132	658	744
133	653	992
134	649	860
135	654	636
136	659	788
137	649	548
138	657	720
139	659	778
140	657	750
(12)	647	420
141	642	600
142	654	794
143	652	754
144	651	722
145	645	570
146	645	810
147	651	932
148	644	970
149	654	592
150	647	740
151	653	426
152	651	854

Ring No.	f_r	Q
153	641	954
154	653	984
155	645	952
156	646	864
157	644	808
158	643	862
159	637	856
160	648	570
(12)	646	416
161	649	817
162	650	728
163	643	898
164	652	974
165	655	886
166	650	814
167		
168	649	746
169	664	710
170	661	724
171	662	752
172		
173	650	834
174	653	506
175	661	956
176	644	948
177	658	1016
178	650	576
179	647	534
180	646	528
(12)	647	412
181	665	810
182	649	730

TABLE 4.3 continued

Ring No.	f_r	Q
183	653	732
184	649	928
185	655	1014
186	645	884
187	655	764
188	651	680
189	651	1026
190	646	483
191	645	796
192	653	836
193	649	836
194	646	828
195		
196	653	672
197	662	898
198	653	956
199	650	844
200	649	788
(12)	647	422

CHAPTER 5

THE DESIGN OF A TUNING FORK TRANSDUCER FOR MEASURING FLUID DENSITY AND VISCOSITY

5.1 INTRODUCTION

A tuning fork can be designed to have tines of large areas with a small separation between them. This traps a thin lamina of liquid on which the vibration of the tines exerts a pumping action. The vibration of the fluid is greatly magnified and the associated kinetic energy adds inertia to the system, reducing its natural frequency. This phenomenon is the basis of the fluid density transducer.

The function of the electronic system is to make the tuning fork vibrate automatically at its natural frequency. The essence of the problem is that, the transducer is passed through a flange in an oil pipe line or a pressure vessel wall. A vital user requirement is the absence of any electrical hazard. To meet this requirement the electrical part of the transducer (the drive and pick-up) is on the outside and the mechanical sensor element (the tines) is on the inside.

The energy is lead through the flange as magnetic flux and is converted to mechanical vibration at the sensor by

magnetostriction. The return signal occurs automatically by energy reciprocity.

A power amplifier is used to generate electrical bursts of oscillations to drive the transducer via a coil wound at the end of the stem on four strips of magnetic material (laminated steel) to produce and to carry a magnetic field to the tines. The magnetic field is converted to mechanical energy by two magnetostrictive strips on the outer surface of the tines. The strips can be attached by any suitable adhesive but direct electroplating gives better performance and allows more flexibility in the mechanical design. The magnetostrictive material must be pre-polarised or supplied with a biasing magnetic field. Figure 5.1 shows a typical transducer used for measuring fluid density.

The energy stored during the drive period decays exponentially (decrement) at the natural frequency of the transducer and is independent of the drive frequency. The decrement signal is received on a separately wound coil.

The control system compares this frequency with that of the drive to produce an error signal. The resultant error signal is reduced to zero by the control loop, making the two frequencies equal. The system functions so long as the decrement signal is sufficient to operate

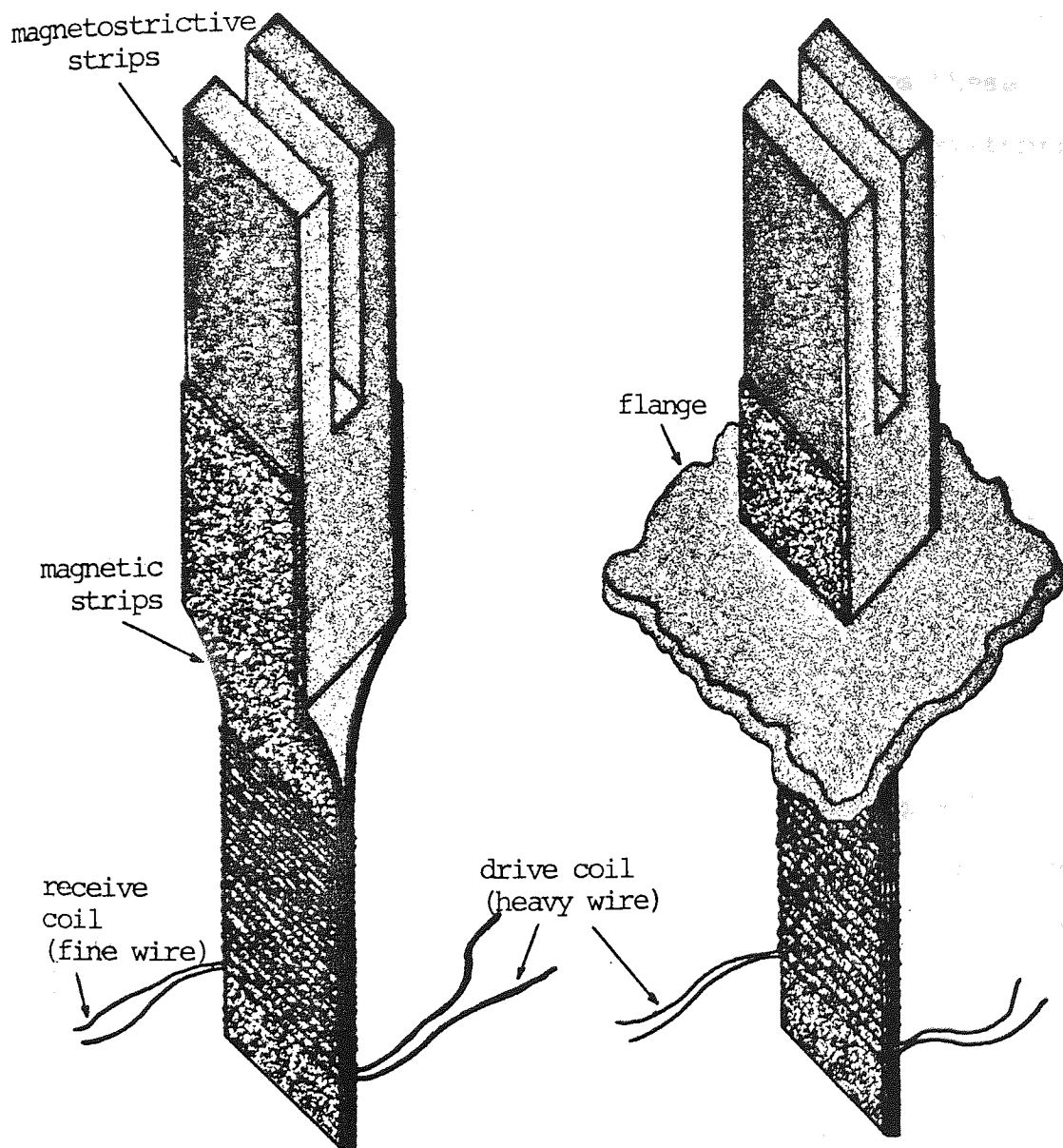


Fig. 5.1 In the transducer shown, the fluid between the tines is pumped in and out as the tines vibrate, constituting an internal load on the vibrating system, hence lowering the frequency. The steel strip carries the magnetic energy to and from the tines. The heavy coil with a small number of turns enables a high driving flux to be generated and the large number of turns in the receiver coil gives a sufficient high decrement voltage to be processed without amplification.

the receiver circuits.

The electronic system required to perform these functions can be divided into the following subsystems:

(1) Driver Circuits - For gating a burst of oscillations from a voltage controlled oscillator (VCO) at an equal mark space ratio.

(2) Receiver Circuits - For decrement identification and processing which occurs during the space interval. The sinusoidal decrement signal is squared using a zero crossing detector and then processing digitally to give a measure of the period.

(3) Error Measurement and Control System - This produces an error signal by comparing in each burst cycle a sample of period derived from the decrement with that of the drive signal.

The functional block diagram of the electronic system is shown in Fig. 5.2. Digital techniques were used as extensively as possible and the technology is based on TTL integrated circuit making minimal use of discrete components and analogue devices.

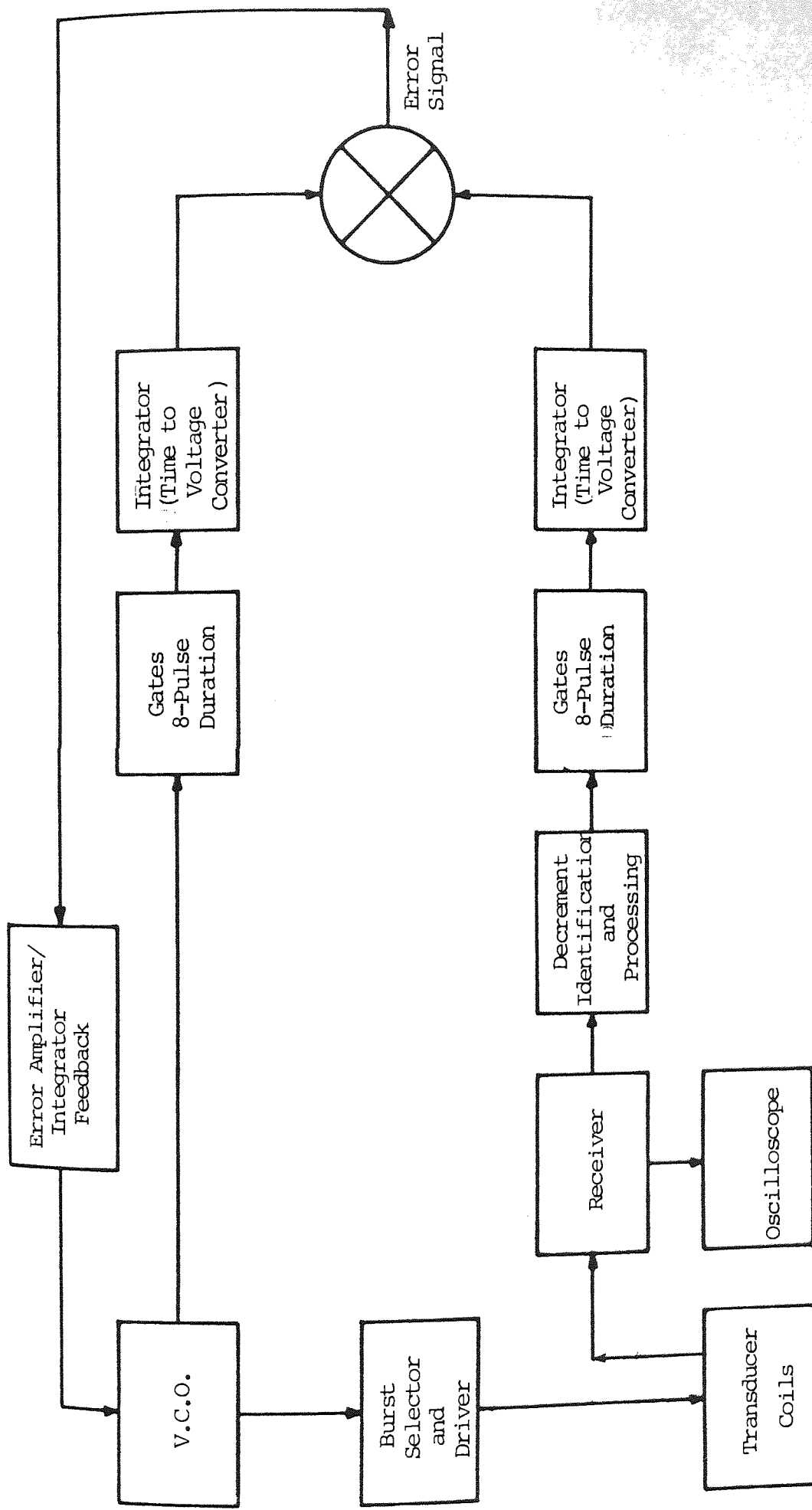


FIG. 5.2 The Functional Block Diagram of the Electronic System.

5.2 DRIVER

5.2.1 Introduction

The function of the driver is to amplify the bursts of oscillations to drive the transducer. A coil of a heavy wire ($\frac{1}{2}$ mm diameter) consisting of a small number of turns wound on four layers of laminated steel, was used to produce the magnetic flux. The lamination steel ($\frac{1}{4}$ mm thickness each) bonded at the stem of the tuning fork was used to carry the magnetic flux to and from the magnetostrictive material plated on the tines. This converts the magnetic energy to mechanical energy which will drive the transducer.

A coil of a fine wire ($1/5$ mm diameter) having a large number of turns was also wound over the drive coil to receive the decrement signal (Receiver Coil) as shown in Fig. 5.1.

5.2.2 Drive Channel

A voltage controlled oscillator producing free running square waves (a TTL integrated circuit type 74124) was used. The VCO range is governed by an external timing capacitor, and the controlling voltage by the same form of potentiometer. In this design, the output of a two input summing amplifier was used. The first input was from a potentiometer, while the second was derived from

the error signal of the control loop. Three frequency ranges were available and coarse and fine tuning facilities were provided for manual adjustment on open loop.

The drive channel shown in Fig. 5.3 produces bursts of oscillations, the number selected was 128 for the drive mode which can be conveniently obtained by binary division. The vibrational energy stored in the transducer during the drive period decays exponentially at its natural frequency. This is the decrement mode which occupies the same time as the drive mode. The two modes are shown in Fig. 5.4 for two transducers.

Two 4-bit Binary Counters and JK flip-flops type 7493 and 7473 respectively were used to count 256 oscillations to produce signal B shown in Fig. 5.5. This signal was used for gating bursts of oscillations from the VCO at an equal mark space ratio.

By operating the VCO at twice the required signal frequency and divided by two, two interlaced signals could be obtained. They were used to operate the two power transistors giving a push pull drive. Gates N_1 and N_2 produce the required signals, which are then applied to high logic level gates (open collector integrated circuit type 7416). The open collector produces high voltage pulses of amplitude 0 to 15 volts which are required to operate the drive transistors.

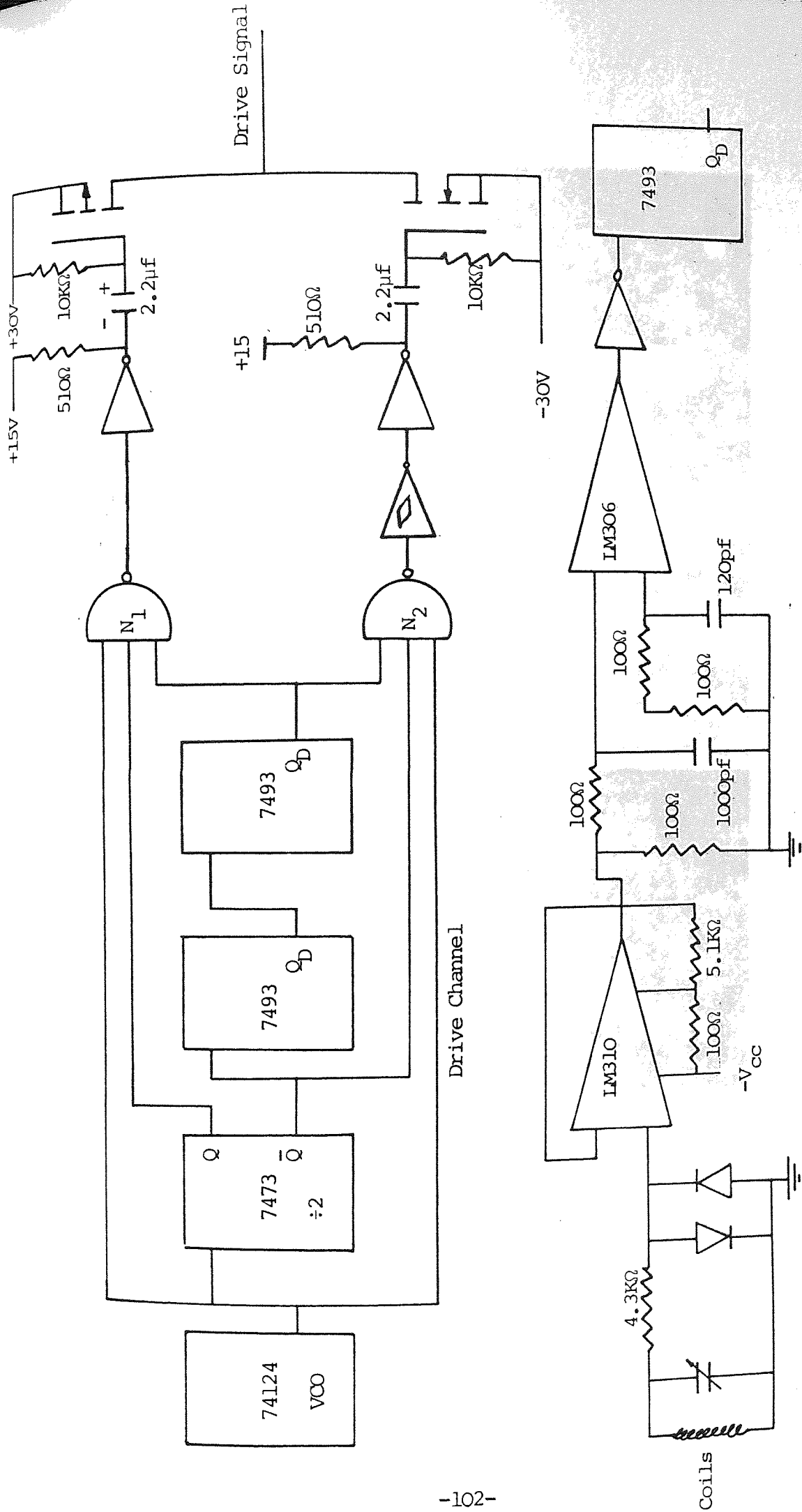
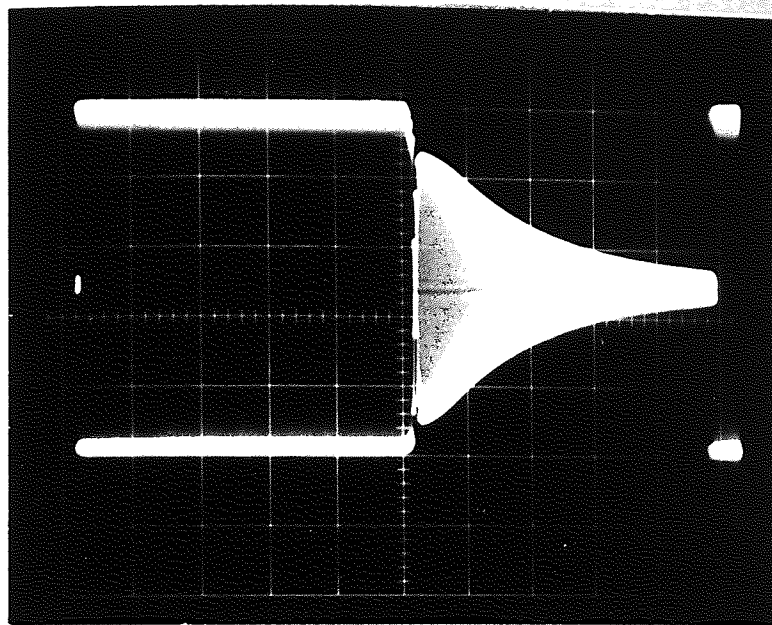
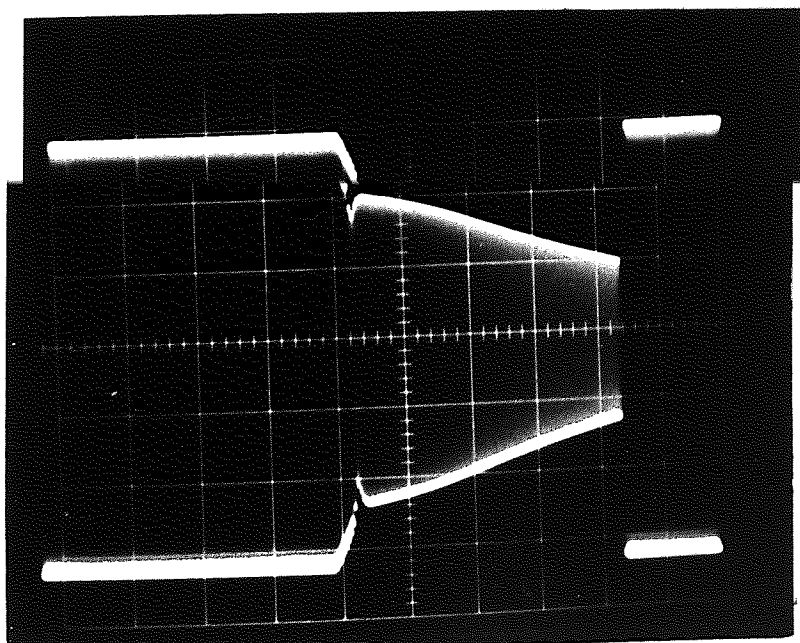


Fig. 5.3 The drive channel for producing bursts of oscillation and the receive channel for decrement identification and processing.



(a)



(b)

Fig. 5.4 The drive and decrement mode.

- (a) Aluminium transducer vibrating in air with a natural frequency of 581 Hz and it has $Q = 250$.
- (b) Aluminium transducer vibrating in air and has a natural frequency of 2242 Hz and $Q = 680$.

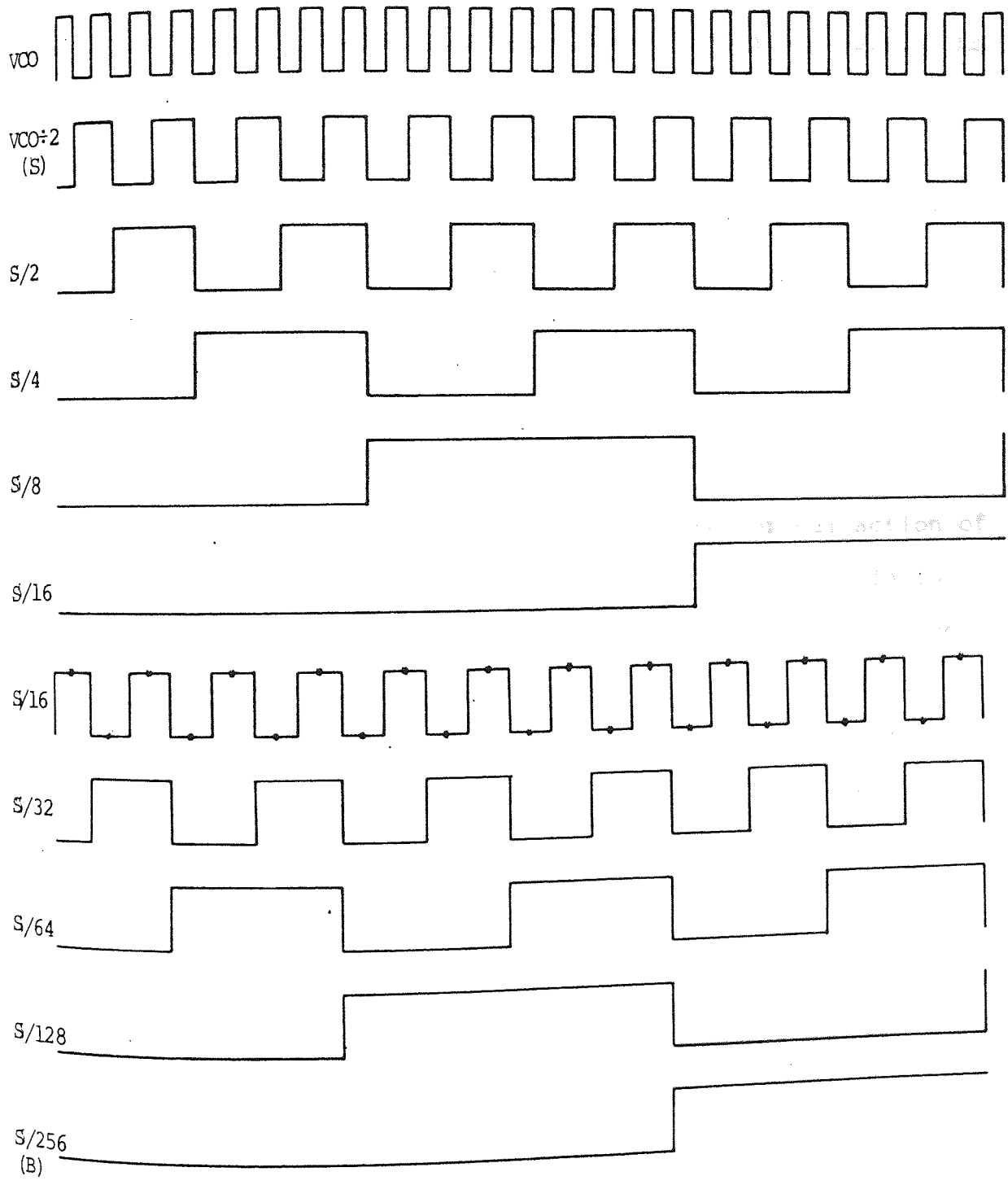


Fig. 5.5 The required waveforms obtained from dividing circuits for gating bursts of oscillations from the VCO at an equal mark space ratio.

The drive power amplifier (shown in Fig. 5.3) consists of two VMOS transistors type BD 512 (p-channel) and BD 522 (n-channel) which connected the load coil alternately to the positive and negative rails (about ± 30 volts). The waveforms at different points are shown in Fig. 5.6. The load coil (the drive coil) produces a high magnet flux which is carried via the steel laminations through the flange to the magnetostrictive strips on the tines which then vibrate.

5.3 RECEIVER AND DECREMENT SIGNAL PROCESSING

5.3.1 Introduction

On switching off the drive, the reciprocal action of the magnetostrictive strip produces an A.C. flux in the magnetic strip. This in turn produces a voltage in the receiver coil which consists of a large number of turns of fine wire wound on the top of the drive coil. It is readily tunable and gives a reasonable large signal.

Two small permanent magnet bars were used to provide the magnetostrictive strips with a D.C. bias. This is necessary because of the non-linearity of the magnetostrictive effect. The bias gives an efficient energy transfer, and improves the overall receiver decrement signal. The magnetostrictive phenomenon is discussed in detail in Chapter 6.

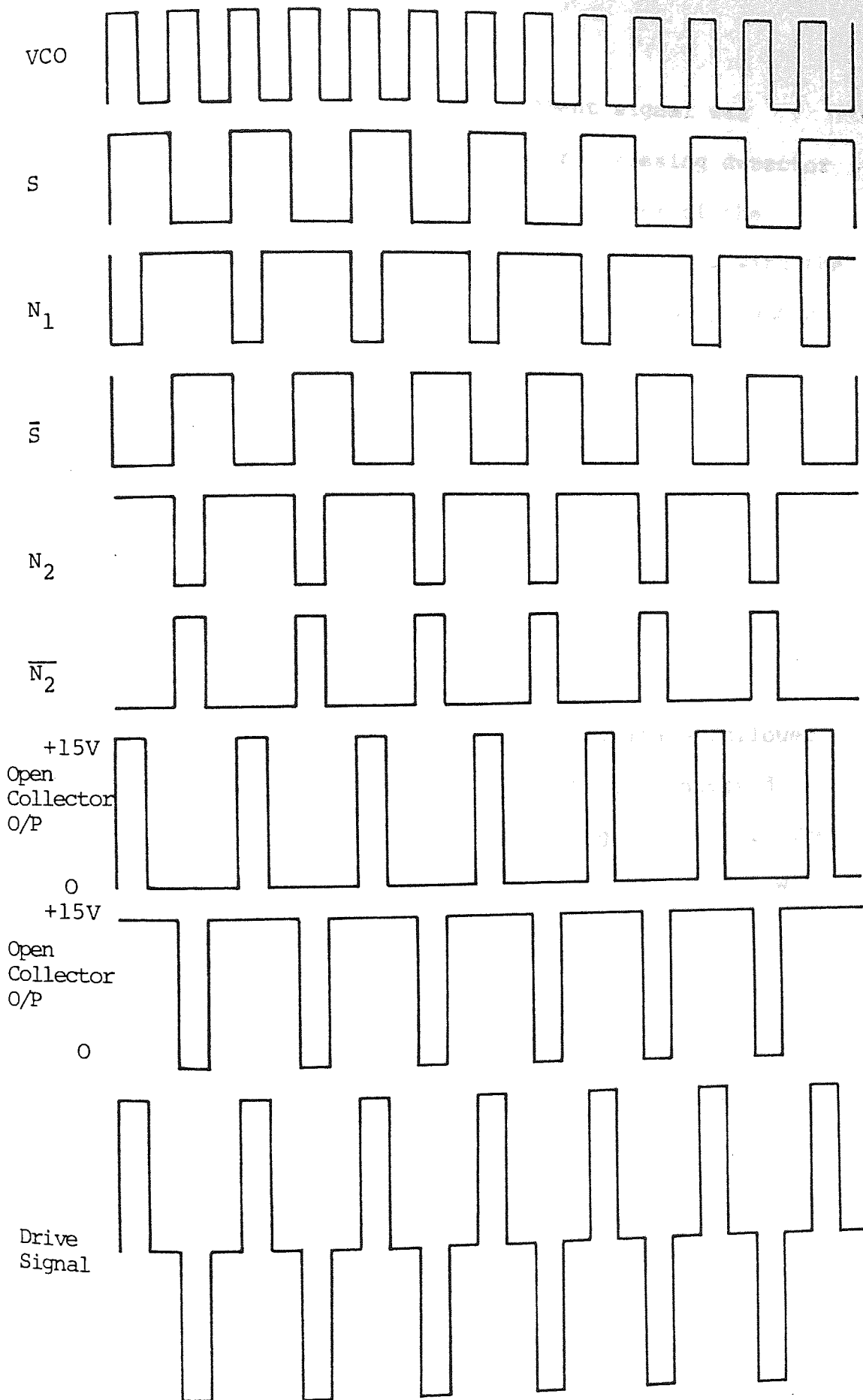


Fig. 5.6 The required waveform to drive the transducer.

Typically the sinusoidal decrement signal was converted to square waves using a zero crossing detector and then processing digitally. A few pulses of the decrement were sampled and the duration compared with the same number of pulses of the drive signal thus producing an error voltage. This will be discussed in detail in the error measurement section. The circuit details of the receiver channel is shown in Fig. 5.3.

5.3.2 Input Voltage Follower

The receiver signal was clamped to ± 0.7 volts using back to back diodes for protection against the very large amplitude drive signal. It drives the voltage follower which is an integrated circuit type LM 310 connected internally as a unity gain non-inverting amplifier. The output impedance is sufficiently low to drive the low input impedance comparator.

5.3.3 Zero Crossing Comparator

The integrated circuit voltage comparator which gives a TTL compatible output was discussed in detail in Chapter 3. It was used to interface the analogue to digital signals.

5.4 ERROR MEASUREMENT

In the error measurement, sixteen pulses after the beginning of the decrement eight pulses were selected. This avoids any initial transient. The duration of the eight pulses was compared with a sample of the same number from the drive signal, to produce the error signal which is proportional to the difference between decrement and drive signal durations. The circuit diagram for sampling the eight pulses from the drive signal (signal channel) is shown in Fig. 5.7. The figure also shows how the sample of eight pulses producing from the decrement channel.

5.4.1 Signal Channel

In this channel three D-type flip-flops were used to delay signal B by a period equal to eight pulses of the drive signal making three different edges of either polarity available. The S/16 waveform, as shown in Fig. 5.8(a), was used as a clock pulse for the first and third flip-flops, while the inverse of that waveform clocked the second flip-flop. The output of gate N_3 is a sample of eight pulses ($8 \times S$) duration of the drive signal.

5.4.2 Decrement Channel

As previously stated, the sinusoidal decrement signal is squared using a zero crossing comparator and then

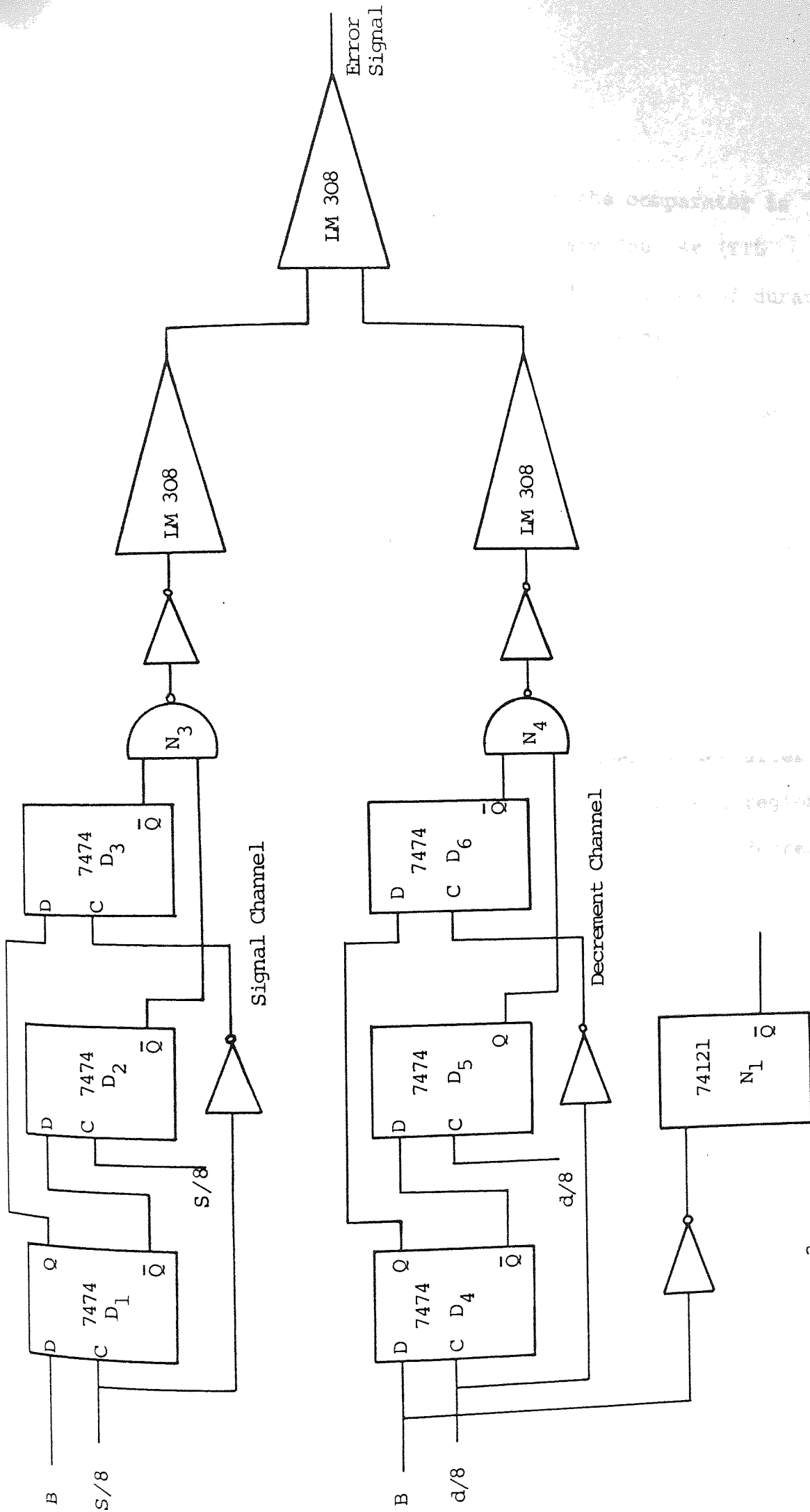


Fig. 5.7 The circuit diagram for sampling the eight pulses from the drive signal (signal channel), and the decrement channel for sampling eight pulses from the decrement

processing digitally. The output of the comparator is divided by sixteen using a 4-bit Binary Counter (TTL integrated circuit type 7493) to produce pulses of duration equal to eight pulses of the decrement ($8 \times D$).

The processing of this channel (Fig. 5.7) is the same as the drive channel. Another three D-type flip-flops were necessary. The $D/16$ waveform was used as a clock for the D_4 and D_6 flip-flops, while the inverse of that waveform was used to clock D_5 .

The output of gate N_4 is a sample of eight pulses ($8 \times D$) duration of the decrement. As in the drive channel the decrement sample was selected sixteen pulses after the start of the decrement to avoid the transient region between the end of the burst and the start of the decrement, as shown in Fig. 5.8(b).

5.5 THE CONTROL SYSTEM

5.5.1 Introduction

The function of the control system is to use the difference between the periodic sample of eight pulses of the decrement with the same number from the drive signal as an error signal. This is proportional to the difference between decrement and drive durations.

The two samples are applied to two separate integrators,

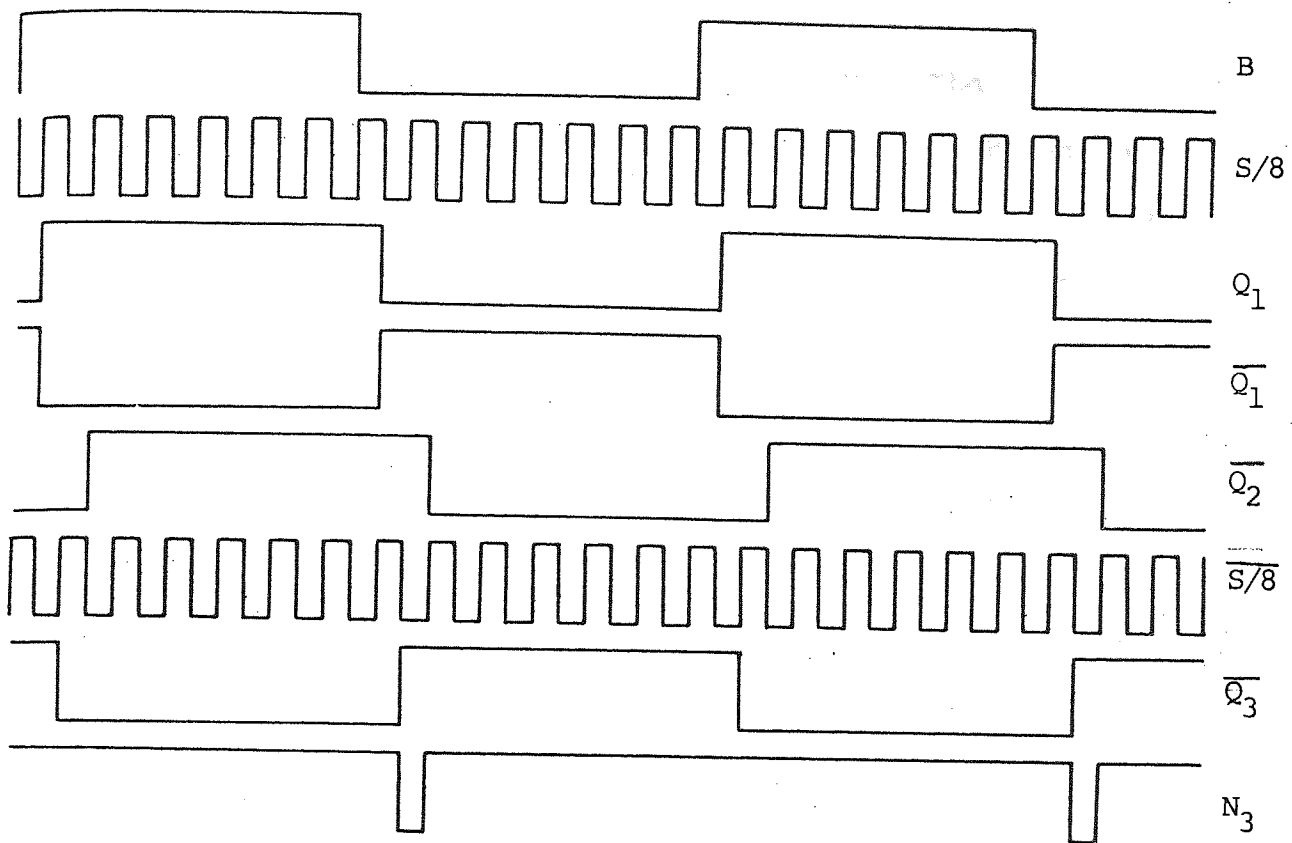


Fig. 5.8(a) Drive Signal Sample

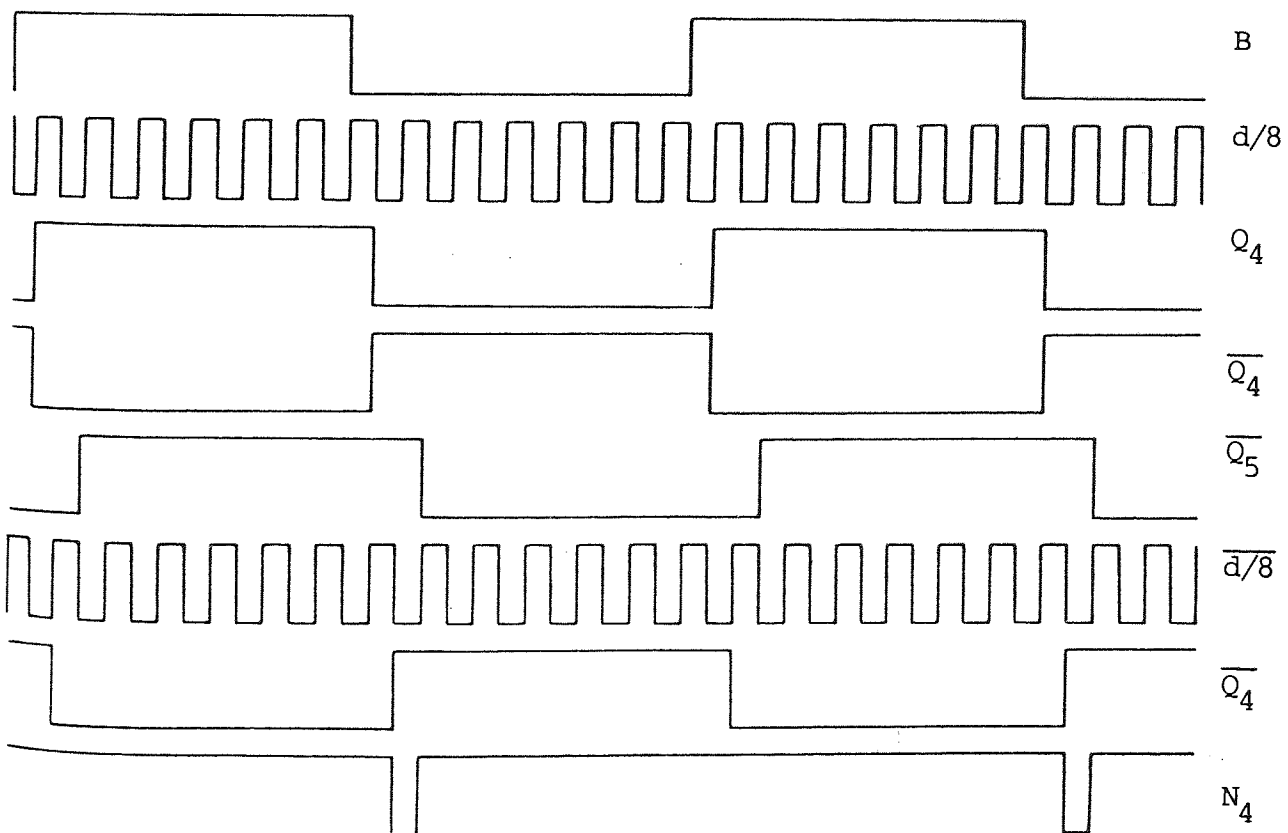


Fig. 5.8(b) Decrement Signal Sample

which act as time to voltage converters. The difference between these two voltages gives the error signal. Fig. 5.9 shows the two samples along with the decrement waveform - it also shows the output of the two integrators.

The values of the resistor and the capacitor in both integrators are exactly equal. Two pnp transistors were used to reset the output of the integrators by applying a negative going pulse (\bar{Q} of monostable M_1 in Fig. 5.7) to the bases of the transistor, switching them on transiently, shorting the integrator capacitor and setting the output voltage to virtually zero. The \bar{Q} of M_1 , the two samples and the output of the integrators are shown in Fig. 5.10.

The output of the two integrators are then applied to the inputs of a difference amplifier with a gain of about three which acts as a discriminator producing the error voltage. This error signal is further amplified by a factor of ten and then applied to a sample and hold integrated circuit type LF 398.

As the error signal this is now integrated over a number of recurrent cycles making the control a second order system. The integrator output makes the VCO period follow the variations in decrement period as it varies with the density of fluid or the viscosity. Fig. 5.11. shows a functional block diagram of the control system.

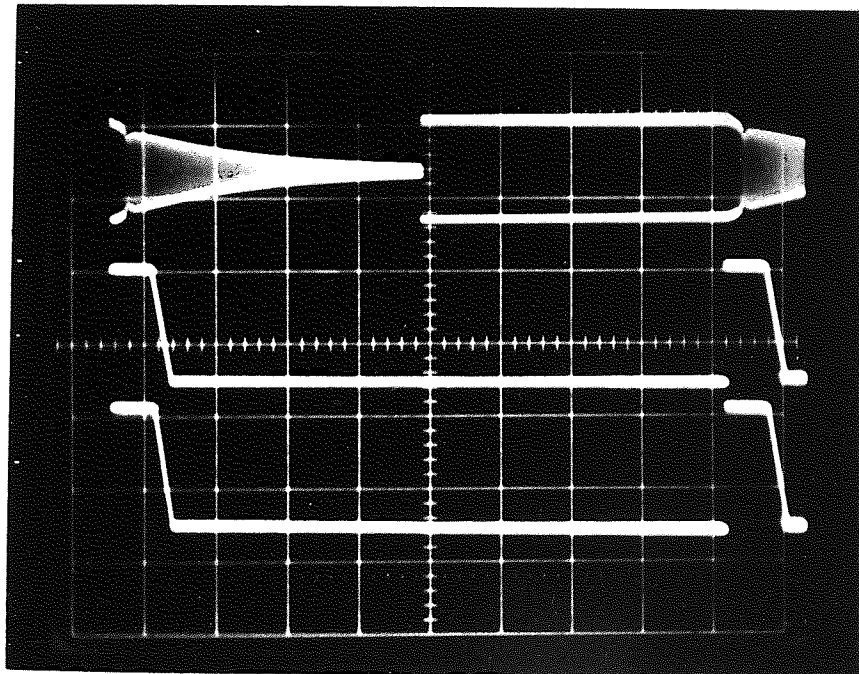
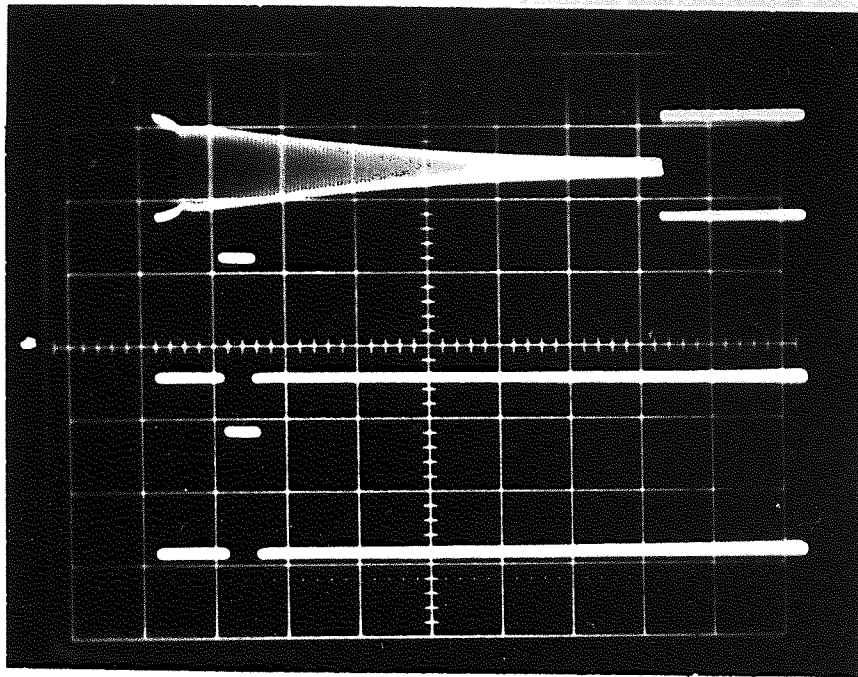


Fig. 5.9 The drive and decrement sample along with the decrement and the output of the two integrators.

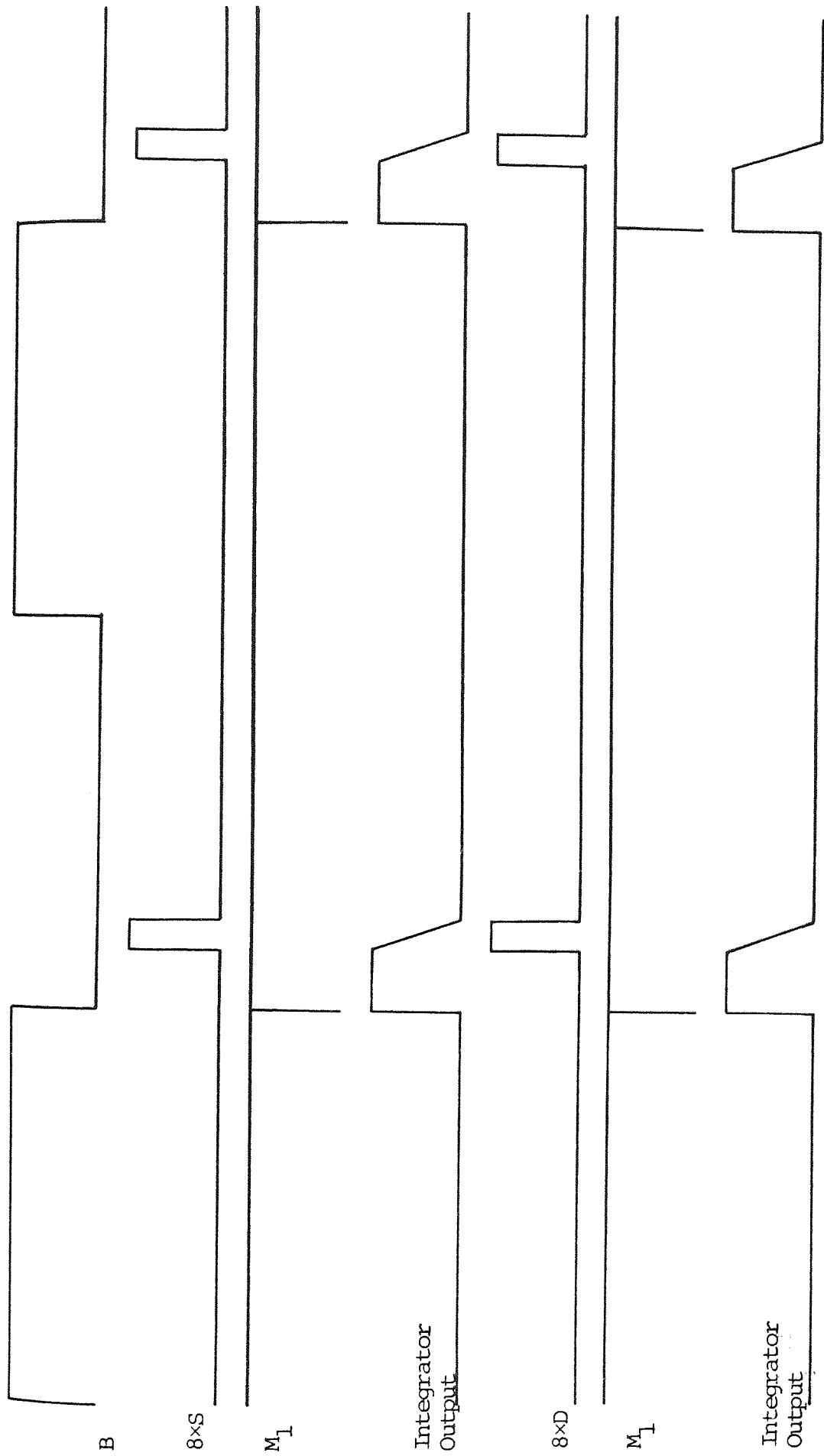


Fig. 5.10 Drive and decrement sample and the output of the two integrators.

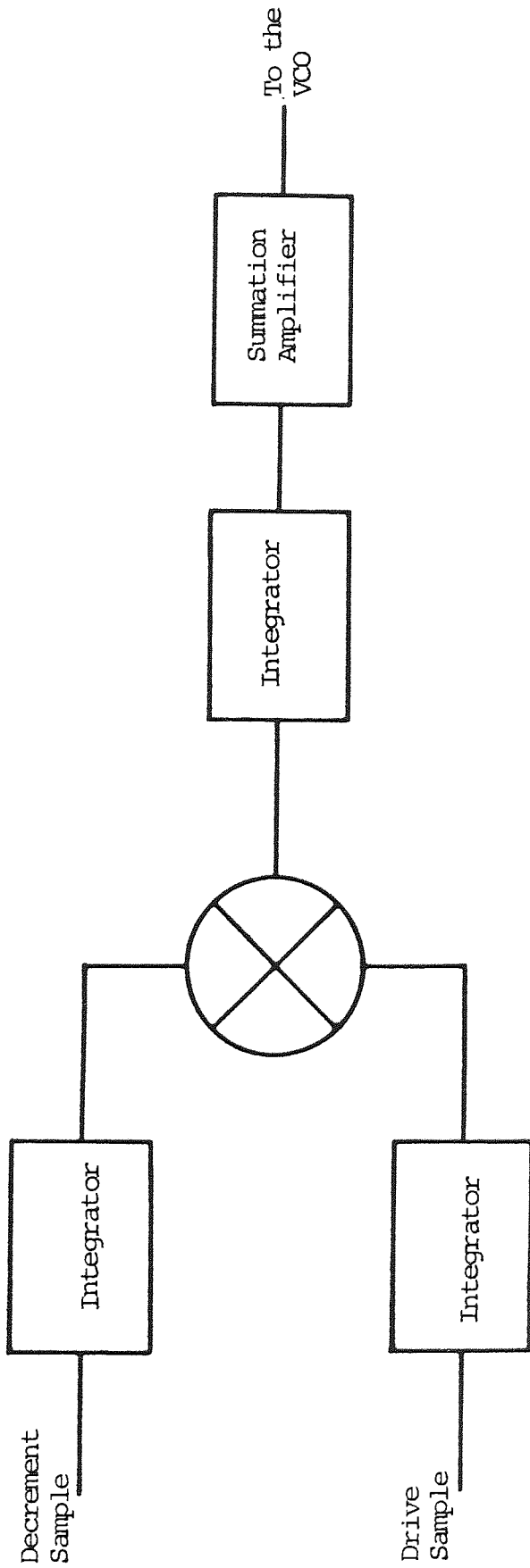


Fig. 5.11 Functional block diagram of the control system.

The control system as shown in Fig. 5.12 makes use of the following system in addition to the two integrators and the discriminator as discussed previously.

(1) Integrator

The error signal produced by the discriminator is integrated over a number of cycles to give a reasonably fast control of the VCO frequency. The integrator which is the essential part of the control loop (making it a second order system), consists of a low drift operational amplifier type LM 308 and a capacitor and resistor of high stability. It is operated in two different modes, in proportional control, a resistor is connected in parallel with the feedback capacitor, and in integral mode, only the capacitor is present. In the second mode the error signal (because it is reduced to zero by the control system) maintain the transducer at its true natural resonant frequency as shown in Fig. 5.13. This is the normal operational mode.

(2) Summation Amplifier

As stated above, the summation amplifier has two inputs, one from the manual control potentiometer and the other, the feedback voltage from the integrator (the error signal). Only a small signal is required to drive the VCO and in fact the summation amplifier reduces the manual control voltage by a factor of three and the

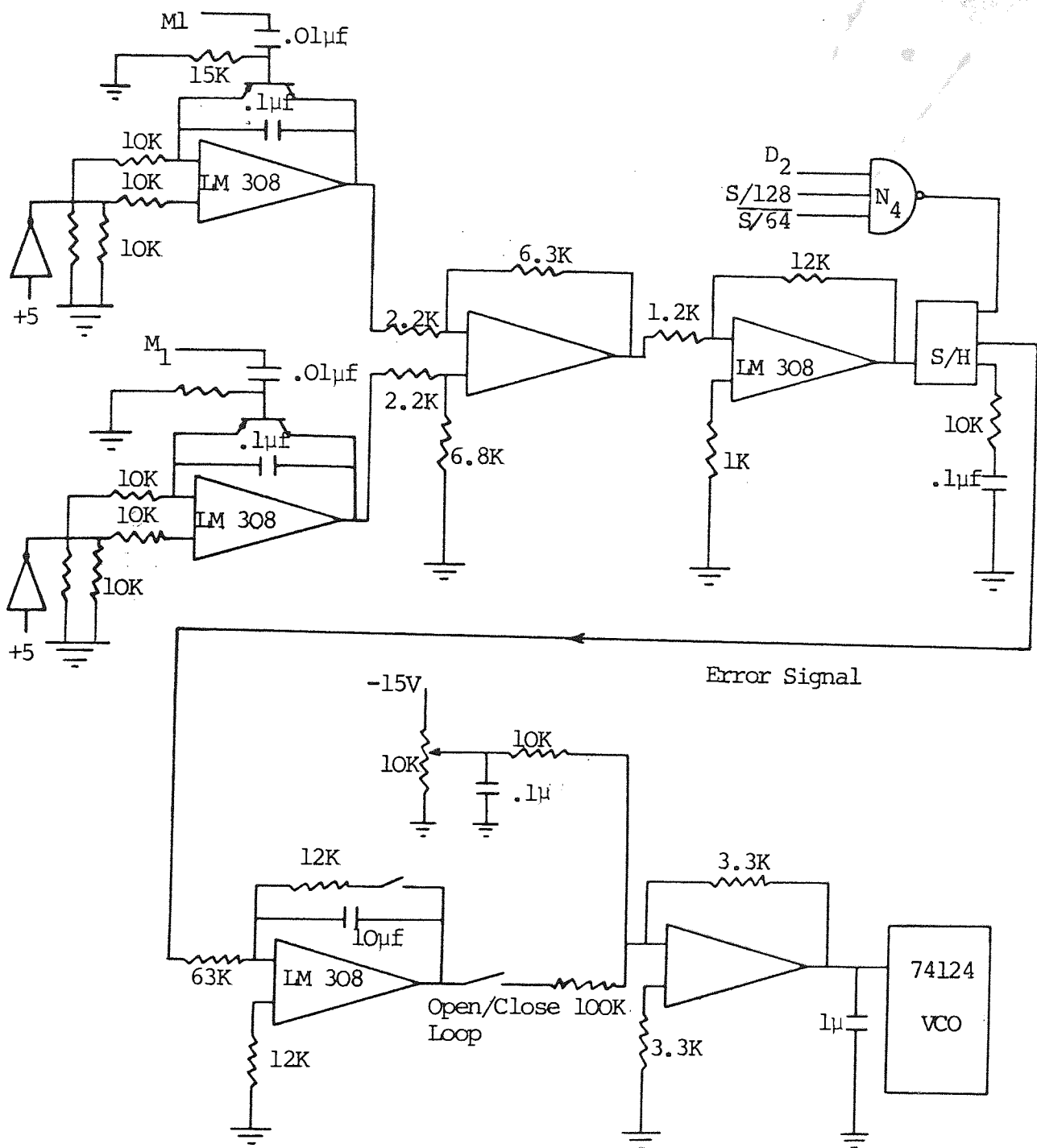


Fig. 5.12 Error Measurement Circuit

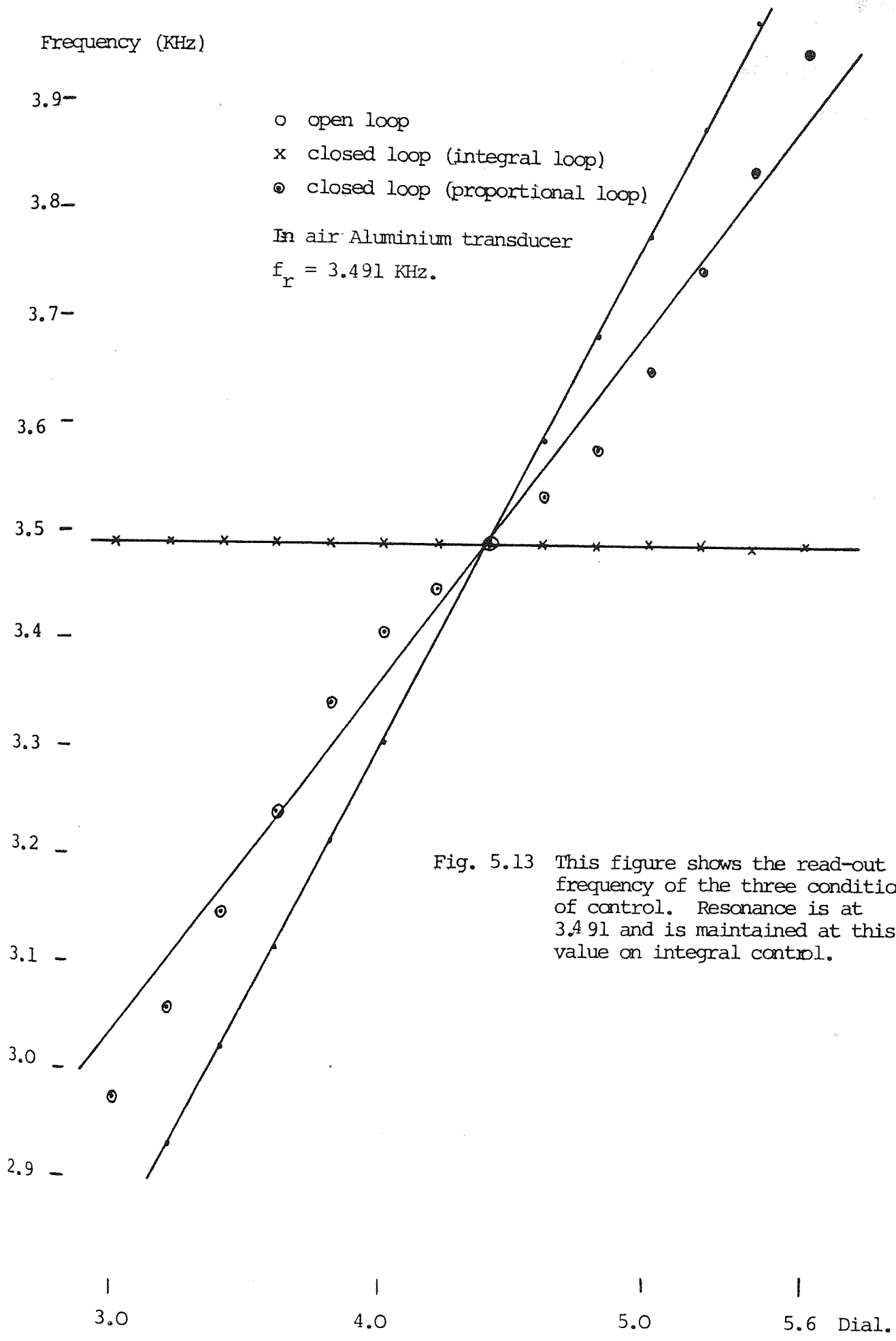


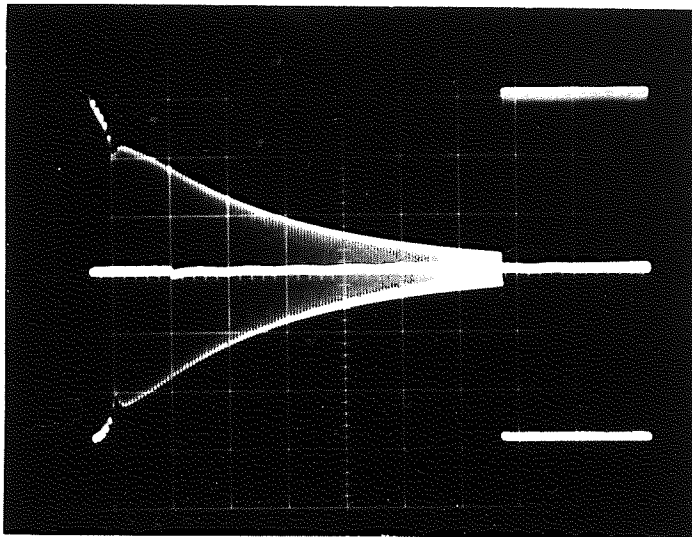
Fig. 5.13 This figure shows the read-out frequency of the three conditions of control. Resonance is at 3.491 and is maintained at this value on integral control.

feedback by thirty. The amplifier which is a standard integrated circuit type LM 308 inverting the signal making the overall feedback negative.

In the closed loop condition the voltage from the manual control and that from the integrator must combine to make the oscillator frequency that of the sensor. Any change in the manual control voltage will follow by a change in the error voltage at the response time of the system to keep the summation amplifier output constant. This is presented in Fig. 5.14 where the system was operating manually to drive aluminium transducers in air with frequency 3.584 KHz.

5.6 TRANSDUCER EVALUATION

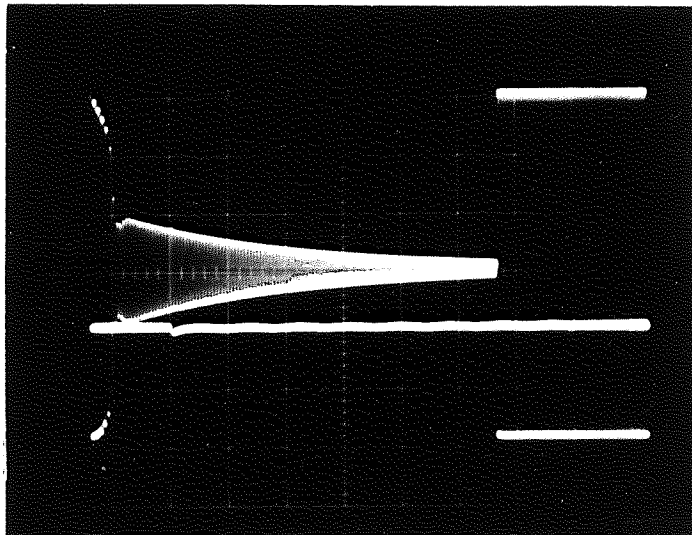
There are three parameters which mainly contribute to the effective performance of the transducer. These are the decrement signal amplitude which is used to obtain the error voltage, the actual value of the decrement itself and the frequency sensitivity i.e. the fractional change in frequency with fluid density. A good signal is essential to the efficient working of the electronic system. A high frequency sensitivity and a low decrement are conflicting requirements and geometrical designs which give a practical compromise were sought after. Typically, for a given transducer geometry, low density aluminium gives high sensitivity but a poor decrement.



3.584

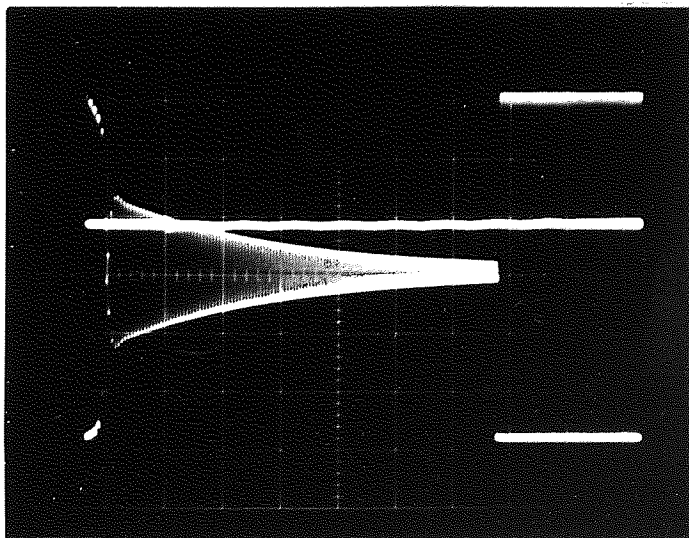
Zero error voltage
at resonance

$$f_r = 3584 \text{ Hz}$$



Negative error
voltage at high
frequency

$$f = 3617$$



Positive error voltage
at low frequency

$$f = 3561$$

Fig. 5.14 The decrement waveform and the error signal for aluminium transducer

Using steel reduces the sensitivity but provides a very usable decrement signal. In general, an increase in the scale of the transducer gives an overall improvement.

The major test applied to all transducers was to look at the magnitude of the frequency fluctuations in various liquids selected on a basis of density and viscosity. In effect, it measures the ultimate resolution of the instrument. This was done by taking the digital output of the frequency meter used and converting it to an analogue signal for use with an X-Y plotter. The results are shown graphically in the following figures.

Fig. 5.15 shows the frequency fluctuation for six 8 minute samples. The system was operated manually to drive aluminium transducers in air, water and oil. The very small variations in frequency of the VCO are associated with the instrument stability for the particular case.

Fig. 5.16 shows the frequency fluctuations for three 8 minute samples where each graph was calibrated for 100 Hz. Nickel silver transducer was used. The variation in frequency expressed gives the ultimate resolution of the instrument.

(a) The transducer is in air and has a natural frequency of 1.423 KHz.

(b) The transducer is immersed in oil and the frequency decreased to 1.255 KHz.

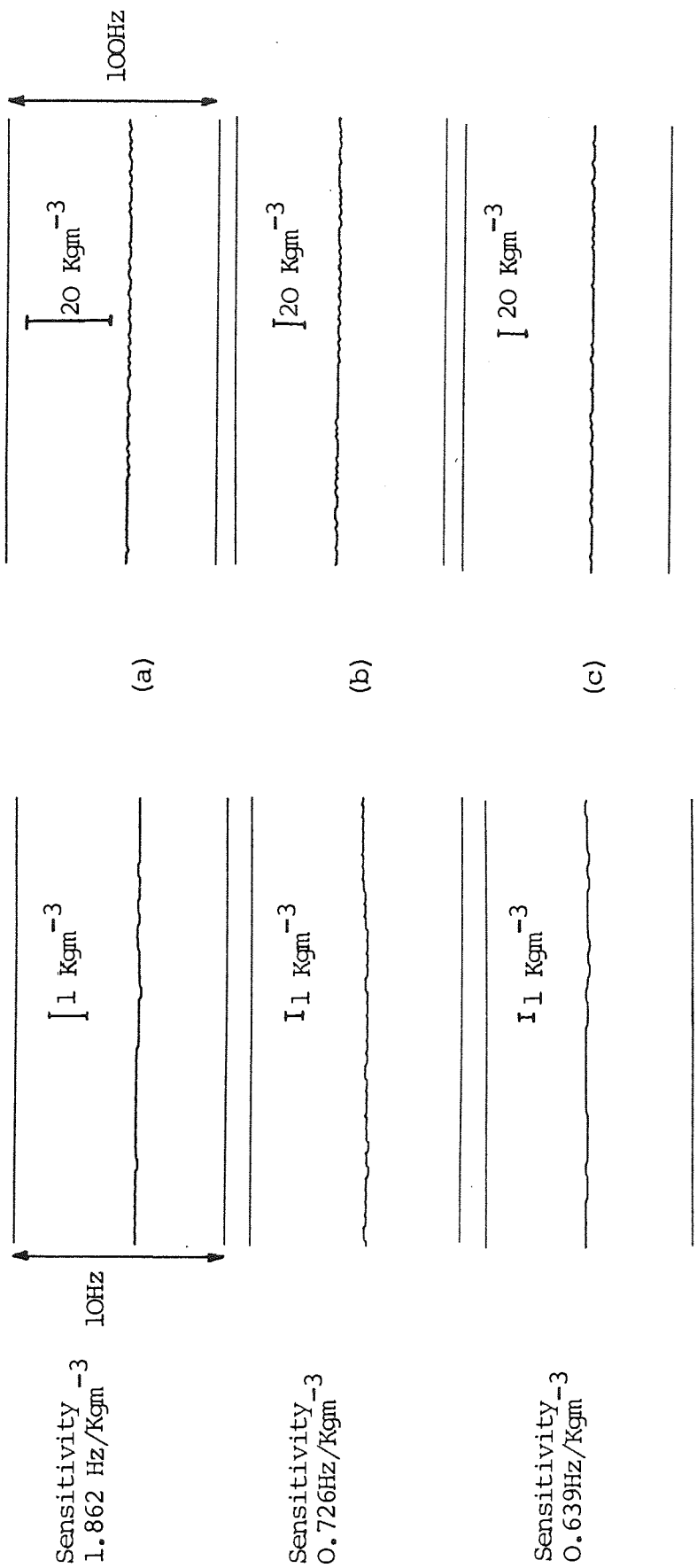


Fig. 5.15 Aluminium Transducer (1)

- (a) In air $f_r = 3581 \text{ Hz}$. 100 Hz corresponding to 53.7 Kgm^{-3}
- (b) In oil $f_r = 2621 \text{ Hz}$. 100 Hz corresponding to 138 Kgm^{-3}
- (c) In water $f_r = 2507 \text{ Hz}$. 100 Hz corresponding to 156 Kgm^{-3}

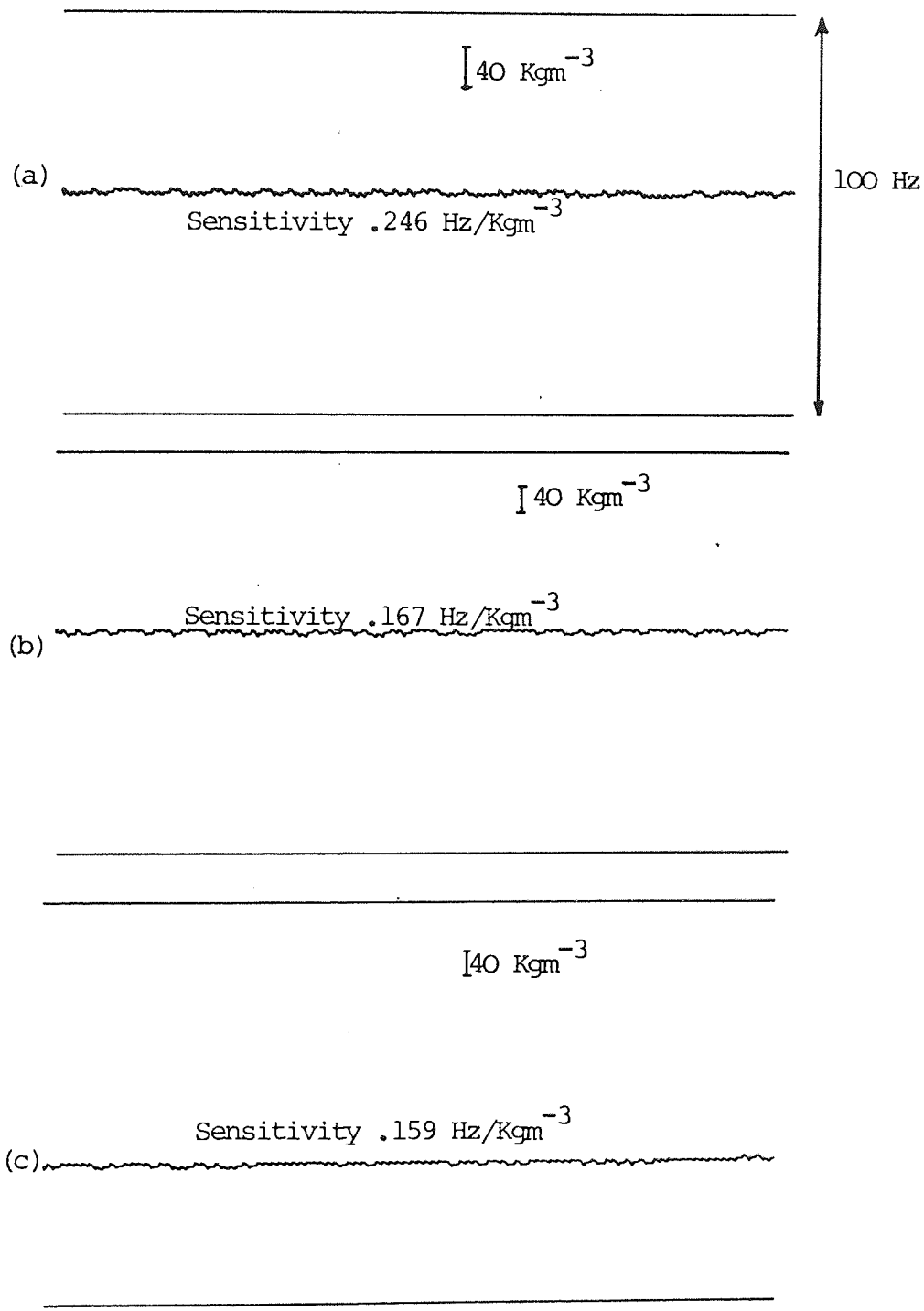


Fig. 5.16 Nickel silver transducer (2)

- (a) In air $f_r = 1423 \text{ Hz}$. 100 Hz corresponding to 407 Kgm^{-3}
- (b) In oil $f_r = 1255 \text{ Hz}$. 100 Hz corresponding to 600 Kgm^{-3}
- (c) In water $f_r = 1225 \text{ Hz}$. 100 Hz corresponding to 630 Kgm^{-3}

(c) The transducer is in water giving a frequency of 1.225 KHz.

Fig. 5.17 shows the frequency fluctuations for three 8 minute samples. The same transducer was used. Each graph was calibrated with parallel lines representing a 10 Hz change of frequency. The noise in the output represents the intrinsic noise of the transducer.

The second group of the experiments was carried out where the fluctuation at the output is greater than the instrumentation noise. This noise was due to the change in the density of liquid or the temperature of the transducer. These experiments investigate the ability of the system to track the natural frequency of the transducer during the whole period of the experiment and to observe any change in the measured parameter. The results are shown graphically in the following figures.

Fig. 5.18 shows the change in the density of the water, when an anti-freeze liquid was added to the water at a different time. An aluminium transducer ($\frac{1}{2}$ " square cross-section) with natural frequency 2.539 KHz in water was used. The graph was calibrated for 100 Hz which corresponds to 16 Kgm^{-3} .

Fig. 5.19 shows the change in the density of the water when a sugar solution was added to the water. The natural frequency of the nickel silver transducer which

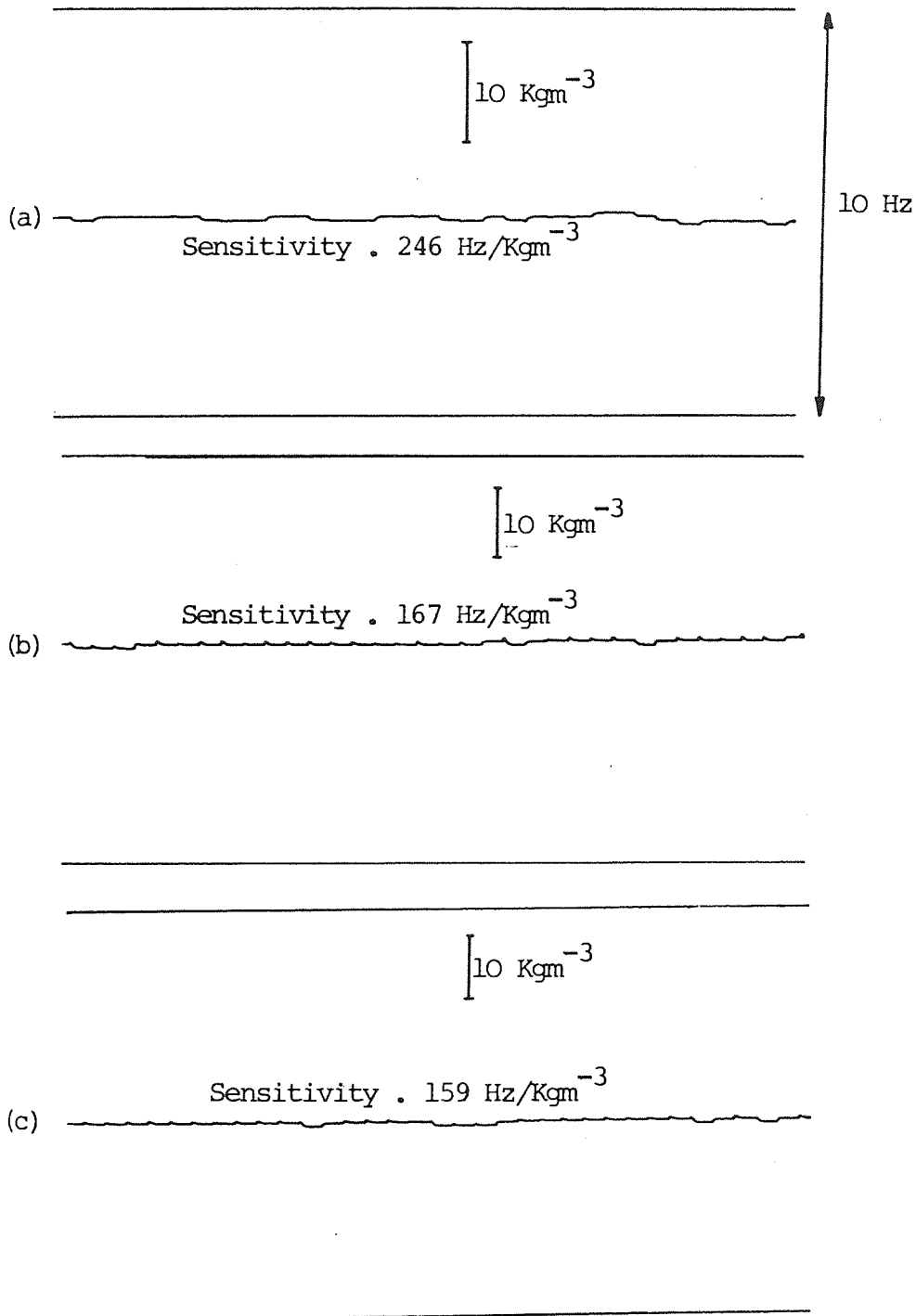


Fig. 5.17 Nickel silver transducer (2)

- (a) In air $f_r = 1423 \text{ Hz} \cdot 10 \text{ Hz}$ corresponding to 40.7 Kgm^{-3}
- (b) In oil $f_r = 1255 \text{ Hz} \cdot 10 \text{ Hz}$ corresponding to 59.9 Kgm^{-3}
- (c) In water $f_r = 1225 \text{ Hz} \cdot 10 \text{ Hz}$ corresponding to 62.9 Kgm^{-3}

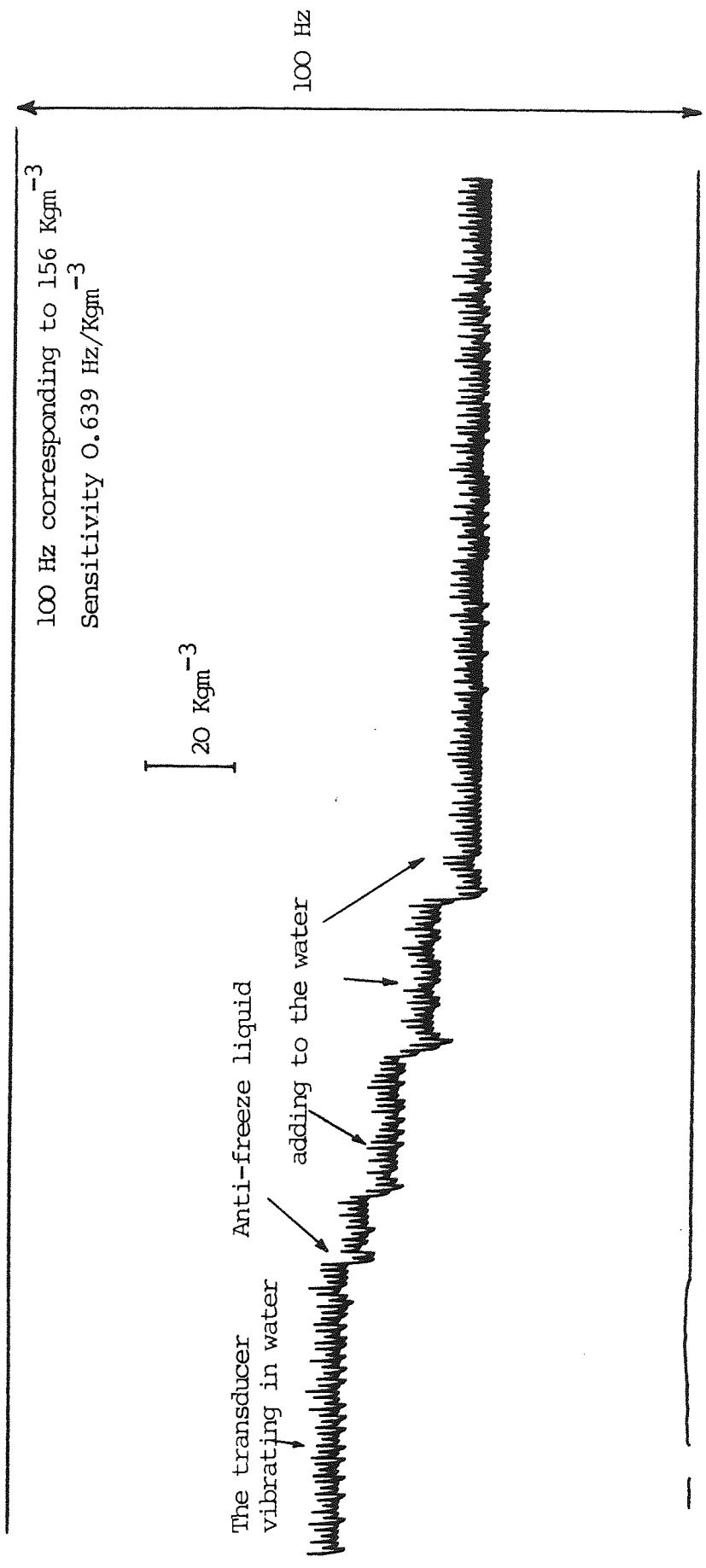


Fig. 5.18 Aluminium transducer (1) in water $f_r = 2539 \text{ Hz}$.

The change in the density of the water, when the anti-freeze liquid was added to the water.

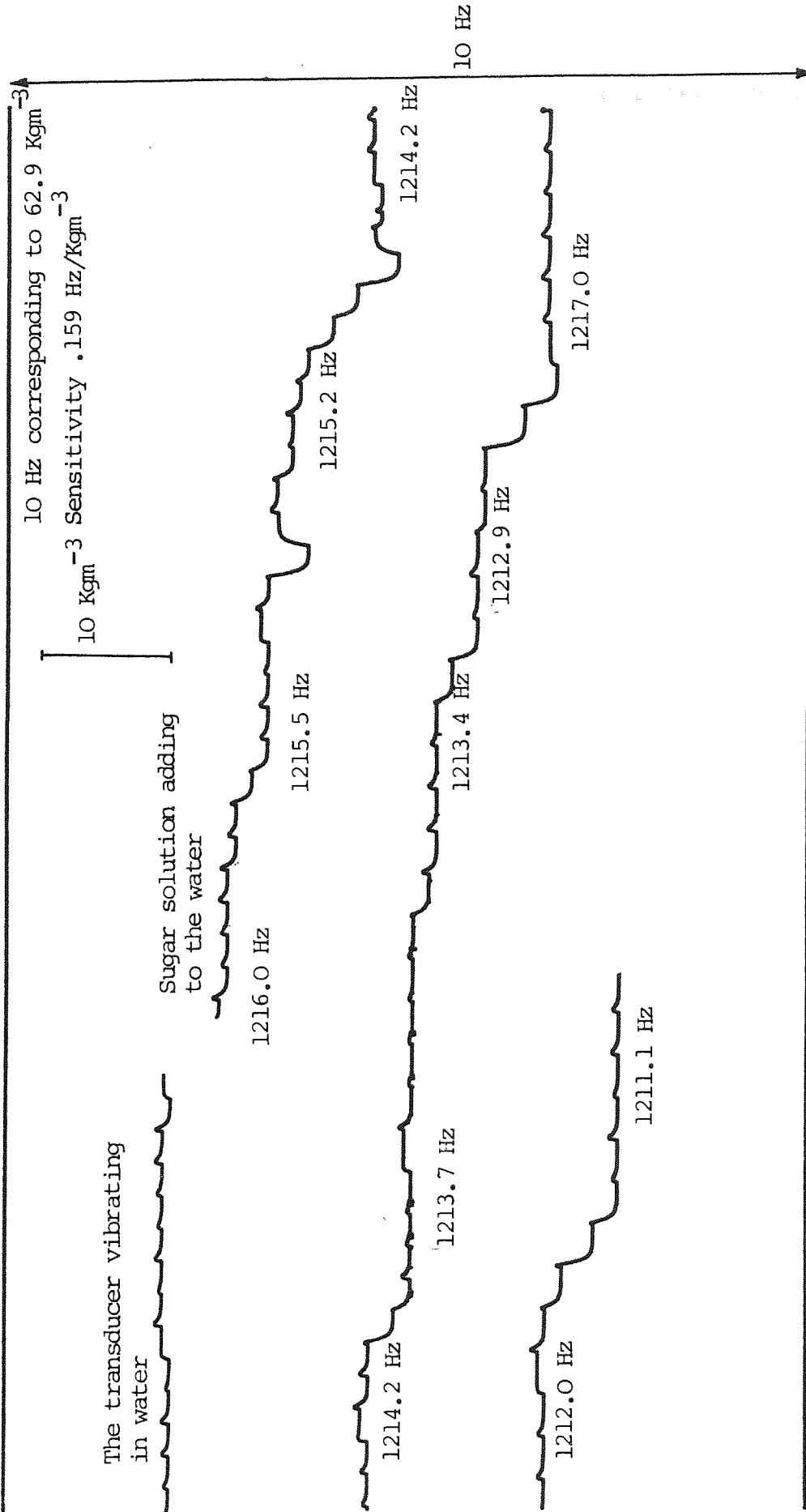


Fig. 5.19 Nickel silver transducer (2) in water $f_r = 1216.7 \text{ Hz}$.

The change in the density of water, when a sugar solution was added to the water.

was 1.217 KHz at the beginning of the experiment decreased with increasing the concentration of the sugar solution in water. The graph is calibrated for 10 Hz which corresponds to 63 Kgm^{-3} .

Fig. 5.20 shows the stability of the electronic system when it was operating automatically to drive the nickel silver transducer in oil and the oil was stirred $2\frac{1}{2}$ minutes after the start of the experiment. The stability of the graph, which was calibrated for 10 Hz, means that there was no disturbance to the transducer (there is no change in the density of the oil).

In general the elasticity and hence the frequency decreases as the temperature increases. In this case, the natural frequency of the transducer will change according to any variation in the temperature. This point is presented in Fig. 5.21 where the electronic system was operating automatically being controlled by the aluminium transducer at frequency 3.559 KHz in air.

From the above experiments, it will be noted that, there are two parameters affecting the transducer frequency. The parameters are, the density of the liquid and its temperature. Fig. 5.22 presents this situation, where an aluminium transducer was vibrating in hot oil. The frequency increased while the oil was cooling.

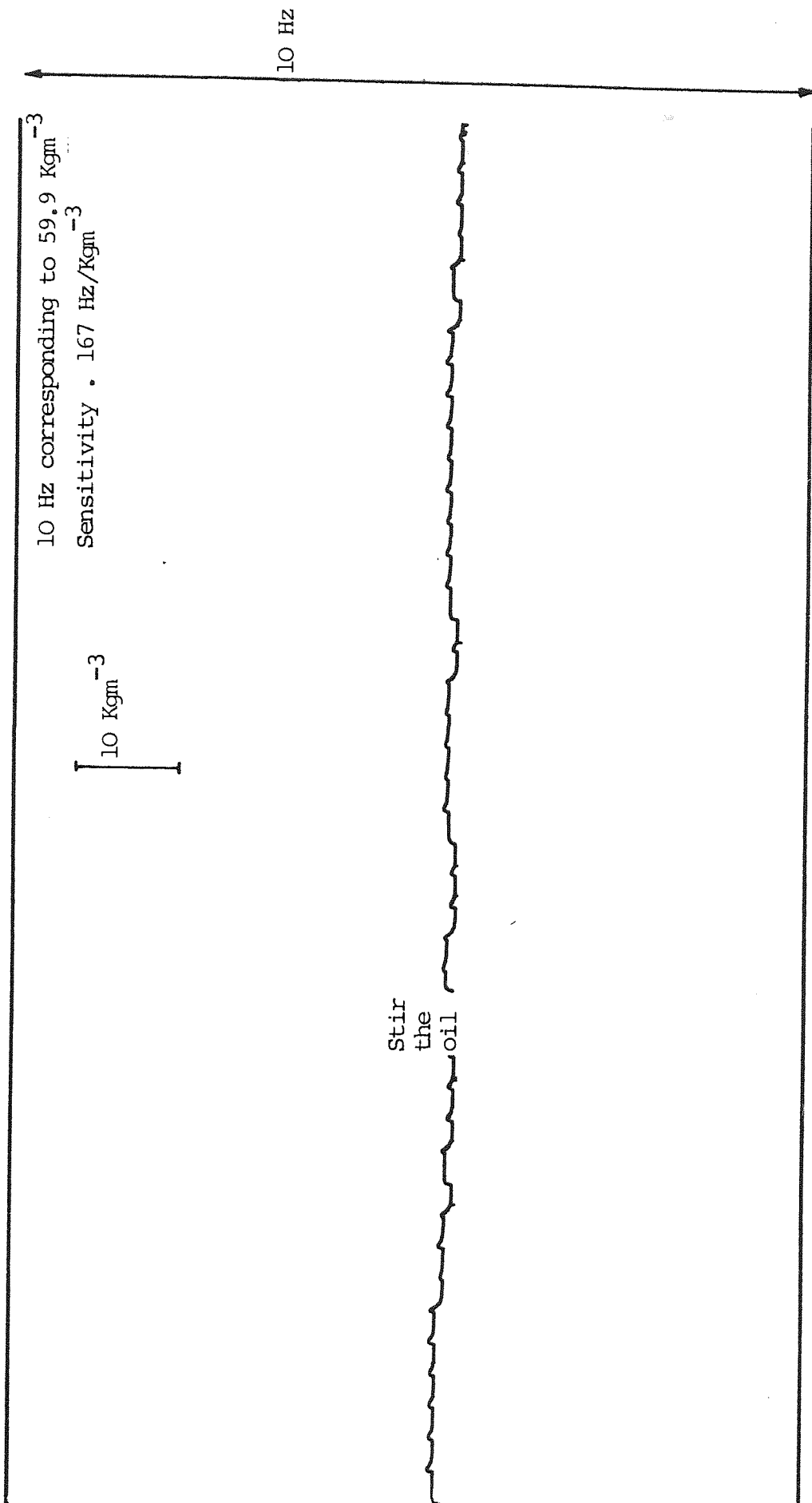


Fig. 5.20 Nickel silver transducer vibrating in oil $f_r = 1250 \text{ Hz}$.

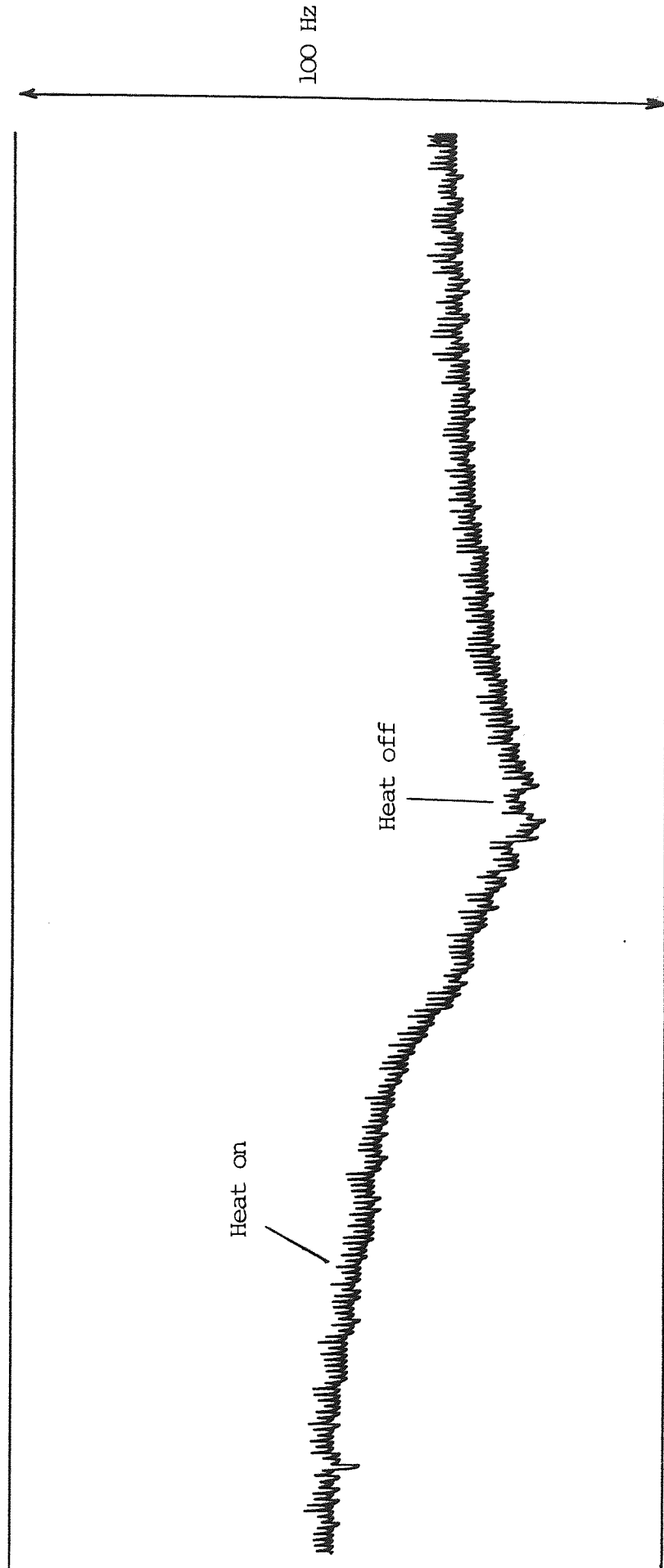


Fig. 5.21 Aluminium transducer (1) vibrating in air $f_r = 3560$ Hz.

The decrease in the frequency as the temperature increases is apparent.

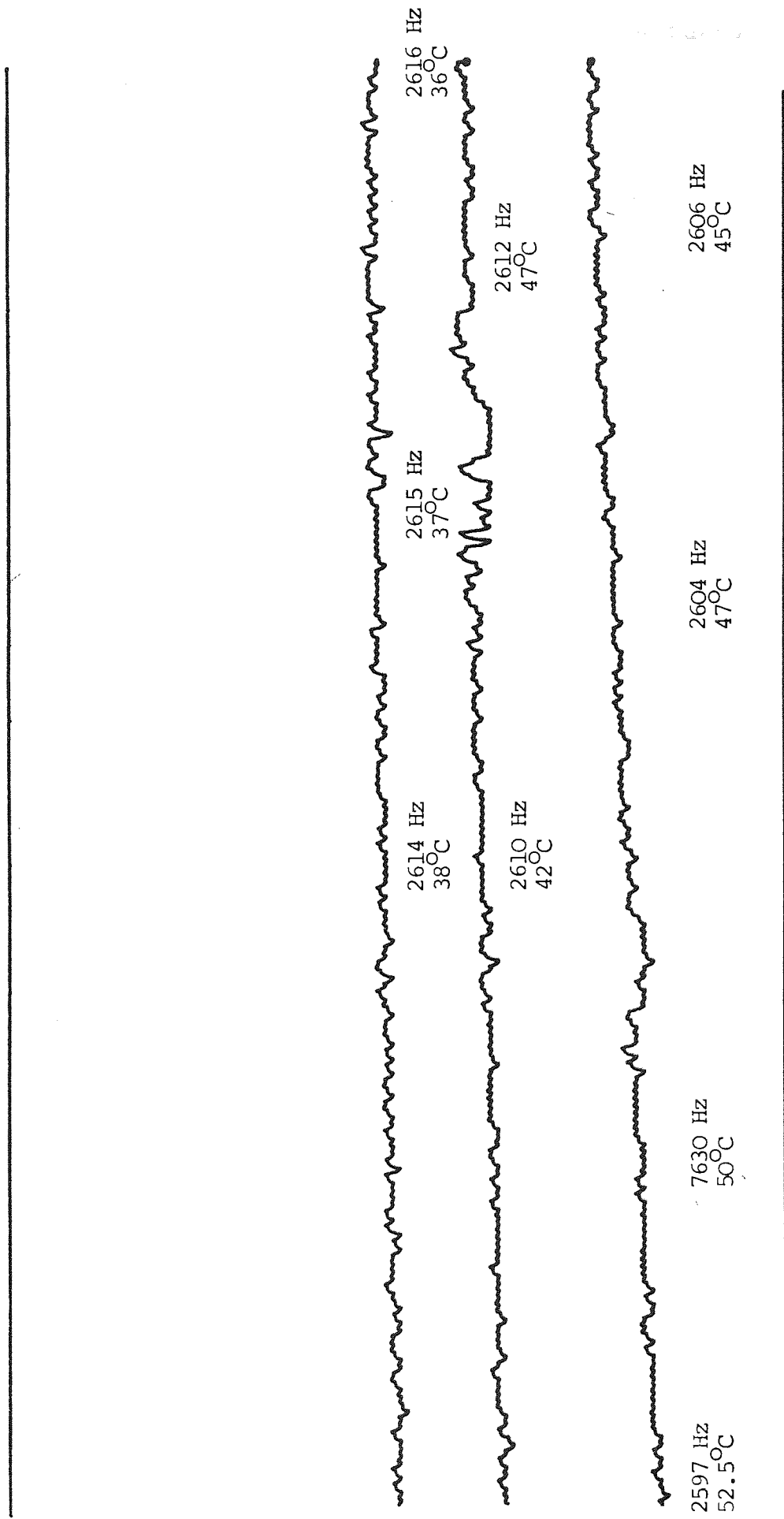


Fig. 5.22 Aluminium transducer (1) vibrating in hot oil.

The increase in the frequency as the oil cools down from 52.5°C to 36°C was 19 Hz.

It is possible to avoid any temperature perturbation on the density measurement by making the transducer from a material with very low temperature coefficient. These materials are not readily obtainable in the geometry required and are not necessarily compatible with the fluid to be measured.

CHAPTER 6

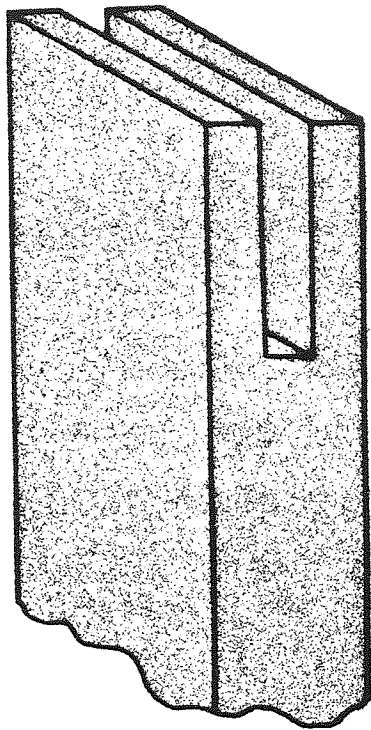
DENSITY AND VISCOSITY MEASUREMENT

6.1 INTRODUCTION

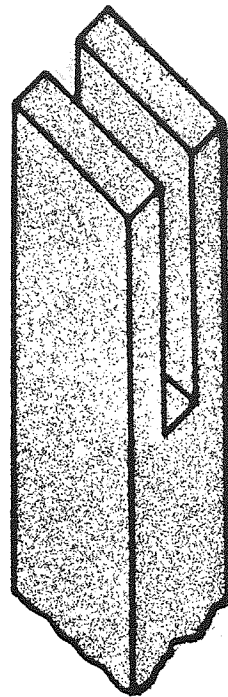
Various transducers using electromechanical resonators were developed in the past for the measurement of physical variables such as fluid density, fluid pressure, temperature, viscosity, etc. These have been reviewed in Chapter 1.

General views of particular resonator structure designed for density transducers are shown in Fig. 6.1. The sensing feature of these resonators is that a thin layer of fluid is trapped between the vibrating tines and becomes part of the resonator. Inertial loading due to the fluid movement lowers the resonant frequency. It is this feature of the design which improves by a large factor transducer sensitivity.

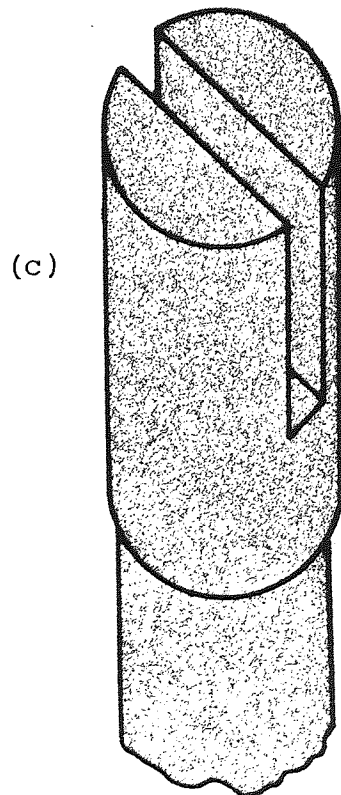
In the viscosity measurement where the width of the transducer is very small compared to the thickness (shown in Fig. 6.2), the pumping action between the tines is insignificant. The tine surfaces now vibrate parallel to themselves and the liquid constitutes a shear loading due to its viscous properties.



(a)



(b)



(c)

The thickness of the tines for (a) and (b) are equal to 6.25 mm while the width of (a) is double that of (b) (45mm). Transducer (c) is a rod of diameter 25.4 mm. The gap between the tines and the length of the tine are equal to 6.25 mm and 44 mm respectively.

Fig. 6.1 A general view of the liquid density transducer.

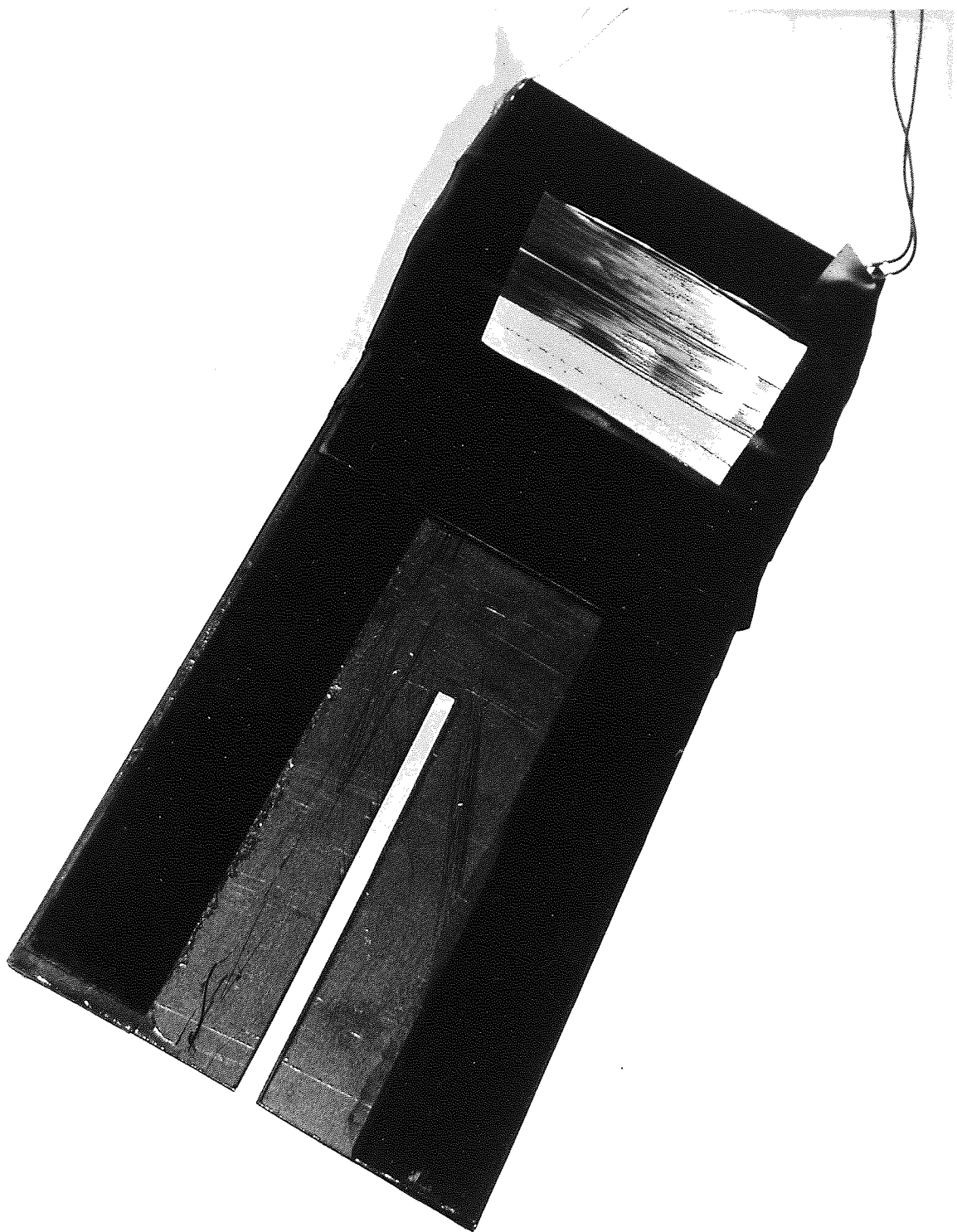


Fig. 6.2 Viscosity transducer design.

6.2 VIBRATING BODY - FLUID INTERACTION

When a vibrating body is immersed in a fluid medium, there are changes in the dynamics of the body due to loading effects of the fluid. This interaction may be used as a basis for designing density transducers. In the past, several such transducers were built with different structures of resonators giving various degrees of success, as discussed in Chapter 1. While based on the same fundamental principle, the present structures have been designed to give large improvement in transducer sensitivity, and at the same time improve the robustness and simplicity.

There are three main classifications that may be given to the loading effects on the structure due to this interaction.

(a) Reactive Loading

A resonator sets the fluid into motion and thus stores additional kinetic energy in the liquid which has a consequent inertia reaction on the resonator dynamics. This effectively is an apparent increase in the mass of the body and results in a decrease in the resonant frequency.

The reactive loading may be expressed by an equation of the form:-

$$\omega_o^2 = \frac{K_e + \Delta k}{M_e + \Delta m} \quad (6.1)$$

where

ω_o is a natural frequency of the resonator.

K_e is the stiffness.

M_e is the mass of its corresponding in vacuum equivalent lumped circuit.

Δk is the effective change in stiffness due to loading.

Δm is the effective change in mass due to loading.

From equation (6.1) it can be seen that there could be a stiffness loading, due to compression of the liquid which raises the resonant frequency. The resultant change depends upon the relative values of Δm and Δk . Δm is related directly to the density of the liquid. Thus a predominant mass effect (negligible stiffness) is the desirable design criterion. This is achieved by choosing a geometry such that the acoustic wavelength at the resonant frequency is very large compared to the resonator dimensions. Δk is then negligible as are acoustic radiation effects.

(b) Sound Radiation Loading

Some energy is radiated away from the resonator in the form of sound. It has a damping effect on the body but, more significantly, can cause standing waves which

change the resonance in a way which is difficult to predict.

The wavelength of sound in the liquid should be considerably larger than the geometrical dimensions of the vibrating body to minimise acoustic effects. The use of flexural resonators simplifies this requirement, Lame (1921), Junger (1972). In view of the above comments, the double resonators were designed to operate at low frequencies (typically below 5 KHz). The low frequency also increases the magnitude of the mass effect. The interpretation given by Junger (1952) is that, at high frequencies the resonator vibrates with such rapidity that the disturbance does not travel far before the action is reversed, whereas with low frequency the resonator tends to accelerate larger quantities of fluid. Again this low frequency helps to keep the unwanted loss due to sound radiation loading at a low value.

Analysis indicates that at low frequencies the mass effect is normally highest at the fundamental flexural mode of vibration of the resonator, Lax (1944). This being the lowest frequency mode also favours geometrical designs. Another practical advantage of this mode is its large frequency separation from other modes.

(c) Viscous Loading

This is the principle of operation of the vibrating transducer to measure viscosity. The motion of the resonator in the fluid induces an alternating shear force which has both a damping and inertial effect on the resonator. The viscosity makes the liquid move with the vibrating surfaces.

The magnitude of the three above mentioned effects depends on such factors as geometrical dimensions and structural configurations of the body, mode of vibration, frequency of resonance and physical properties of the fluid.

6.3 DRIVING TECHNIQUES

Various techniques can be found in the literature for driving and pick-up from a mechanical system. Methods include electromagnetic, magnetostrictive, piezoelectric and electrostatic. Any particular technique has its merits and demerits, depending upon the particular situation. Coupling efficiency, effect on Q-factor of the resonator and mechanical simplicity are some important features which generally influence the choice. A brief discussion of them in context to the present resonator follows:

(a) Coupling Efficiency

Coupling efficiency may be defined as the ratio of

the power picked up from the resonator to the power utilised for driving it. Thus the more the coupling efficiency, the less power is required to maintain the oscillation. In this respect the driving method presented in Chapter 5 seems to be superior to the piezoelectric method which, although it has the higher coupling efficiency, the presence of the crystal lowers the Q by an overwhelming amount.

(b) Mechanical Simplicity

In this respect again the drive and receiver methods seems to have some advantages. The positioning of the two coils (drive and receive) is not so stringent as in the traditional electromagnetic and electrostatic units. In the piezoelectric method, the small drive and pick-up elements can be bonded on the resonator, but the two elements being voltage operated must be insulated for the liquid measurements.

(c) Effect on the Q-factor of the Resonator

The transducer system is essentially an electronic oscillator using the mechanical resonator as the frequency controlling element. Therefore, keeping the Q-factor of the resonator at a reasonable value has several important advantages. Firstly, the energy required to maintain the system oscillating is kept low which, reduces heat

dissipation and power demand. Design problems are potentially simpler for the electronic system when using the PLL as a controller rather than the present error determining method.

In this respect both electromagnetic and electrostatic methods are better than piezoelectric. As in the former two cases there is no mechanical contact with the resonator, therefore the Q-factor is virtually unaffected. In the latter case, however, the piezoelectric elements are to be directly bonded to the resonator and thereby the Q-factor is adversely affected.

The factors that are responsible for overall signal performance may be classified into two broad divisions. The first includes losses in the mechanical and electromechanical systems.

These losses are due to

- (a) the internal friction of the resonator material,
- (b) signal loss due to coupling.

Choosing the resonator material has an important factor on the stability and the sensitivity of the system. It is quite evident that the lighter the resonator material, the more will be the sensitivity of the transducer. Preliminary experiments performed with resonators made of aluminium and stainless steel have supported this feature. However, the consideration of the internal friction and

temperature coefficient are very important where the minimisation of the loss in the resonator is a vital criterion for the transducer.

To overcome the unwanted temperature effect, a material with very small thermal coefficient is desirable, otherwise a compensating system is to be incorporated. Therefore a material having the properties of low internal friction and low temperature coefficient may be used. Fused quartz which is a low density material with very low internal friction and virtually zero temperature coefficient would be ideal. Other materials may be used, for example Solartron Limited uses Ni-span-C902 for both their gas and liquid density transducers.

Nickel-iron-cobalt alloys also have low temperature coefficients.

However because of the ease in machining and nickel plating aluminium, nickel silver alloy and stainless steel transducers have been used in most of the initial experimental work. Aluminium has a low density ($2.71 \times 10^3 \text{ Kg m}^{-3}$) and low internal friction but it has a high temperature coefficient (320 ppm/Kelvin). Nickel silver and stainless steel have a high density $8.5 \times 10^3 \text{ Kg m}^{-3}$ and $7.9 \times 10^3 \text{ Kg m}^{-3}$ respectively, but they have lower temperature coefficients, (180 ppm/Kelvin) and (120 ppm/Kelvin). respectively. Both materials have low internal friction.

In the present driving technique the only thing that may affect the Q-factor of the resonator is the way of attaching the magnetostrictive strips at the tines. After a number of tests it was found that a thermosetting bond or direct electroplating was the most satisfactory way of securing the nickel drive. This gave a very stable mechanical and electrical performance.

In the second the losses are due to acoustic radiation and viscosity.

It is a well established fact that the acoustic energy radiated by a resonator decreases as the ratio of its geometrical dimension to the wavelength of sound in the fluid decreases. As already mentioned this ratio has been designed to be small making the loss minimal.

As the thin layer of liquid is set into motion there is a considerable viscous loss. In fact it has been found that this is a dominant factor in determining Q of any resonator immersed in a liquid.

A series of measurements were carried out using different resonators vibrating in air and different liquids to measure the Q-factor (as will be discussed later). Many experiments have also been carried out by Hassan (1980) in air and vacuum for the same purpose. Thus the decrease in Q can be taken as a measure of the viscous loss. The transducer as designed could be made to give a viscosity

as well as a density readout, either by direct measurement of decrement or by signal level in the electronic control loop.

6.4 THEORETICAL CONSIDERATION

6.4.1 Introduction

For the analysis of the interaction problem various techniques can be found in the literature. Two techniques impedance and energy methods are widely adopted and suitable, particularly for finding the loading effects on the body which are of primary concern in the present work. A brief discussion of the two techniques and a review of the loading effects on some structures has been reported by Hassan (1980).

A rigorous theoretical analysis of the interaction problem for the rectangular geometry chosen together with viscosity and acoustic radiation is too difficult to be of value. Thus a normal procedure in the literature is to solve a particular case under some consistent assumptions and approximations, thereby simplifying the situation.

The present resonator as well as the disc resonator has been analysed under similar general assumptions and approximations. The assumptions for each particular resonator will be discussed later. These general assumptions are:-

(1) The fluid viscosity is negligible and only the mass loading between the tines is considered. Thereby, the analysis will give a formulation only for the change in frequency of the resonator (which is of course the primary object of the present work).

(2) The frequency of oscillation is low (typically below 5 KHz) so that the wavelength in the fluid is much greater than the geometrical dimensions of the resonator. Therefore the loss and standing wave effects due to the radiation of sound is also negligible. Thus the analysis has been carried out taking only fluid mass loading on the resonator.

6.4.2 Centre Clamped Circular Plates; (Antiresonant Mode)

This case is taken since it is reported most extensively in the literature. It is the polar equivalent of a tuning fork. This is because of the fact that the symmetry of a resonator helps to simplify the analysis while the lack of symmetry of the present transducer (rectangular tuning fork) makes it extremely difficult. To simplify the problem some assumptions and approximations have already been discussed.

It is assumed that two rigid circular discs are clamped at the centre as shown in Fig. 6.3. By considering the clamped centre and free perimeter and the flexural

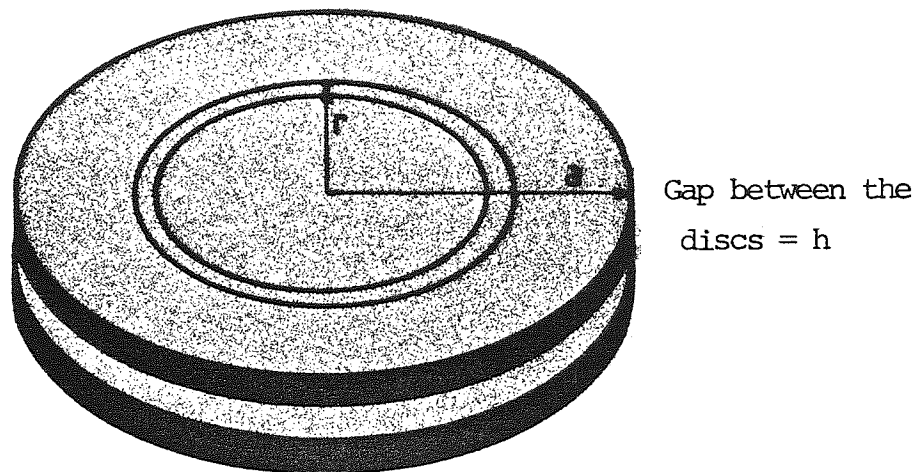


Fig. 6.3 Centre clamped circular plates (circular tuning fork).

mode of vibration they may be classified as a type of tuning fork.

The volume of liquid within radius r is given by

$$V = \pi r^2 h \quad (6.2)$$

where h is the gap between the two discs.

Differentiate equation (6.2) with respect to time

$$0 = 2\pi r h \dot{r} + \pi r^2 \dot{h} \quad (6.3)$$

Velocity magnification can be defined from equation (6.3) as

$$\frac{\dot{r}}{\dot{h}} = -\frac{r}{2h} \quad (6.4)$$

The Kinetic energy of an annular ring considered between r and $r+\Delta r$ is given by

$$\text{K.E.} = \frac{1}{2} (2\pi r h \Delta r \rho_l) \dot{r}^2 \quad (6.5a)$$

$$= \frac{1}{2} (2\pi r h \Delta r \rho_l) \frac{r^2}{4h^2} \dot{h}_r^2 \quad (6.5b)$$

The total Kinetic energy of the liquid between the discs is given by

$$\text{Total K.E.} = \int_0^a \frac{1}{2} \left(\frac{\pi \Delta r \rho_l r^5}{2ha^2} \right) \dot{h}_a^2 \quad (6.6)$$

where a is the radius of the disc

$$\dot{h}_r = \dot{h}_a \left(\frac{r}{a} \right)^2$$

Therefore the total Kinetic energy can be found from equation (6.6) as

$$\text{Total K.E.} = \frac{1}{2} \left(\frac{\pi \rho_l a^4}{12h} \right) \dot{h}_a^2 \quad (6.7)$$

The term in the brackets is the dynamic mass of the

fluid. The actual fluid mass is given as

$$\pi a^2 h \rho_{\ell} \quad (6.8)$$

From equations (6.7) and (6.8) the mass magnification (which is defined as dynamic mass/ actual mass) can be found in terms of the radius of the resonator and the gap between the tines as

$$\text{mass magnification} = \frac{1}{12} \left(\frac{a}{h} \right)^2 \quad (6.9)$$

It may be mentioned here that in terms of added mass Δm , the change in frequency is given by the expression (6.10) which is derived from equation (6.1).

$$\frac{f_{\ell}}{f_0} = \frac{1}{\sqrt{1 + \frac{\Delta m}{M}}} \quad (6.10)$$

where

f_{ℓ} = frequency in the fluid

f_0 = frequency in air

M = dynamic mass of the plate

Δm = the added mass due to the fluid loading.

It is possible to find the dynamic mass of the resonator by the same analytical method, as will be discussed later for the rectangular tuning fork only.

It will be noted that equation (6.10) can be used for calibration when put in the form of equation (6.11) where

K_0 is a measure of the sensitivity

$$\rho_\ell = \left| \left(\frac{f_0}{f_\ell} \right)^2 - 1 \right| \frac{1}{K_0} \quad (6.11)$$

6.4.3 The Fluid Loading Effects in Practical Designs

In the analysis of the circular resonator the added mass (Δm) due to the loading effect of the fluid was obtained as

$$\Delta m = \frac{\pi a^4}{12h} \rho_\ell \quad (6.12)$$

where

- ρ_ℓ = fluid density
- a = radius of the discs
- h = gap between the discs

In the case of the rectangular resonator, two separate cases can be considered for the analysis of the interaction problem. In the first case, the tuning fork is narrow compared to the length, and the fluid is assumed to move laterally while in the second case the tuning fork is wide and the fluid movement is in length only. The two cases will be analysed below.

6.4.3.a Fluid Loading Effects on the Narrow Tuning Fork

As mentioned above, in addition to the general assumption and approximation discussed in section 6.4 to

analyse the interaction problem, the fluid between the tines is pumped laterally only.

By considering the tuning fork, Fig. 6.4, and a short segment Δy of the liquid. The mass of fluid trapped between $x=0$ and x is given by

$$\text{Mass} = \Delta y h x \rho_l \quad (6.13)$$

Assuming that the fluid is incompressible, as h changes x will change, the velocity magnification can be obtained by differentiating equation (6.13) with respect to time

$$\frac{\dot{x}}{\dot{h}} = - \frac{x}{h} \quad (6.14)$$

The Kinetic energy of an element Δx is obtained by

$$\text{K.E.} = \frac{1}{2} (\Delta x \Delta y h \rho_l \frac{x^2}{h}) \dot{h}^2 \quad (6.15)$$

The total K.E. of the short segment Δy of the fluid, can be obtained by integrating equation (6.15) between $-\frac{w}{2}$ and $+\frac{w}{2}$, where w is the width of the transducer.

$$\text{Total K.E.} = \int_{-w/2}^{+w/2} \frac{1}{2} (\Delta x \Delta y \rho_l \frac{x^2}{h}) \dot{h}^2 \quad (6.16)$$

$$= \frac{1}{2} \left(\frac{\Delta y \rho_l w^3}{12h} \right) \dot{h}^2 \quad (6.17)$$

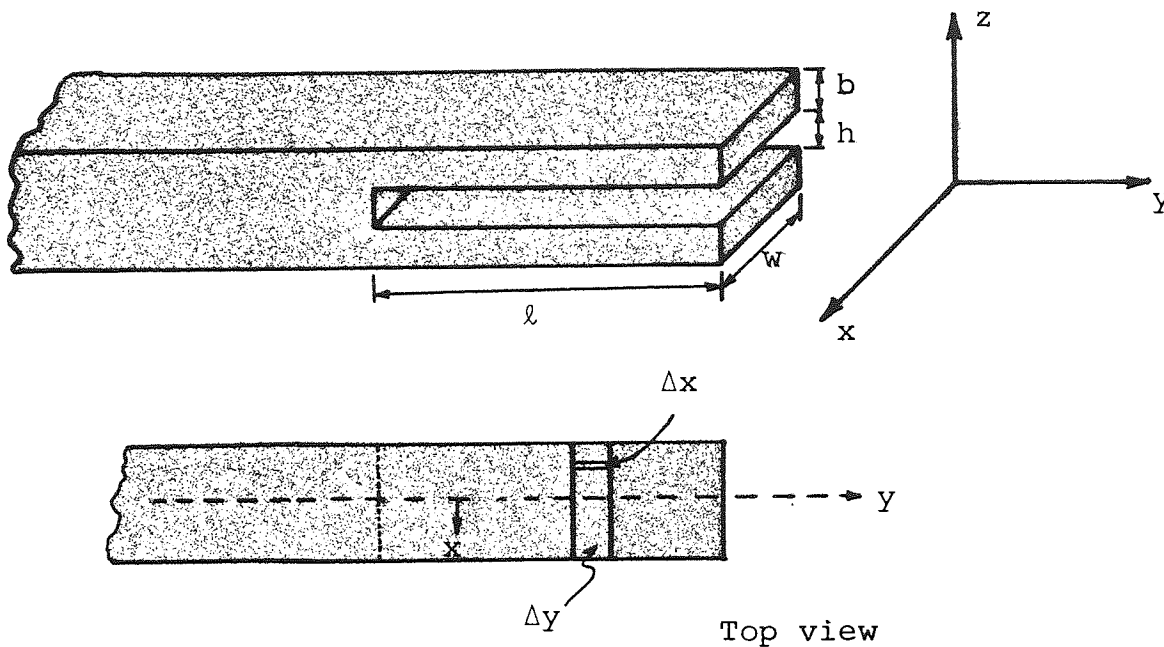


Fig. 6.4 Narrow tuning fork. In this design the fluid between the tines assumed to pump laterally only.

The term in the brackets is the dynamic mass of fluid of the short segment Δy , while its actual mass is $\Delta y w h \rho_l$.

To obtain the total K.E. of the fluid between the tines, equation (6.17) must be integrated from $y=0$ to $y=l$ assuming the vibration profile along the length is

$$\dot{h}_y = \dot{h}_l \left(\frac{y}{l}\right)^2 \quad (6.18)$$

$$\text{Overall K.E.} = \int_0^l \frac{1}{2} \left(\frac{\rho_l w^3}{12h} \right) \frac{y^2}{l^2} \Delta y \dot{h}^2 \quad (6.19)$$

$$= \frac{1}{2} \left(\frac{\rho_l w^3 l}{36h} \right) \dot{h}^2 \quad (6.20)$$

The term in the brackets is the total dynamic mass of the fluid. It is the Δm of equation (6.1). The actual mass is $wl\rho_l$. Therefore the overall mass magnification can be found as

$$\text{Overall Mass Magnification} = \frac{w^3 l \rho_l}{36h\rho_l w l h} \quad (6.21)$$

$$= \frac{1}{36} \left(\frac{w}{h}\right)^2 \quad (6.22)$$

6.4.3.b Fluid Loading Effects on the Wide Tuning Fork

In this case the fluid between the tines is pumped in the y direction (in the length direction) only as shown in Fig. 6.5. The volume of liquid trapped between 0 to y is given by

$$\text{Volume} = wyh \quad (6.23)$$

where

h = the gap between the tines

w = width of the tines.

The velocity magnification can be obtained by differentiating equation (6.23) with respect to time as

$$0 = \dot{y}h + y\dot{h} \quad (6.24)$$

The Kinetic energy of strip of liquid Δy is given by

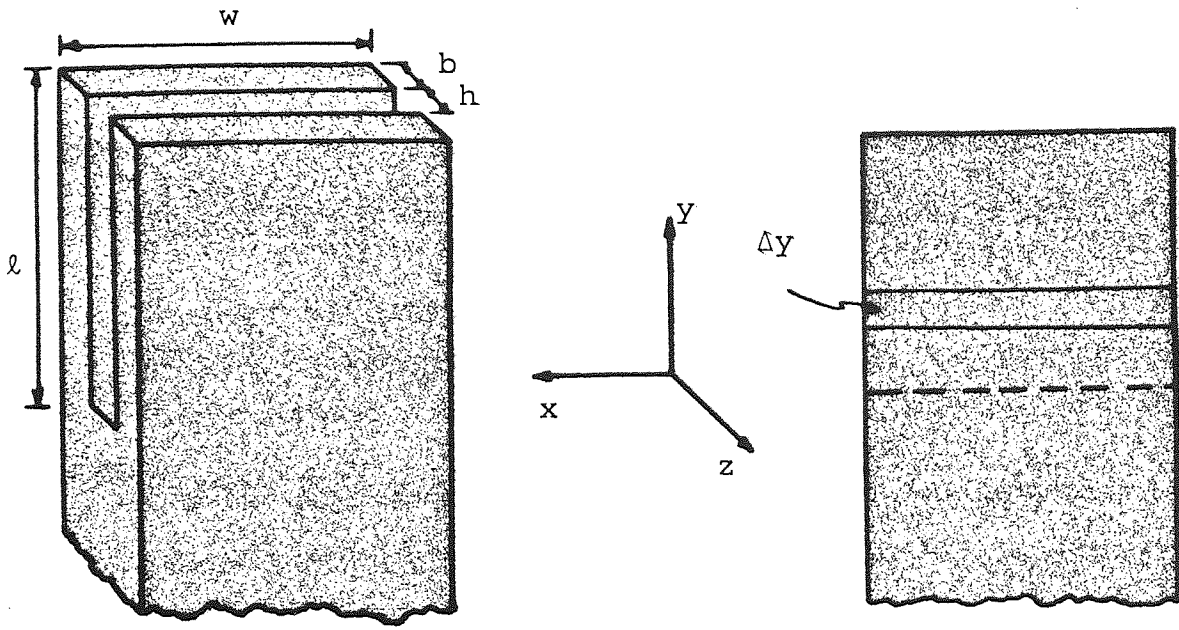


Fig. 6.5 Wide tuning fork. The liquid between the tines assumed to pump in y direction only.

$$\text{K.E.} = \frac{1}{2} (wh\Delta y\rho_\ell \frac{y^2}{h}) \dot{h}^2 \quad (6.25a)$$

$$= \frac{1}{2} (w\Delta y\rho_\ell \frac{y^2}{h}) \dot{h}^2 \quad (6.25b)$$

$$\dot{h}_y = \dot{h}_\ell \left(\frac{y}{\ell}\right)^2 \quad (6.25c)$$

Taking the assumption of equation (6.25c) the total K.E. of the fluid can be obtained by integrating equation (6.25b) from 0 to ℓ

$$\text{Total K.E.} = \int_0^\ell \frac{1}{2} \left(\frac{w\Delta y}{h\ell^2} y^4 \rho_\ell \right) \dot{h}_\ell^2 \quad (6.26)$$

$$= \frac{1}{2} \left(\frac{w\ell^3}{5h} \rho_\ell \right) \dot{h}_\ell^2 \quad (6.27)$$

The term in bracket is the dynamic mass of the fluid,

while the actual mass is $wlh\rho_l$. Therefore the mass magnification can be obtained as

$$\text{Mass magnification} = \left(\frac{wl}{5h}\rho_l\right)l/wlh\rho_l \quad (6.28)$$

$$= \frac{1}{5}\left(\frac{l}{h}\right)^2 \quad (6.29)$$

6.4.4 The Dynamic Mass of the Resonator

The total Kinetic energy of the tines can be found by the same analytical method as discussed before obtaining the dynamic mass of the liquid trapped between the tines.

The Kinetic energy of a short segment Δy considered in Fig. 6.5 is given by

$$\text{K. E.} = \frac{1}{2}(wb\Delta y\rho_m) \frac{\dot{h}_y^2}{4} \quad (6.30)$$

where

$\frac{\dot{h}}{2}$ = the velocity of the tine

b = the thickness of the tine

ρ_m = the density of the resonator material

\dot{h}_y^2 = the velocity magnification as defined by equation (6.18)

The total K. E. can be found by integrating equation (6.30) between $y=0$ to $y=l$

$$\text{Total K.E.} = \int_0^{\ell} \frac{1}{2} \left(\frac{wby^2 \Delta y}{4\ell^2} \rho_m \right) \dot{h}_\ell^2 \quad (6.31)$$

$$= \frac{1}{2} \left(\frac{wb\ell}{12} \rho_m \right) \dot{h}_\ell^2 \quad (6.32)$$

The term between the brackets is the dynamic mass of one tine, it is equal to $\frac{1}{12}$ of the actual mass of one tine ($wb\ell\rho_m$). Equation (6.32) gives the dynamic mass for both tines. It will be noted that the value obtained for the sensitivity is not particularly sensitive to assumption 6.25-c as it applies to the tine and fluid motions.

$$\text{Total K.E. for both tines} = \frac{1}{2} \left(\frac{wb\ell}{6} \rho_m \right) \dot{h}_\ell^2 \quad (6.33)$$

Hence the term $\left(\frac{wb\ell}{6} \rho_m \right)$ is the dynamic mass of the rectangular tuning fork resonator and is the M term in equation (6.10).

The dynamic mass of the tines can be found experimentally by cementing two identical small weights on the tines which represent the added mass (Δm) of equation (6.10)

$$\frac{f_x}{f_o} = \frac{1}{\sqrt{1 + \frac{\Delta m}{M}}}$$

From the above equation the dynamic mass M can be found where

f_o = the frequency of the transducer in air

f_x = the frequency of the transducer with the two weights loading the tines.

The above mathematical model can be represented by a lumped mechanical vibrator system. Such a system as shown in Fig. 6.6 consists of a spring of stiffness K , a mass M and a small mass Δm represents the added mass.

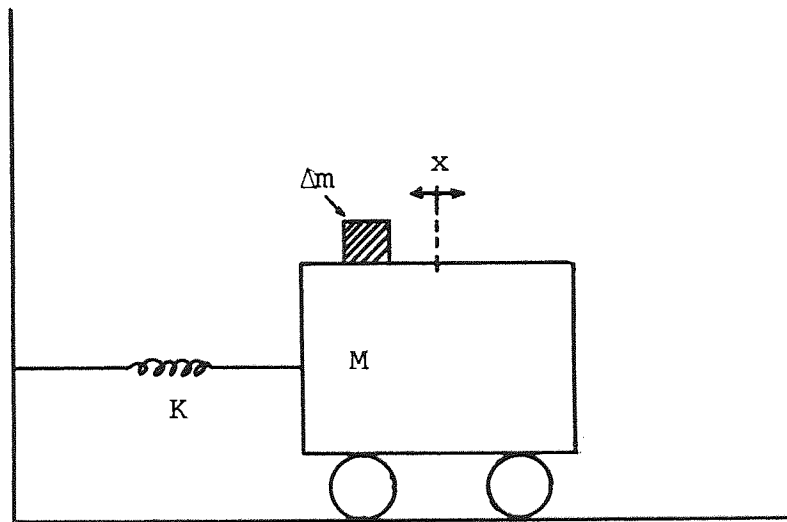


Fig. 6.6 Mechanical vibrator system, with mass M and spring.

This system represents the equation $\frac{f_x}{f_0} = \frac{1}{\sqrt{1 + \frac{\Delta m}{M}}}$ where M is the dynamic mass of the resonator, Δm is the added mass of liquid and f_x and f_0 are the corresponding frequencies.

6.5 EXPERIMENTS AND CALIBRATION

The frequency of the various transducers was measured

in air and liquids. The transducers were designed from different materials and different geometries as shown in Table 6.1 This enabled factors obtained in the analyses to be tested qualitatively.

The sensitivity and Q of the transducer are dependent on its geometry. Thus for an optimal design compromises are to be made in selecting geometrical dimensions of the transducer. For example, for a narrow transducer, the sensitivity can be found from equation (6.11), (6.20) and (6.33) as

$$\left(\frac{f_l}{f_o} \right)^2 = \frac{1}{1 + \frac{w^2 \rho_l}{6hb \rho_m}} \quad (6.34)$$

$$\rho_l = \frac{6hb}{w^2} \rho_m \left| \left(\frac{f_o}{f_l} \right)^2 - 1 \right| \quad (6.35a)$$

alternately

$$\rho_l K_o = \left| \left(\frac{f_o}{f_l} \right)^2 - 1 \right| \quad (6.35b)$$

where

K_o is the scale factor which equal to

$$K_o = \frac{1}{6} \left(\frac{w^2}{hb} \right) \frac{1}{\rho_m} \quad (6.36)$$

From equation (6.35b) it is quite evident that the higher the K_o is a measure of the sensitivity of the

TABLE 6.1

The Characteristics of the Transducers used for Liquid Density Measurements

Transducer Number	1	2	3
Material	Aluminium	Nickel Silver	Aluminium
Dimensions of the tines (mm)	29x12x4 ($a \times w \times b$)	53x22x8	44x24.3x6.25
Gap between tines (mm)	4	6	6.25
f_r (Hz)	3585	1422	2302
$Q \times 10^3$	0.185	3.4	3.0
Magnetostrictive material (mm)	One (6x.025) annealed strip nickel bonded at each tine.	The tines are plated with nickel, .025mm thickness	One (16x.025) annealed nickel strip bonded at each tine.
Scale factor K_o theoretical	0.554 (narrow) 23.275 (wide)	0.195 (narrow) 8.139 (wide)	0.930 (narrow) 21.946 (wide)
K_o experimental	1.030	0.340	1.375
Magnetic Material	Two layers bonded each side.	Two layers bonded each side.	Two layers bonded each side.

TABLE 6.1 Continued

Transducer Number	4	5	6
Material	Stainless Steel	Stainless Steel	Stainless Steel
Dimensions of the tine (mm)	44x24.3x6.25 ($l \times w \times b$)	45x49.5x6.25	24.5 mm diameter rod
Gap between tines (mm)	6.25 (h)	6.25	6.25
f_r (Hz)	2303.3	2253.3	2744.7
$Q \times 10^3$	3.6	1.7	3.1
Magnetostrictive material	One (16mmx.025mm) annealed nickel strip bonded at each tine.	One (49mmx.025mm) annealed nickel strip bonded at each tine.	The tines are plated with nickel, .025 mm thickness.
Magnetic Material	Two layers bonded each side.	Two layers bonded each side.	The coil is wound on the rod itself.
K_o Theoretical	0.318 (narrow) 7.500 (wide)	1.318 (narrow) 8.153 (wide)	
K_o Experimental	0.54	0.900	0.400

transducer. Thus sensitivity can be increased by reducing the gap (h) between the tines to the limit set by the requirement of free sampling of the surrounding liquid and also to maintain a sharp resonance. The thickness of the tine (b) can also be decreased for increasing sensitivity to the limit set by a choice f_0 a robust structure. By increasing the width (w), sensitivity can be increased, again this is limited by the associate viscous damping.

In this design the parameter ℓ has only a second order effect on the sensitivity. Therefore the size of the unit can be reduced by decreasing ℓ without affecting sensitivity, but this is limited by the liquid compressibility which becomes significant with the increase of frequency and undesired acoustic effects begin to appear.

The sensitivity of a wide transducer is approximated by equations (6.11), (6.27) and (6.33) as

$$\rho_{\ell} = \frac{1}{K_0} \left| \left(\frac{f_0}{f_{\ell}} \right)^2 - 1 \right| \quad (6.37)$$

where the scale factor K_0 is given by

$$K_0 = 1.2 \frac{\ell^2}{hb} \frac{1}{\rho_m} \quad (6.38)$$

From the equation above, one point can be added, that according to the theoretical expression (6.38), the sensitivity should be proportional to ℓ^2 . Again this method

of increasing the sensitivity by the increase of λ , is limited by the fall in 'Q' due to viscosity. The Q and sensitivity appear to be inseparable inverse functions for a given liquid.

However, the sensitivity for any given geometrical design can be increased by choosing a material of low density for the transducer.

The results of the experiment into which the frequencies of the various transducers were measured in air and liquids are shown in Table 6.2 and Fig. 6.7. In agreement with the above theoretical models the sensitivity of transducer 3 because of the low density aluminium is more than that of transducer 4. While transducer 5 is more sensitive than transducer 4, because the sensitivity is increased by the increase in the width of the transducer.

The frequency of transducer 3 is reduced by 35% from air to water (i.e. for a density change of $0-1000 \text{ Kg m}^{-3}$), while for transducer 4 the figure is 20% and for transducer 5, 30%. The stability of the particular electronic maintaining circuits was about 1 in 10^4 .

6.6. DEVELOPMENT OF THE TRANSDUCER

Further developments were carried out on the electronic design of the transducer. The new design uses a very much simpler electronic system.

TABLE 6.2

Density of Liquids	Air	Inhibisol 1.3156	Glycerol 1.2204	Water 1.000	Oil 0.864	Oil 0.837	Acetone 0.7901	Resonance Frequency (Hz)
3	2423.2	1449.2	1477.8	1576.3	1636.7	1659.7	1676.5	
4	2303.3	1785.2	1802.3	1879.7	1915.8	1934.4	1941.0	
5	2253.7	1525.6	1553.2	1642.1	1686.3	1706.6	1724.6	
6	2744.7	2239.0	2253.8	2309.8	2371.9	2376.98	2381.8	
3		1.365	1.384	1.363	1.380	1.352	1.378	$(\frac{f_{air}}{f_x})^2 - 1/\rho \times 10^{-3}$ (K ₀)
4		0.505	0.519	0.502	0.515	0.499	0.516	
5		0.898	0.906	0.884	0.910	0.889	0.896	
6		0.382	0.396	0.412	0.392	0.398	0.415	
3	1.000	2.796	2.689	2.363	2.192	2.132	2.089	$(\frac{f_{air}}{f_x})^2$
4	1.000	1.665	1.633	1.501	1.445	1.418	1.408	
5	1.000	2.182	1.105	1.884	1.786	1.744	1.708	
6	1.000	1.503	1.483	1.412	1.340	1.333	1.328	

The experimental results of measuring frequencies in a range of liquids for the four transducers described in Table 6.1. In group 2 the values for a given fork will be constant for the simple lumped mode. In group 3 the parameter should be linear with density (See Fig. 6.7). The experiments were carried out at room temperature.

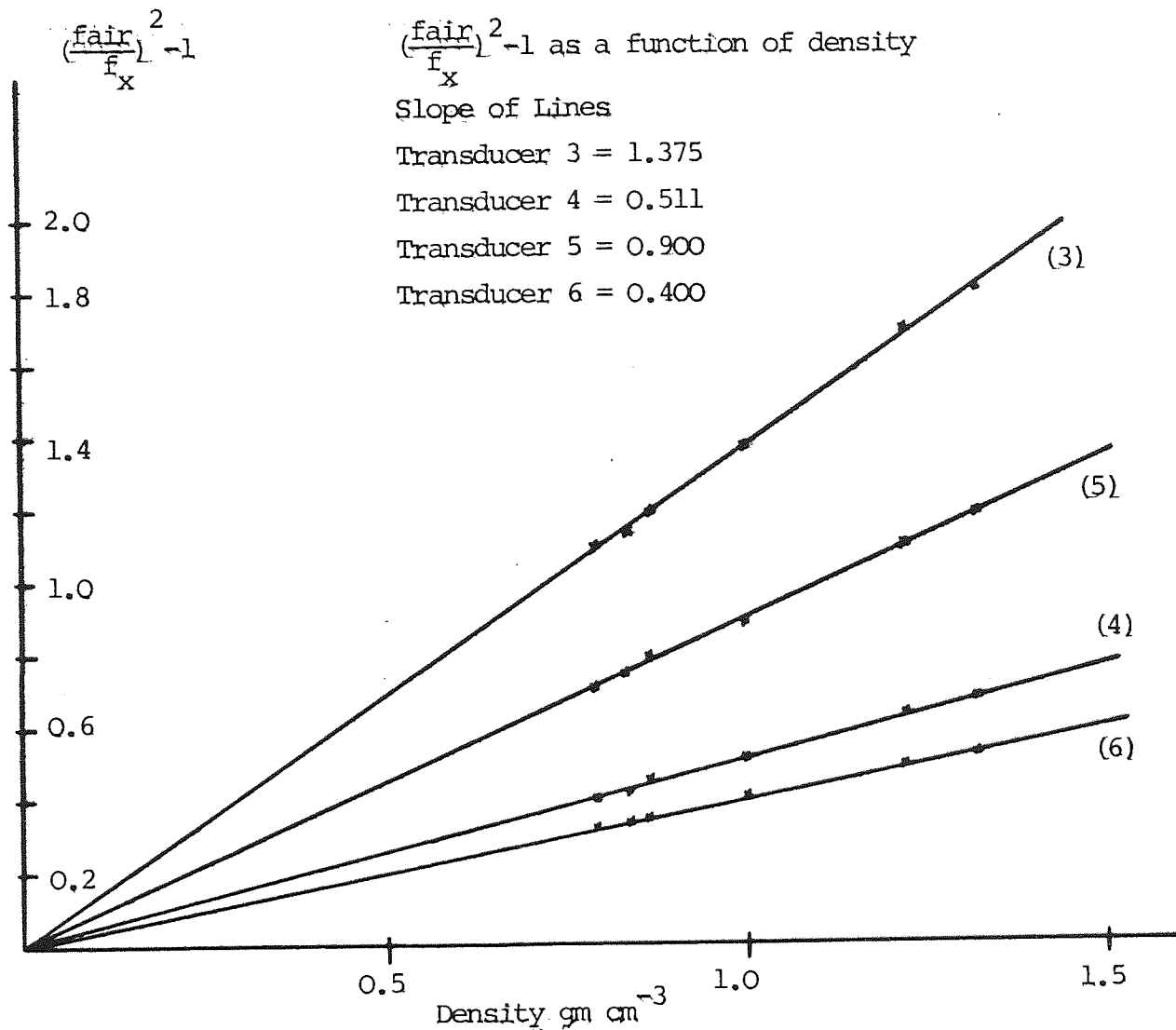


Fig. 6.7 The calibration curves for 4 transducers using a range of liquids. It will be noted that the lines are straight and go through the origin. The slopes are equal to the scale factor K_0 of the transducer. In transducers 3 and 4, the value of K_0 shows the effect of the material density where the gap and the dimensions of the tines are the same. While in transducers 4 and 5 the material density and the gap are the same and K_0 values shows the effect of tine area.

In this development the magnetostrictive effect is used for the drive only which is now continuous. A suitable piezoceramic crystal is used to pick-up the vibration propagated through the flange. (in the previous design the reciprocal magnetostrictive effect was used). These vibrations are converted to electrical signals by the crystal and a charge amplifier.

The output supplies the controlling input of the phase sensitive detector of a PLL. (The PLL has been discussed in detail in Chapter 4). The reference phase comes from the voltage controlled oscillator of the PLL which also supplies the drive unit. In this case, the frequency of the voltage controlled oscillator is directly controlled by the transducer and being a phase sensitive system has a frequency stability proportional to the 'Q' factor. The circuit diagram is shown in Fig. 6.8.

A major simplification of the sensor (the mechanical vibrator) was achieved. The sensor is now in the form of a circular rod tuning fork (shown in Fig. 6.9) plated with nickel to give the magnetostrictive drive and the flux coil is wound on the rod itself hence avoiding the use of laminated magnetic strips.

An experiment was carried out using transducer 5 to investigate the stability of the transducer system. A digital to analogue converter was used to give an x-y plot

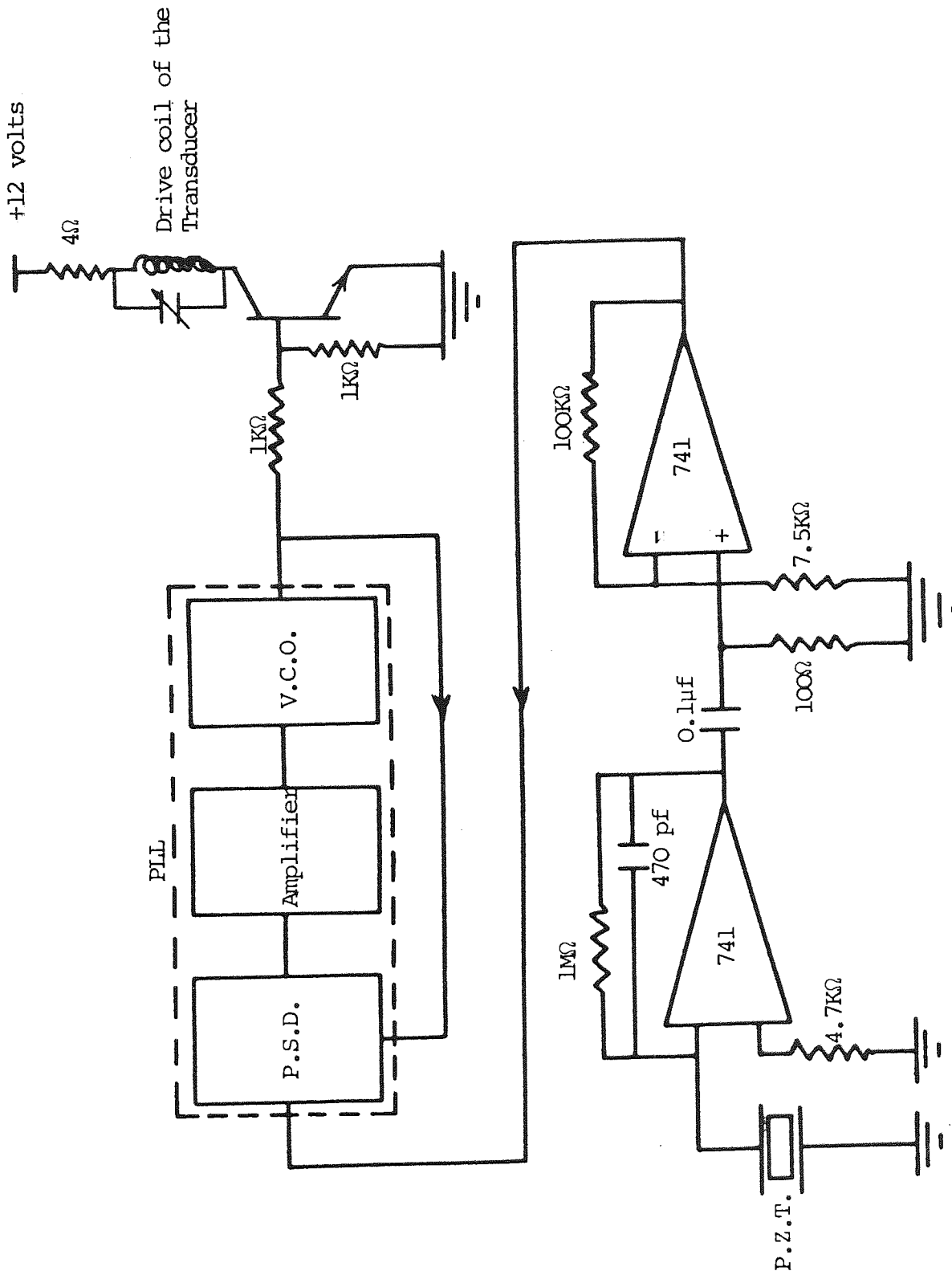


Fig. 6.8 The electronic design used to drive and pick-up the vibration of the transducer.

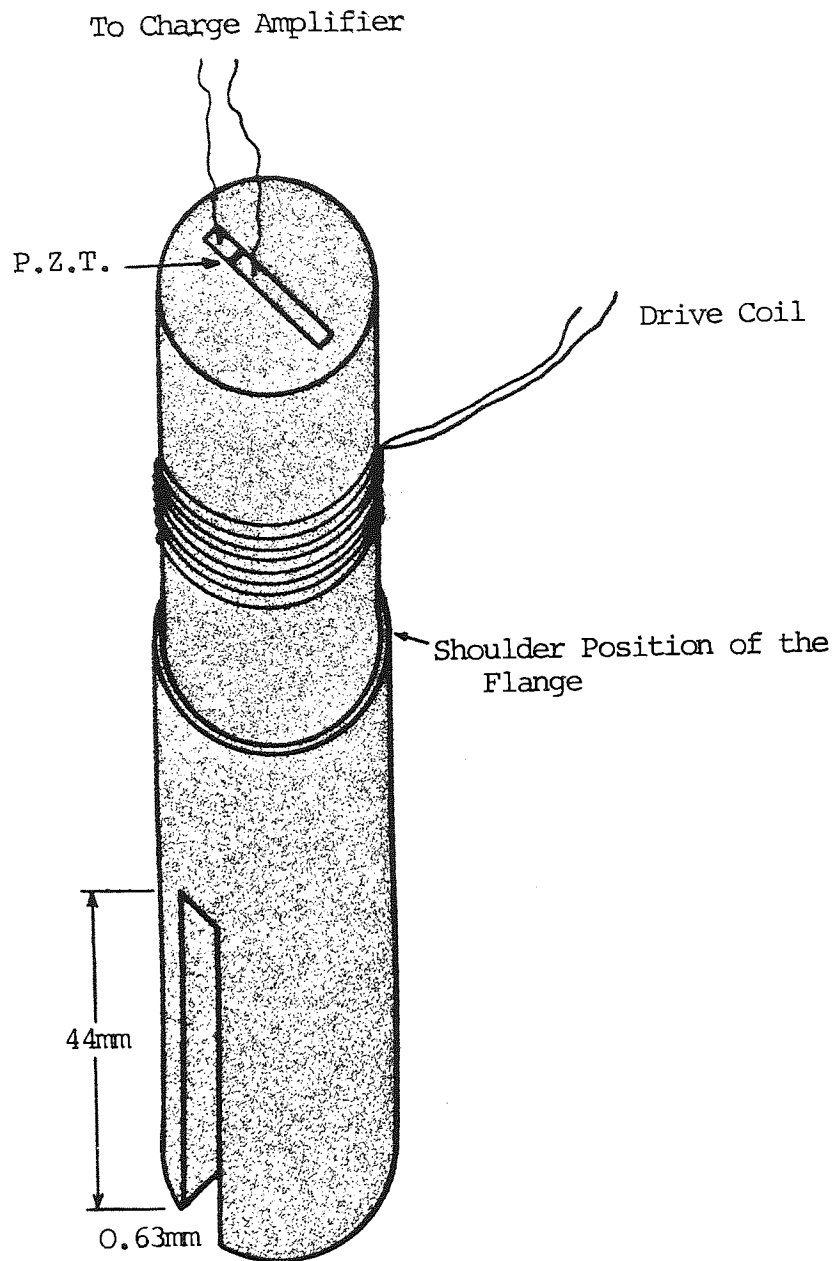


Fig. 6.9 The final transducer design (6). In this design it will be noted that, one coil is used for the drive and a P.Z.T. used to pick-up the vibration.

of frequency. The system thus operated automatically to display the magnitude of the frequency changes. A typical display is shown in Fig. 6.10.

The stability in air ($Q=1.7K$) was about 1 in 10^6 . The improvement in the stability arises from the high Q of the transducer as previously discussed.

6.7 RECOMMENDATION FOR VISCOSITY TRANSDUCERS

6.7.1 Introduction

Viscosity is an important physical property of fluid being a sensitive measure of its physical state. It can be very sensitive to temperature and composition. Viscosity has been measured by a number of methods and devices. Laboratory instruments have used a rotation viscous drag on a falling ball and a liquid flow through capillaries Van Wazer (1963). Some of the more recent instruments are based on vibrational methods to set up an alternating shear wave in the test liquid instead of maintaining a steady shear rate, by means of longitudinally vibrating plates, cylindrical or spherical pendulums vibrating in torsion or flexural oscillations in a thin rod or wire.

In the literature it can be found that there are two methods applied to the vibrational viscosity transducer. One method is based on the resonant system, where the transducer formed part of a self-oscillating circuit, so

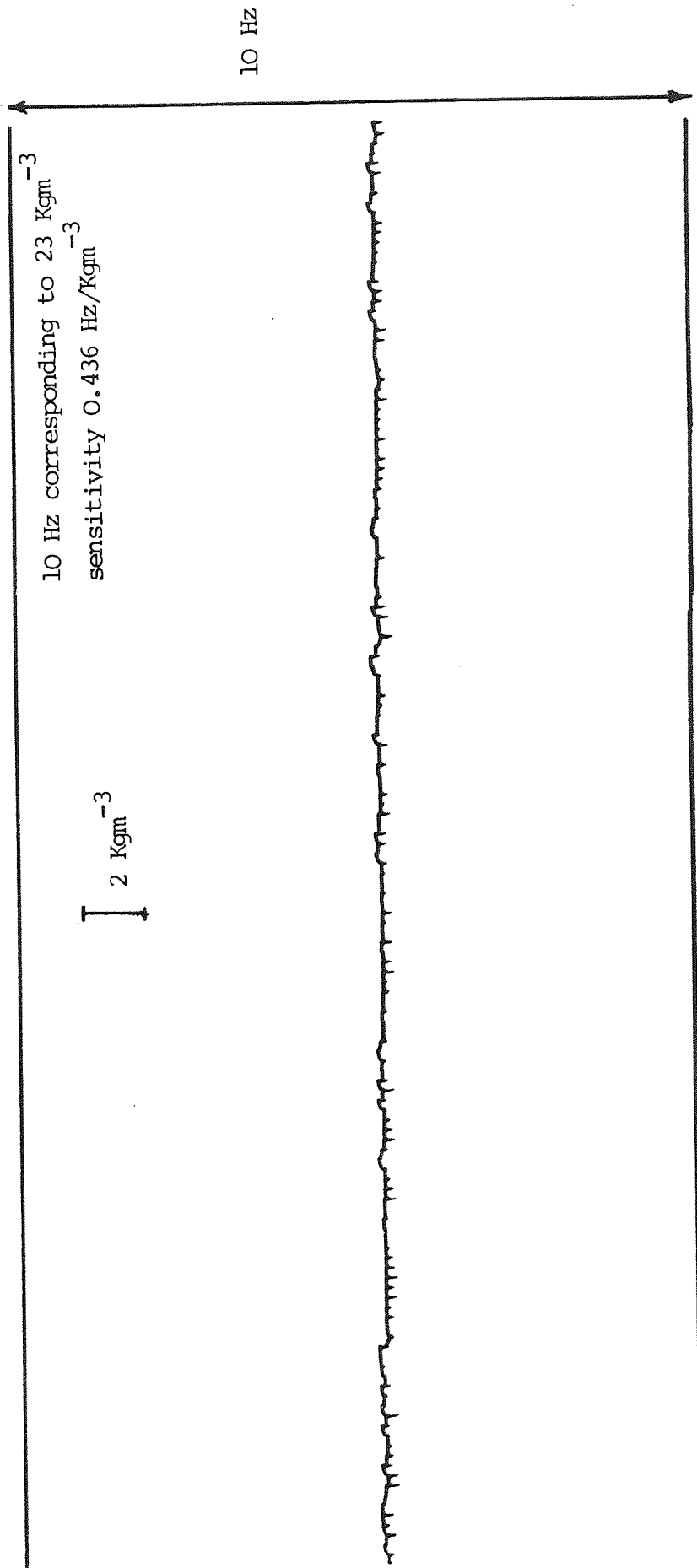


Fig. 6.10 Stainless steel transducer 5 vibrating in oil of density 837 Kgm^{-3} at frequency 1706 Hz.

that it always operated at a resonant frequency, Mason (1947), Haynes (1973) and Kremlevskii (1975). Those of Chung (1973), Berger (1978) and Roth and Rich (1953) are based on the second method which depends upon the measurement of the amplitude decrement of the driven resonator.

6.7.2 Viscosity Measurements

The present design of the density transducer can be developed to operate using either method (resonance or damping) to measure liquid viscosity.

To measure the damping amplitude, experiments were carried out using different transducers vibrating continuously in oil and water. The vibrations were picked up by a crystal bonded at the end of the stem (shown in Fig. 6.9). This pick-up signal was then fed to the decrement Q-meter (discussed in Chapters 3 and 4) and the Q was measured by counting the number of oscillations between two defined amplitude levels and the results are shown in Table 6.3.

The viscosity measurement by the resonant method using the present design require considerable efforts to reach a good practical device.. However, promising results (shown in Table 6.4) were obtained using a new sensor design.

TABLE 6.3

Experimental results of measuring 'Q' factor
as a function of viscosity of different liquids

Transducer Number	Q			
	Water 1000 Kgm ⁻³	Oil 864 Kgm ⁻³	Oil 837 Kgm ⁻³	Air
1	125	-	90	185
2	595	251	235	3400
3	405	103	195	3000
4	650	215	437	3600
5	470	266	-	1700

The experiments were carried out at room temperature.

TABLE 6.4

Experimental results of measuring frequency
as a function of viscosity of different liquids

Transducer Number	Resonant Frequency			
	Water 1000 Kgm ⁻³	Oil 864 Kgm ⁻³	Oil 837 Kgm ⁻³	Air
1	4160	4158	4183	4329
2	2927	2895	2936	2942

The experiments were carried out at room temperature.

The aim of this model (shown in Fig. 6.2) where a tuning fork is designed to reduce the pumping action of the fluid between the tines, and to set up an alternating shear wave in the liquid which has a damping and inertial effect on the transducer. Thus the density effect is minimised and the viscous effect enhanced.

The tuning fork is required to have a very large thickness compared to the width. The drive and receive method is the same as that of the density transducer where two coils were used.

The results were obtained using two transducers described in Table 6.5.

6.8 MAGNETOSTRICTIVE MATERIAL

The magnetostrictive material is a vital part in the transducer design. Magnetostriction is the term applied to the effect of magnetic induction on the dimensions of ferro-magnetic material which is known as Joule effect. The change in length per unit (strain) length is approximately proportional to the square of the flux density.

The reciprocity of the Joule effect is the change in the induction field resulting from an externally applied stress which is known as Villari effect.

A reversal of the induction field brings about the same change; for example during each half of an alternating

TABLE 6.5

The characteristics of the transducers
used for viscosity measurements

Transducer Number	1	2
Material	Aluminium	Zirconium
Dimensions of the tine (mm)	60×3.3×23 $l \times w \times b$	54×0.5×23
Gap between the tines (mm)	3	2
f_r Hz	4329	2942
Q	High	High
Magnet- ostrictive material	One (12mm×.025mm) annealed nickel strip bonded at each side of each tine.	One (12mm×.025mm) annealed nickel strip bonded at each side of each tine.
Magnetic Material	Two layers bonded each side.	Two layers bonded each side.

field, a nickel rod would undergo a complete cycle of contraction and return to normal length, a performance resulting in frequency doublings as shown in Fig. 6.11.

Three disadvantages of this frequency doubling excitation are excessive harmonic distortion, greater hysteresis losses and the fact that efficient power conversion is obtained only at high power level. These handicaps may be avoided by maintaining a fixed magnetizing field in the material on which the a.c. exciting field is imposed as shown in Fig. 6.12.

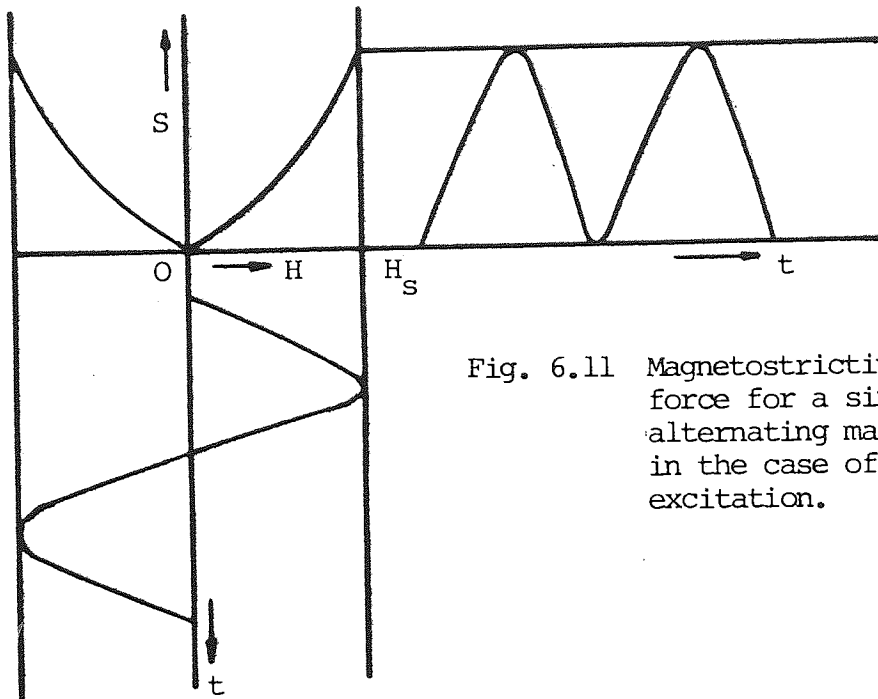


Fig. 6.11 Magnetostrictive driving force for a sinusoidally alternating magnetisation in the case of non-biased excitation.

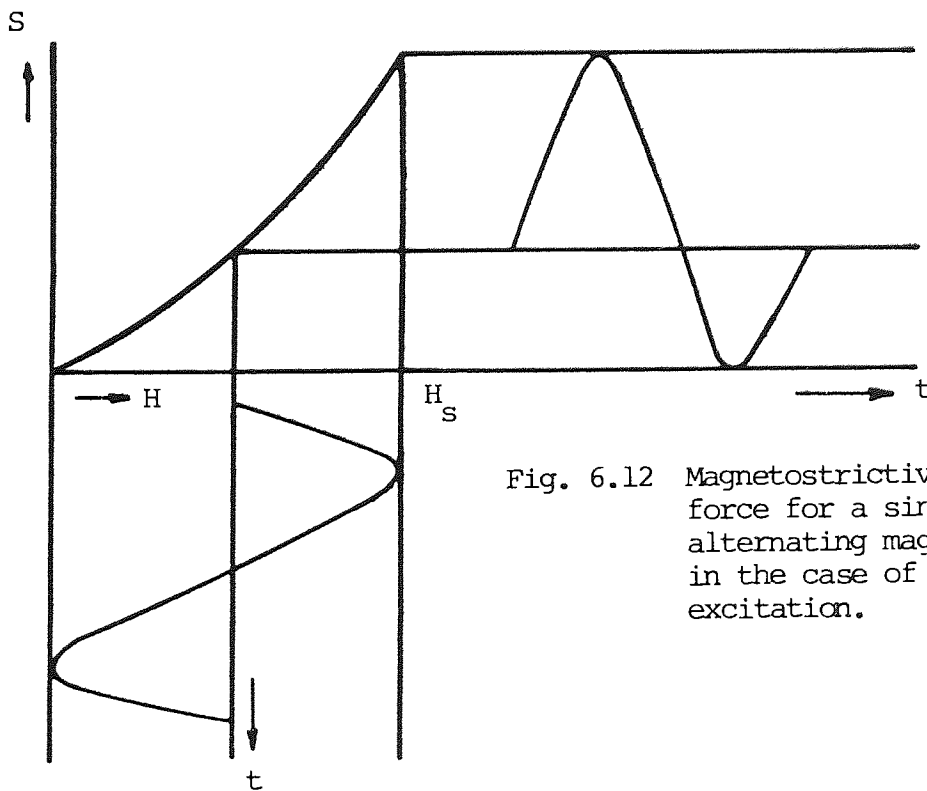


Fig. 6.12 Magnetostrictive drive force for a sinusoidally alternating magnetisation in the case of biased excitation.

6.9 CONCLUSIONS

A variety of transducer designs have been examined for measuring liquid density. It was found that the added mass of the liquid and the dynamic mass of the transducer (i.e. the mass magnification) are functions of the geometry of the transducer. As discussed in Section 6.4, the higher the mass magnification the more the transducer is sensitive, therefore the sensitivity can be controlled by the geometry of the transducer, (i.e. increasing the size of the transducer with the same gap and the same material the sensitivity will increase). This becomes evident by comparing the sensitivity of transducers 4 and 5, the sensitivity of transducer 5 is increased by a factor three of transducer 4 as found experimentally while the theoretical value is about four.

The sensitivity can also be controlled by the density of the material transducer, where the sensitivity is proportional to $1/\rho_m$. This also found experimentally to have a good agreement with the theory, where the sensitivity of transducer 3 increased by a factor of about three by using a material of lower density than that of transducer 4 by a factor of three.

In general the experiments theoretical support have given a good insight into transducer design. It is now possible to design transducers to measure both density

and viscosity for a large range of values and physical situations.

A primary feature of the development is that it enables the transducer, which can be regarded as a circular rod probe, to operate through a metal flange. This isolates the driving which is outside the flange from the measuring sensor (The tines).

Due to the high mechanical simplicity of this system, the present transducer can be built in the form of simple convenient probe for use in the pipe lines or as a direct probe.

LIST OF SYMBOLS

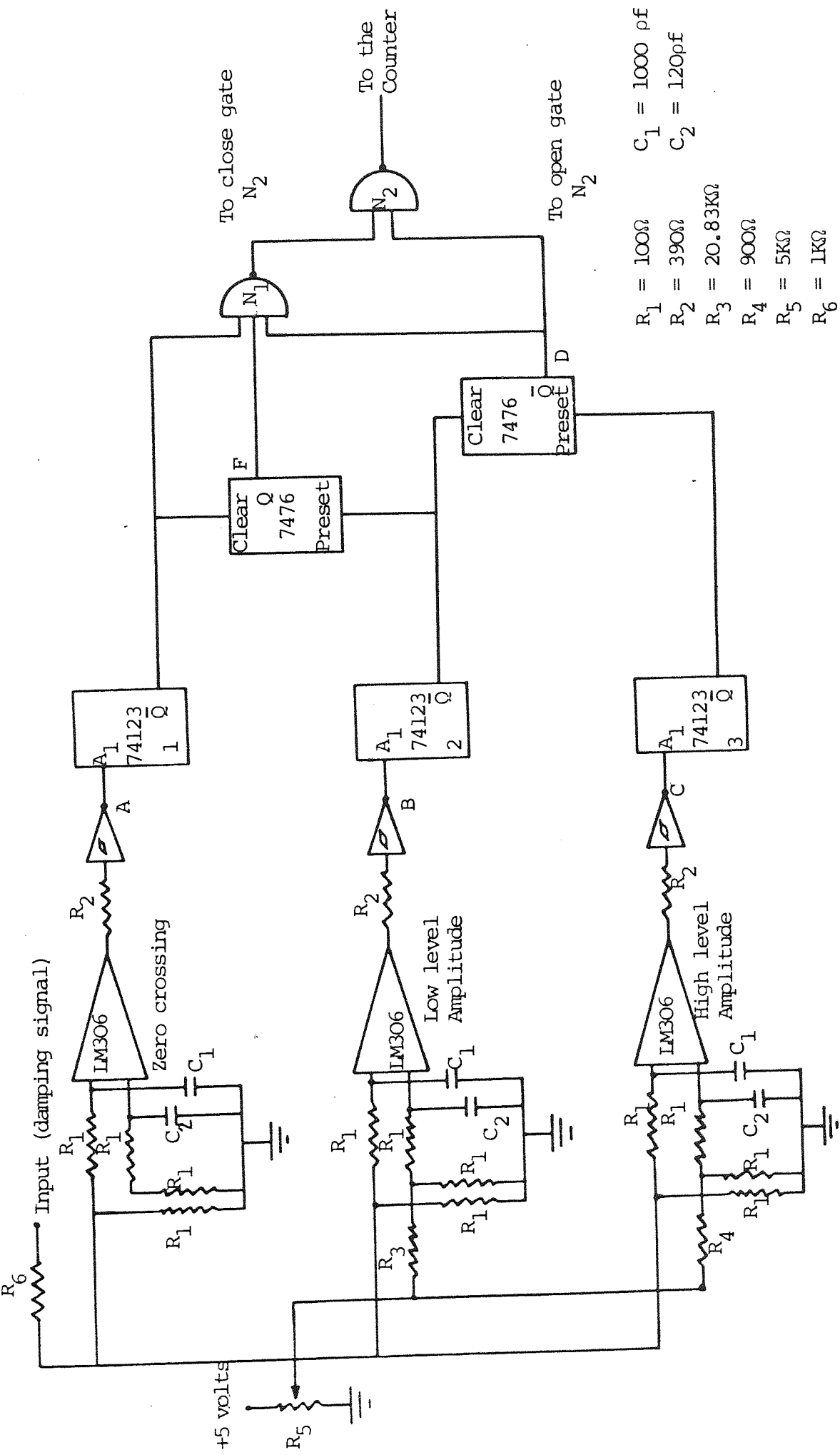
A_0	Amplitude at $t=0$
A_n	Amplitude after a number of oscillations
t	Time
n	The number of oscillations, mode order
Q	Quality factor
M	Mass
R_m	Viscosity damping
K	Spring stiffness, radius of gyration
$F \cos \omega_0 t$	Driving force
ω_0	Angular frequency in air
f_0	Natural frequency
Δf	Band width
f_1, f_2	The frequencies at half power points
X	Displacement in x-direction
Y	Displacement in y-direction
\dot{X}	$\frac{dx}{dt}$
\ddot{X}	d^2x/dt^2
E_0	Energy at $t=0$
E_n	Energy after a number of oscillations
T	Period
ℓ	Inductance, Length of the tine
L	Length of the bar
b	Thickness of the bar, thickness of the tine
a	Radius of rod, radius of the disc
C_0	Velocity of waves
B_n	Factor determining the overtones

r	Resistance, radius of annular ring
R	Resistance
C	Capacitance
E	Young's modulus
ρ	Density of the bar
h	Gap between the tines
w	Width of the tine
f_r	Natural frequency in air
f_ℓ	Frequency in a liquid of density ρ_ℓ ,
ρ_ℓ	Liquid density
K_o	Sensitivity factor
Q_D	Quality factor measured by decrement method
Q_B	Quality factor measured by bandwidth technique
\bar{Q}	Mean value of Q
Δk	The effective change in stiffness due to loading
Δm	The effective change in mass due to loading
V	Volume of liquid
K.E.	Kinetic energy

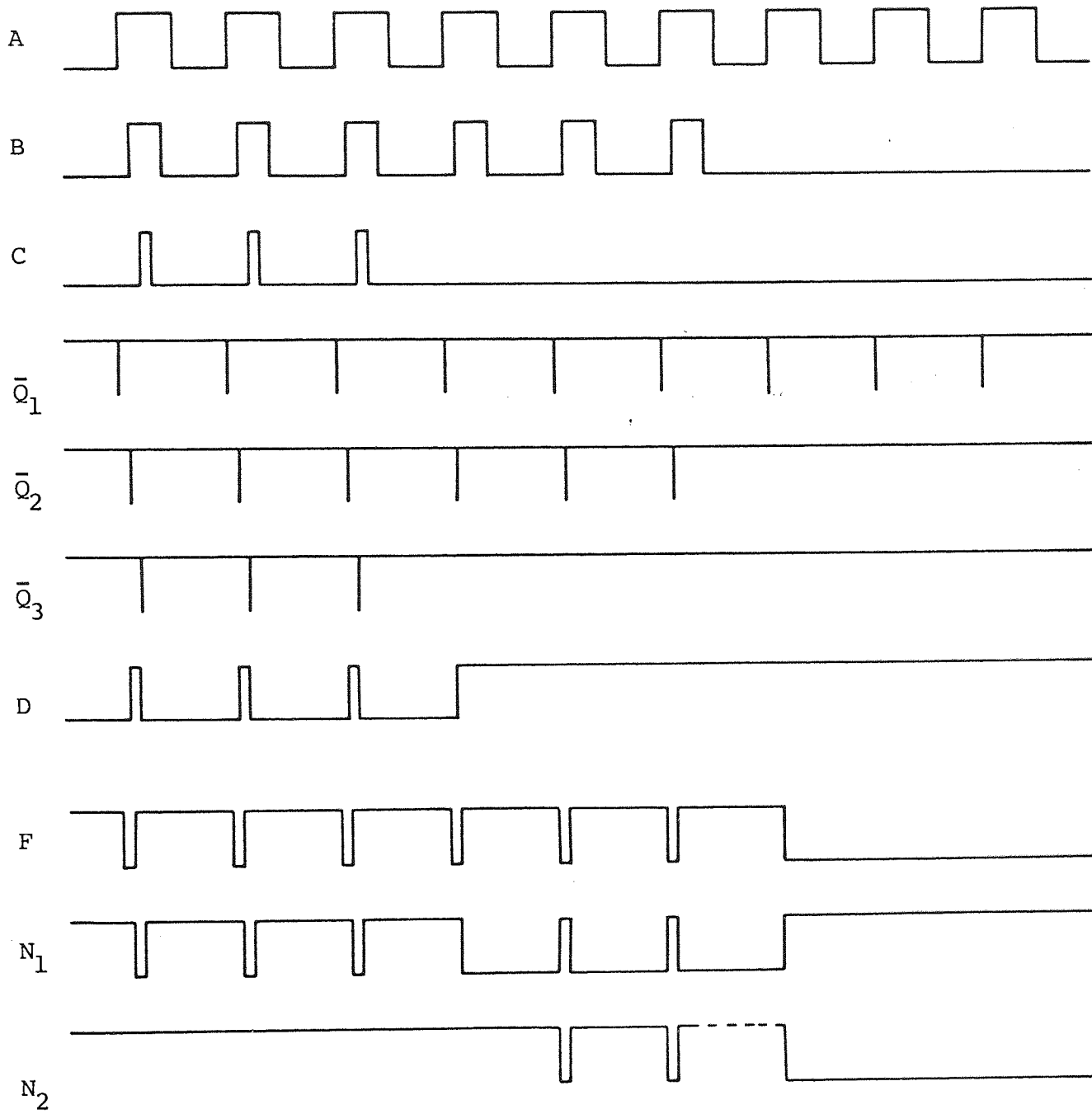
APPENDIX A

The circuit diagram and the waveforms at different points.

The low pass filters in the input circuits were necessary to suppress parasitic oscillations.



- $R_1 = 100\Omega$
- $R_2 = 390\Omega$
- $R_3 = 20.83K\Omega$
- $R_4 = 900\Omega$
- $R_5 = 5K\Omega$
- $R_6 = 1K\Omega$
- $C_1 = 1000\text{ pf}$
- $C_2 = 120\text{ pf}$



REFERENCES

- AGAR, J.
The vibration spool fluid density meter.
Instrument Practice, pp. 437-439, June 1969.
- BELL, J. F. W.
Ultrasonic thermometry using resonance techniques.
Proc. 5th Symp. on Temperatures, Washington D.C., 1971.
- BERGER, S. A. et al.
A new electromechanical viscometer designed for biological fluids.
IEEE Trans. on biomedical Eng. BME-25, pp. 64-70, Jan. 1978.
- BICKFORD, R. H. et al.
The evaluation of acoustic impact technique for detection of incipient cracks in aircraft company.
Airforce Materials Laboratory, Wright-Patterson Airforce Base and the Boeing Vertal Company AFML-TR-73-146, 1973.
- CHUNG, P. L.
A linear oscillatory viscometer.
Rev. of Sci. Inst., 44, pp. 1669-1670, 1973.
- EDER, O. J. and SCHWARA, R.
A fast digital method for the measurement of internal friction and elastic moduli of solids.
J. of Phy. E.: (Scientific Instruments), 7, pp. 476-480, 1974.
- FATHIMANI, A. A.
The automation of resonant thermometer probe measurements.
Ph.D. thesis, University of Aston in Birmingham, 1976.
- FORSTER, F.
Z. Metallk, 29, 109, 1937.
- FUSFELD, H. I.
Apparatus for rapid measurement of internal friction.
The Rev. of Sci. Inst., 21, pp. 612-616, 1950.
- HASSAN, A.
Electromechanical resonators as measuring transducers.
Ph.D. thesis, University of Aston in Birmingham, 1980.

HAYNES, W. M.
Viscosity of gaseous and liquid Argon.
Physica., 67, pp. 440-470, 1973.

HOLT, W. J.
A tuning fork for high Q resonator.
Electronics, No. 21, p. 108, 1960.

JAMES, G. S.
Tuning fork frequency standard.
J. Acous. Soc. Am., Vol. 33, pp. 1649, 1961

JUNGER, M. C. and FEIT, D.
Sound structure and their interaction.
MLT Press Cambridge, 1972.

JUNGER, M. C.
Vibrating of elastic shells in a fluid medium and the
associated radiation of sound.
J. of Appl. Mechanics, pp. 439-445, Dec. 1952.

KALMARCZIE, P. J.
Energy trapped resonances in solid structures.
Ph.D. thesis, University of Aston in Birmingham, 1976.

KLIMASARA, A., FIORE, N. F. and KUCZYNSKI, G. C.
Automated resonance - bar damping measurement system.
Rev. Sc. Inst., 47, pp. 1163-1166, 1976.

KREMLEVSKII, V. P. and STEPICHEN, A. A.
Measurement of viscosity and density of a liquid by means
of a vibrating transducer.
Soviet Physics - Acoustics, 21, No. 7, July-August, 1975.

LAMB, H.
On the vibration of an elastic plate in contact with water.
Proc. Ray. Soc., 98, pp. 205-216, 1921.

LAX, M.
The effect of radiation of the vibration of the circular
diaphragm.
J. Acoustic Soc. Am., 16, pp. 5-13, 1944.

LAZAN, B. J.
Damping studies in materials science and materials
engineering.
A.S.T.M., STP, 378, Am. Soc. Testing Mats., 1964.

LEISSA, A. W.
The free vibration of rectangular plates.
J. of Sound and vibration, 31, pp. 257-293, 1973.

LLOYED, P. A.
Material testing by impact response analysis.
Ph.D. thesis, University of London, 1976.

MASON, J. M. and LEVENTHALL, H. G.
The efficiency of various free-free supports systems for
a flexing beam.
Acustica, 23, pp. 348-350, 1970.

MASON, J. M. and LEVENTHALL, H. G.
Rapid measurement of the decay rate of vibrations.
J. of Physics, E. (Scientific Instrument) 2, pp. 1104-1107,
1969.

MASON, W. P.
Measurement of the viscosity and shear elasticity of
liquids by means of a torsionally vibrating crystal.
A.S.M.E. Transactions, May 1947.

MAX, H.
Frequency-adjustable tuning fork type vibrator for an
electrically energized timepiece.
J. Acoustic.Soc. Am., 35, p. 950 , 1963.

MORSE, P. M.
Vibration and sound.
McGraw-Hill, 1948.

NORWICK, A.
Progress in metal physics, (Internal friction in Metals)
Intersciences Publishers Inc., New York, Vol. IV, pp. 1-70,
1953.

POTTER, P. N.
Frequency domain transducers and their applications.
Instrument Practice, pp. 849-853, Dec. 1969.

PATTISON, J. R.
An apparatus for the accurate measurement of internal friction.
Rev. of Sci. Inst., 25, pp. 490-496, 1953.

LORD RAYLEIGH
Theory of Sound, Vol. 1.
Macmillan, London, 1894.

REEFMAN, W. E.
Tuning fork measure frequency.
Electron Prod. Mag., No. 6, pp. 32-34, 1964.

ROTH, W. and RICH, S. R.
A new method for continuous viscosity measurements. General
theory of the ultra viscoson.
J. Appl. Phys., 24, pp. 940-950, 1953.

SETH, T. N.
Ultrasonic pyrometer for industrial applications.
Ph.D. thesis, University of Aston in Birmingham, 1974.

SIMPSON, H. M. and SOSIN, A.
Automatic internal friction and modulus measurement
apparatus utilising a PLL.
Rev. of Sci. Inst., 48, pp. 1392-1396, 1977.

STEPHENS, R. W. B. and BATE, A. E.
Acoustics and vibrational physics.
Arnold, London, 1966.

SWARTZ, J. C.
Circuit to measure decay rate of a low frequency signal.
Rev. of Sci. Inst., 35, pp. 1573-1574, 1964.

TARABA, O.
Some thoughts on viscosity measurement with ultrasonic
transducer.
Ultrasonics, pp. 248-250, Oct. 1967.

VAN WAZER, J. R. et al.
Viscosity and flow measurement. A laboratory handbook of
Rheology Interscience, 1963.

WACHTMEN, J. B.
Effect of suspension position on apparent values of internal
friction determined by Forster's method.
Rev. of Sci. Inst., 29, pp. 517-520, 1958.

WHITE, M. S. and SOLOMONS, C.
Linear oscillation viscometer.
Rev. of Sci. Inst., 40, pp. 339-346, 1969.

WULFSBERG, K. N..
A tuning fork filter.
J. Acous. Soc. Am., Vol. 22, pp. 847-849, 1950.

YASUHIRO MIYAKE and YOSHINOBU IZUM,
Static and dynamic viscosities in the binary mixture
microbenzene-n-hexan near a critical point.
Phy. Review A, 15, pp. 2065-2068, 1978.

ZENER, C.
Elasticity and an elasticity of metals.
University of Chicago Press, 1948.